

# Heat Exchanger Performance and Optimisation

A dissertation submitted to

**University of Southern Queensland**

by

**Terrence Clarke**

Supervised by

**Dr Khalid Saleh**

For the award of

**Bachelor of Engineering (honours)**

**Mechanical Engineering Major**

Submitted

**12<sup>th</sup> of October 2021**

# Abstract

Heat exchangers are used throughout industry, in various forms, to remove excessive heat created and allow continual operation of the equipment. A common type of heat exchanger is the liquid/liquid non-direct heat exchanger, typically with flow rates adjusted using a butterfly control valve to maintain desired operating temperatures. A modern option for reducing some of the system inefficiencies of heat exchangers is replacing the fixed output pump and butterfly control valve system with a variable speed pump which does not require a control valve. This improvement provides:

- Improved efficiency as the variable speed pump uses less power
- Longer pump life by reducing cavitation from throttling
- Longer life and efficiency out of the heat exchanger core due to less ‘hot-spots’ resulting in fouling.

An extensive literature review was carried out, however little published information is available on the effects of a butterfly control valve at the entry of a heat exchanger. This dissertation investigates the knowledge gap surrounding the influence of a control valve at the entry of a heat exchanger. It addresses both the global heat distribution and the local transfer wall temperatures near the entry region. The following stepwise phases were completed in succession and form the structure of this investigation:

- **Phase 1:** Conduct physical experiments of a simple heat exchanger arrangement and gather experimental data
- **Phase 2:** Undertake a computational fluid dynamics (CFD) simulation of a heat exchanger modelled on the physical experiment
- **Phase 3:** Compare the results of the experimental and simulation studies. Refine the CFD model until the results are within an acceptable error range
- **Phase 4:** Conduct a physical experiment and CFD modelling of a simple heat exchanger using a control valve at the process water entry point and analyse the temperature distribution at a global level.
- **Phase 5:** Analyse the temperature distribution at the entry of the heat exchanger for localized hot spots on the transfer wall
- **Phase 6:** Scale the CFD model to the size and boundary conditions of the real-life application and repeat global and localized analysis.

With respect to the global heat distribution, the study found that both the USQ experimental jig and scaled analysis showed no influence from the control valve at the entry. However, for the local transfer wall distribution, the simple experimental jig and the scaled analysis both showed that the maximum temperature on the wall was significantly higher in the region 1.9 to 2.9x the diameter of the valve diameter into the heat exchanger. The study also found that as the angle of the control valve became more closed, both the average and maximum temperature across the transfer wall in the 1.9-2.9x valve diameter region increased.

These results indicate a variable speed pump reduces temperature spikes on the transfer wall and is preferable to a fixed speed pump with butterfly control valve.

## Limitations of Use

The Council of the University of Southern Queensland, its Faculty of Health, Engineering and Sciences, and the staff of the University of Southern Queensland, do not accept any responsibility for the truth, accuracy or completeness of material contained within or associated with this dissertation.

Persons using all or any part of this material do so at their own risk, and not at the risk of the Council of the University of Southern Queensland, its Faculty of Health, Engineering and Sciences or the staff of the University of Southern Queensland.

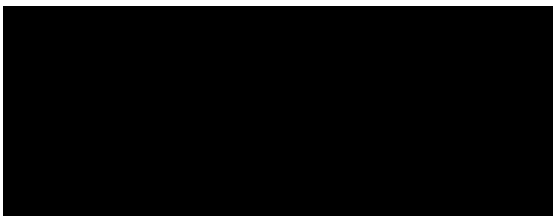
This dissertation reports an educational exercise and has no purpose or validity beyond this exercise. The sole purpose of the course pair entitled “Research Project” is to contribute to the overall education within the student’s chosen degree program. This document, the associated hardware, software, drawings, and any other material set out in the associated appendices should not be used for any other purpose: if they are so used, it is entirely at the risk of the user.

# Certification

I certify that the ideas, designs and experimental work, results, analyses, and conclusions set out in this dissertation are entirely my own efforts, except where otherwise indicated and acknowledged.

I further certify that the work is original and has not been previously submitted for assessment in any other course or institution, except where specifically stated.

**Terrence Braden Clarke**



*Signature*

*12 October 2021*

*Date*

# Acknowledgements

The experimental work within and the writing of this dissertation has been a challenging journey and would have been near impossible without the help of a few special people along the way. Firstly, a big thank-you to my supportive supervisor Dr Khalid Saleh from the USQ teaching staff. His constant communication via emails, calls, video conferencing and face to face support to guide and educate was critical to the success of this work. Also, from the USQ teaching staff, I would like to thank Assoc Prof Andrew Wandel. Whilst not my formal supervisor he took the time to assist and educate by being a third set of eyes on some of my early CFD challenges and got me on track.

Starting out on this dissertation my daughter, my first child, had just turned three months old. Along the way my wife Jenna has been understanding and patient well beyond what could be expected from a marriage. My work and study commitment has required her to make significant personal sacrifices and raise our daughter without my full support. If not for the dissertation she would normally deserve and receive that support. Without her this dissertation would never have been a success. In what personal time Jenna does get, she has also taken the time to proofread this dissertation and highlight areas where I made grammatical errors. I am very thankful to have a wife willing to go above and beyond for our family.

As mentioned, with a young child, time management has been a challenge throughout this dissertation. Thanks to the members of my extended family who have helped along the way, especially when my wife was completing her nursing placement. An extra special thank-you goes to my Mum who travelled down from Mackay to stay in our spare room for a couple of months offering her continual household assistance.

Reflecting on the end of my Bachelor degree I wish to acknowledge my employer: Cummins South Pacific. Cummins identified potential in me many years ago and gave me an entry level “Engineering” position knowing I did not yet have my qualifications. Over the seven years of my undergraduate degree Cummins have supported me both financially and with study leave to complete on-site requirements and exams. I am very appreciative of this opportunity and with the confidence they have shown with me.

Finally, I am thankful of the very thorough education the University of Southern Queensland have provided me. Not only through theoretical learning, but also the personal and profession development the university experience offered. I started this degree with a retrospectively poor attitude that it was just something I ‘had to do’ to get my job, but it very quickly became apparent there was much to learn from the USQ courses and teaching staff. Thermodynamics and fluid dynamics were the two fields where I struggled most, and got the poorest marks in, during my degree. I have chosen to do my thesis in this area to challenge myself and reinforce my learning. I don’t think I would have ever decided to take the hard road without the values USQ has taught me. Thank you to all the teachers and mentors that have contributed to my development along this journey.

# Table of Contents

Abstract .....	ii
Limitations of Use.....	iii
Certification .....	iv
Acknowledgements .....	v
Table of Contents .....	vi
List of Figures .....	x
List of Tables .....	xiv
Nomenclature .....	xv
Glossary of Terms.....	xvi
References.....	113

## **Chapter 1: Introduction**

1.1	Background.....	1
1.2	Idea Generation .....	2
1.3	Expected Outcomes .....	2

## **Chapter 2: Literature Review and Knowledge Gap**

2.1	Heat Exchanger Technologies .....	4
2.1.1	Direct Contact Heat Exchangers.....	4
2.1.2	Storage-Type Exchanger .....	4
2.1.3	Indirect-Contact Heat Exchangers.....	5
2.2	Heat Exchanger Efficiency and Optimisation .....	7
2.3	Heat Exchanger Inefficiencies.....	7
2.3.1	Heat Exchanger Flow Maldistribution.....	7
2.3.2	Heat Exchanger Fouling .....	8
2.3.3	Heat Exchanger Nucleate Boiling .....	9
2.4	Heat Exchanger CFD modelling.....	9
2.4.1	Mathematical Modelling.....	9
2.4.2	Computation Fluid Dynamic (CFD) Modelling .....	11

2.4.3	Physical Experiments .....	12
2.5	Heat Exchanger Entry Conditions .....	12
2.6	Control Valve Types.....	13
2.7	Butterfly Valve Modelling.....	13
2.7.1	Mathematical Modelling.....	14
2.7.2	Computational Fluid Dynamic Modelling.....	15
2.8	Turbulence Modelling .....	15
2.9	Similar CFP and Physical experimental Studies .....	16
2.10	Knowledge Gap .....	17

### **Chapter 3: Study Methodology**

3.1	Experimental Methodology .....	18
3.2	Limitations.....	18
3.2.1	Student.....	18
3.2.2	Heat Exchanger Technology .....	18
3.2.3	ANSYS Student Edition .....	19
3.3	Scope .....	19
3.4	Methodology Used and Expected Outcomes.....	19
3.5	Study Planning/Timeline .....	19
3.6	Resource Planning .....	21
3.6.1	Physical Experimental Jig .....	21
3.6.2	Software.....	21
3.6.3	Computer Lab Access.....	21
3.6.4	Confidentiality of Proprietary Information.....	21
3.7	Project Risk .....	22

### **Chapter 4: Physical and Computational Modelling**

4.1	Phase 1: Verification Physical Modelling .....	23
4.1.1	Experiment Equipment.....	23
4.1.2	Design of Experiment.....	24
4.1.3	Experimental HSE Risk.....	25
4.1.4	Experiment Details .....	25

4.1.5	Results .....	26
4.2	Phase 2: Verification ANSYS Modelling.....	28
4.2.1	Assumptions Made .....	28
4.2.2	Model Creation.....	30
4.2.3	Results .....	39
4.2.4	Mesh Independence Study.....	42
4.3	Phase 3: Verify and Optimize the Model .....	45
4.3.1	Expected Errors .....	45
4.3.2	Results .....	45
4.3.3	Model Optimisation.....	46
4.3.4	Results after Optimisation .....	47
4.4	Phase 4: Global Temperature Distribution with Control Valve .....	49
4.4.1	Physical Model with Control Valve .....	49
4.4.2	CFD Model with Control Valve .....	51
4.5	Phase 5: Analyse Cold Water Entry Region.....	60
4.5.1	Design of Experiment.....	60
4.5.2	Verification Model Creation.....	60

## **Chapter 5: Scale and Optimisation**

5.1	Introduction .....	82
5.2	Design of Experiment.....	82
5.3	Data for Model .....	82
5.4	Calculations .....	83
5.5	Global Distribution model.....	91
5.5.1	Model Creation.....	91
5.5.2	Analysis .....	96
5.5.3	Findings .....	97
5.6	Local Distribution Model .....	98
5.6.1	Model Creation.....	98
5.6.2	Analysis .....	104
5.6.3	Findings .....	107

5.7 Valve Angle Influence..... 108

**Chapter 6: Conclusion**

6.1 Findings and Discussions ..... 110  
Global Temperature Distribution..... 110  
Local Transfer Wall Maximum Temperatures ..... 111  
Valve Angle Influence..... 111  
6.2 Recommendations ..... 111  
6.3 Further Work ..... 112

**Appendix**

Appendix A – Project Specification..... 116  
Appendix B – Project Planning Timeline..... 117  
Appendix C – Risk Assessment for Physical Experiments ..... 118  
Appendix D – Mesh Independence Study for Heat Exchanger..... 121  
Appendix E – Mesh Independence Study for Cold-water Entry Region ..... 122  
Appendix F – Local Temperature Distribution Data for Section 4.5.6 ..... 123  
Appendix G – Local Temperature Distribution Data for Section 5.6.2 ..... 124  
Appendix H – Mesh Independence Study for Scaled Entry Region ..... 125  
Appendix I – Temperature Distribution Data for Section 6.1 ..... 126

# List of Figures

Figure 1-1: Engine dynamometer cooling system (Icons made by Freepik from <a href="http://www.flaticon.com">www.flaticon.com</a> ). .....	2
Figure 2-1: A typical single pass tube and shell heat exchanger arrangement (Shah & Sekulic 2003). .....	5
Figure 2-2: A typical double pipe heat exchanger arrangement (Shah & Sekulic 2003). .....	6
Figure 2-3: A typical gasketed plate-type heat exchanger arrangement (Shah & Sekulic 2003). .....	6
Figure 2-4: Cocurrent flow (a) and Countercurrent flow (b) (Taler 2019). .....	10
Figure 2-5: Butterfly valve simplified model and example from industry (Janusz 2006). .....	13
Figure 2-6: Butterfly valve advertised Cv values. ....	14
Figure 2-7: Flow transition from laminar to turbulent flow (Rao 2017). .....	15
Figure 3-1: Project risk matrix.....	22
Figure 4-1: Armfield HT36 extended heat exchanger experiment in USQ laboratory.....	23
Figure 4-2: Hot and cold-water measurements with hot water 3lpm and cold water 1lpm flow rate. ....	26
Figure 4-3: Hot and cold-water measurements with hot water 3lpm and cold water 2lpm flow rate. ....	27
Figure 4-4: Armfield HT36 extended heat exchanger (Armfield 2015). .....	28
Figure 4-5: Photo and nomenclature of Armfield HT36 heat exchanger end transfer arrangement. ....	29
Figure 4-6: Counter-current flow diagram (Armfield 2015). .....	30
Figure 4-7: The Armfield HT36 fluid path 3D model. ....	30
Figure 4-8: Segments for heat loss through convection. ....	31
Figure 4-9: Resulting mesh for initial verification. ....	32
Figure 4-10: Resulting mesh for initial verification – sectioned through the centre of cold-water corner.....	32
Figure 4-11: Model naming – Thermocouple location and hot water domain. ....	33
Figure 4-12: Model naming – Cold water domain and insulated wall. ....	34
Figure 4-13: Model naming – Convection wall and Transfer wall.....	34
Figure 4-14: Residuals of test case 1. ....	39
Figure 4-15: Residuals of test case 2. ....	39
Figure 4-16: Mass flow rate at inlet and outlet for Test Case 1.....	40
Figure 4-17: Mass flow rate at inlet and outlet for Test Case 2.....	41
Figure 4-18: Temperature contour through the X-Z plane for Test Case 1.....	41
Figure 4-19: Temperature contour through the X-Z plane for Test Case 2.....	41
Figure 4-20: Mesh Independence Study results showing stability after approximately 275,000 elements.....	43
Figure 4-21: Chart showing physical vs CFD results – experiment 1 (1 lpm). .....	46
Figure 4-22: Chart showing physical vs CFD results – experiment 2 (2 lpm). .....	46
Figure 4-23: Chart showing physical vs CFD results – experiment 1 (1 lpm). .....	48
Figure 4-24: Chart showing physical vs CFD results – experiment 2 (2 lpm). .....	48
Figure 4-25: The manual control valve at the heat exchanger entry point. ....	50
Figure 4-26: Online protractor tool to measure the valve angle. ( <a href="https://www.ginifab.com/feeds/angle_measurement/">https://www.ginifab.com/feeds/angle_measurement/</a> 2021). .....	51
Figure 4-27: Control valve created in CFD model. ....	52

Figure 4-28: Cross section of the mesh around the valve feature showing inadequate mesh. ....	52
Figure 4-29: Cross section of the mesh around the valve feature showing refined mesh. ....	53
Figure 4-30: Velocity contour around throttling valve to verify modelling. ....	56
Figure 4-31: Plot of the results of the physical and CFD experiment at 1lpm without the valve.....	57
Figure 4-32: Plot of the results of the physical and CFD experiment at 1lpm with the valve.....	57
Figure 4-33: Plot of the physical experimental results with and without the valve.....	58
Figure 4-34: Plot of the CFD experimental results with and without the valve. ....	59
Figure 4-35: ANSYS model of entry region of the heat exchanger. ....	61
Figure 4-36: External mesh in ANSYS model of entry region of the heat exchanger. ....	62
Figure 4-37: Sectioned mesh of ANSYS model showing detail around valve.....	62
Figure 4-38: Named sections: hot and cold inlets and outlets. ....	63
Figure 4-39: Named sections: transfer wall, valve and hot water domain. ....	63
Figure 4-40: Named sections: cold water domain and insulated wall. ....	64
Figure 4-41: Residuals of entry region validation case .....	66
Figure 4-42: Temperature contour showing correct transfer of heat. ....	67
Figure 4-43: Velocity contour showing expected velocity profile around valve. ....	67
Figure 4-44: Image showing correct balance of mass flow. ....	67
Figure 4-45: 2D streamline on X-Z plane using k- $\epsilon$ turbulence model. ....	69
Figure 4-46: 2D streamline on X-Z plane using k- $\omega$ turbulence model. ....	69
Figure 4-47: 2D streamline on X-Z plane using SST turbulence model. ....	69
Figure 4-48: 3D streamline using k- $\epsilon$ turbulence model. ....	70
Figure 4-49: 3D streamline using k- $\omega$ turbulence model. ....	70
Figure 4-50: 3D streamline using SST turbulence model. ....	70
Figure 4-51: 2D velocity contour on X-Z plane using k- $\epsilon$ turbulence model.....	71
Figure 4-52: 2D velocity contour on X-Z plane using k- $\omega$ turbulence model.....	71
Figure 4-53: 2D velocity contour on X-Z plane using SST turbulence model.....	71
Figure 4-54: 2D temperature contour on X-Z plane using k- $\epsilon$ turbulence model. ....	72
Figure 4-55: 2D temperature contour on X-Z plane using k- $\omega$ turbulence model.....	72
Figure 4-56: 2D temperature contour on X-Z plane using SST turbulence model.....	72
Figure 4-57: Mesh independence study results showing stability after approximately 375,000 elements.....	74
Figure 4-58: Residuals for the entry region model without valve. ....	75
Figure 4-59: 2D velocity streamlines for the entry region model without valve.....	76
Figure 4-60: 3D velocity streamlines for the entry region model without valve.....	76
Figure 4-61: 2D velocity contour for the entry region model without valve.....	76
Figure 4-62: 2D temperature contour for the entry region model without valve. ....	77
Figure 4-63: Example of sample cut to measure min, max and average temperature close to transfer wall...	77
Figure 4-64: Minimum temperature at the transfer wall region at various valve positions.....	78
Figure 4-65: Maximum temperature at the transfer wall region at various valve positions. ....	79

Figure 4-66: Average temperature at the transfer wall region at various valve positions. ....	79
Figure 4-67: Maximum temperature at the transfer wall region at various valve positions refined to 0-16mm. .....	80
Figure 4-68: Maximum temperature at the transfer wall region at various valve positions refined to 15-31mm. .....	80
Figure 5-1: System diagram of scaled model for maximum cooling capacity.....	84
Figure 5-2: System diagram of scaled model at operating conditions.....	87
Figure 5-3: Initial values in Excel. ....	89
Figure 5-4: Solved values in Excel.....	89
Figure 5-5: Valve flow rate percent vs valve opening percentage (Johnson Controls 1996). ....	90
Figure 5-6: 3D Model for the scaled model.....	91
Figure 5-7: Valve in the entry region of scaled model. ....	92
Figure 5-8: Exterior view of the mesh elements for the global model. ....	92
Figure 5-9: Sectioned view of the mesh elements for the global model.....	93
Figure 5-10: Residuals for the scaled global model without valve.....	95
Figure 5-11: Mass Flow Rates of the scaled global CFD model without the valve. ....	96
Figure 5-12: Temperature distribution of the scaled global CFD model without the valve. ....	96
Figure 5-13: Global temperature distribution at various valve angles.....	97
Figure 5-14: 3D model for the entry region scaled model.....	98
Figure 5-15: Valve in the entry region of scaled model. ....	98
Figure 5-16: Initial mesh for the entry region scaled model. ....	99
Figure 5-17: Residuals for the scaled entry region model without valve. ....	101
Figure 5-18: Mass flow rates of the scaled entry region CFD model without the valve. ....	101
Figure 5-19: Mesh Independence Study results showing stability after approximately 375,000 elements...	103
Figure 5-20: Example of sample cut to measure min, max and average temperature close to transfer wall.	104
Figure 5-21: Minimum temperature at the transfer wall region at various valve positions.....	105
Figure 5-22: Maximum temperature at the transfer wall region at various valve positions. ....	106
Figure 5-23: Average temperature at the transfer wall region at various valve positions. ....	106
Figure 5-24: Maximum temperature at the transfer wall region at various valve positions refined for 0-250mm. .....	107
Figure 5-25: Maximum temperature at the transfer wall region at various valve positions refined for 250- 500mm.....	107
Figure 5-26: Maximum temperature at transfer wall by units of valve diameter. ....	108
Figure 5-27: Maximum temperature at transfer wall for various valve open angles (smoothed).....	109
Figure 5-28: Average and maximum temperature differential with various valve open angles.....	109
Figure B-1: Screenshot of project plan showing project approval and project specification plans.....	117
Figure B-2: Screenshot of project plan showing research plans.....	117

Figure B-3: Screenshot of project plan showing dissertation and presentation plans. ....	117
Figure C-1: Risk assessment header information. ....	118
Figure C-2: : Risk register and analysis.....	119
Figure C-3: Action plan and approval. ....	120
Figure D-1: Mesh independence study results – for section 4.2.4.....	121
Figure E-1: Mesh independence study results – for section 4.5.4. ....	122
Figure F-1: Data set from section 4.5.6 reporting temperatures at various distances by valve angle. ....	123
Figure G-1: Data set from section 5.6.2 reporting temperatures at various distances by valve angle.....	124
Figure H-1: Mesh independence study results – for section 5.6.1.....	125
Figure I-1: Mesh independence study results – for section 5.6.1. ....	126

# List of Tables

Table 3-1: Major project milestones.....	20
Table 4-1: Physical experiment test conditions.....	25
Table 4-2: Table of results from experiment 1.....	26
Table 4-3: Table of results from experiment 2.....	26
Table 4-4: ANSYS verification model material properties.....	35
Table 4-5: ANSYS verification model boundary conditions.....	35
Table 4-6: ANSYS verification model Fluent parameter setup.....	38
Table 4-7: Temperature distribution reported at fixed locations throughout the heat exchanger.....	40
Table 4-8: Ideal boundary conditions for mesh independence study.....	42
Table 4-9: Results comparing physical model vs CFD results.....	45
Table 4-10: Tabular results comparing physical model vs CFD results after optimisation.....	47
Table 4-11: Physical experiment boundary conditions with valve.....	49
Table 4-12: Results from physical experiment with the valve.....	50
Table 4-13: ANSYS initial valve model material properties.....	53
Table 4-14: ANSYS initial valve model boundary conditions.....	54
Table 4-15: ANSYS initial valve model fluent parameter setup.....	54
Table 4-16: Temperature distribution reported at fixed locations throughout the heat exchanger.....	55
Table 4-17: Results of the physical and CFD experiment at 1lpm with and without the valve.....	56
Table 4-18: Data comparing the differences between experiments with and without the valve.....	58
Table 4-19: Entry region model material properties.....	64
Table 4-20: Entry region model material properties.....	64
Table 4-21: Entry region model boundary conditions.....	65
Table 4-22: ANSYS entry region model Fluent parameter setup.....	65
Table 4-23: Temperature validation of entry region CFD model.....	66
Table 4-24: Summary of approximate scaled residuals for the different turbulence models.....	73
Table 5-1: Material properties of heat exchanger fluids.....	83
Table 5-2: Scaled model material properties.....	93
Table 5-3: Scaled model boundary conditions.....	94
Table 5-4: Scaled model parameter setup.....	94
Table 5-5: Comparison of mathematical vs CFD model outlet temperatures.....	95
Table 5-6: Results of global temperature distribution at various valve angles.....	97
Table 5-7: Scaled entry region model boundary conditions.....	99
Table 5-8: Scaled model parameter setup.....	100
Table 5-9: Comparison of mathematical vs CFD model outlet temperatures.....	101

# Nomenclature

A	Area ( $m^2$ )
$c_p$	specific heat ( $\frac{J}{kg K}$ )
CFD	Computational Fluid Dynamics
CLCS	Closed Loop Cooling System
D	Diameter (m)
e	Energy per unit mass (J)
$h$	Heat Transfer Coefficient ( $\frac{W}{m^2 K}$ )
HHP	High Horsepower
HVAC	Heating, Ventilation and Air Conditioning
$K_{eff}$ or $\lambda$	Thermal Conductivity ( $\frac{W}{m K}$ )
Lpm	Litres per minute
$\dot{m}$	Mass flow rate ( $\frac{kg}{s}$ )
$\rho$	Density ( $\frac{kg}{m^3}$ )
p	Fluid pressure (Pa)
$\dot{Q}$	Heat Energy Transfer (W)
Re	Reynolds Number
T	Temperature (K)
$\Delta T_m$	Mean Temperature Difference (K)
U	Overall heat transfer coefficient ( $\frac{W}{m^2 K}$ )
USQ	University of Southern Queensland
$\mu$	Viscosity ( $\frac{kg}{m s}$ )
$\dot{V}$ or $Q$	Flow rate ( $\frac{m^3}{s}$ )

# Glossary of Terms

Adiabatic:	A process in which no heat is transferred in or out of a system.
Annulus:	The area between two concentric circles.
Baffle:	A device to restrain the flow of fluid.
Boolean:	A process in ANSYS software to add or subtract two bodies.
Chamfer:	A cut out on an edge of corner.
Computational Fluid Dynamics:	Use of computer programs to perform analysis and solve problems involving fluid flows.
Computations:	Mathematical calculations.
Concentric:	Having a common centre.
Dynamometer:	A device for measuring the speed and torque of an engine.
Eddies:	Swirling of fluid in turbulent fluid flow.
Electric field:	A physical field around electrically charged particles which can influence other particles.
Extrude:	A process in ANSYS for extending a 2D sketch in a linear direction to form a 3D shape.
Geometries:	Dimensional properties of an object including size, shape, and position.
Iterations:	Repeating of a process using the previous results as the start of the process.
Logarithmic:	The inverse function of an exponential which can be used to display numerical values of a wide range in a compact way.
Maldistribution:	Uneven distribution of something.
Methodologies:	A system of methods used to solve a problem.
Nucleate boiling:	A stage of the boiling process which produces bubbles.
Negligible:	So small or unimportant it can be ignored.
Oscillation:	Repetitive variation around a central value.
Out-of-chassis engine:	An engine which has been removed from, or not yet fitted to, its normal operating location.
PID controller:	A control system which uses current, past, and expected future performance to control the system.

Solubility: Degree of which a substance will dissolve into a solvent.

Tetrahedron: A triangular pyramid 3-dimensional shape.

Thermocouples: An electrical device made of two dissimilar metals used to measure temperature.

Volume: The amount of space and object occupies.

# 1.0 Chapter 1: Introduction

## 1.1 Background

There are many industrial applications generating heat that could not be used for their intended purpose without appropriate cooling. There are also many everyday devices that generate little heat, such as a modern lightbulb not requiring specialised cooling. In contrast some heavier equipment and plant generate significant amounts of heat, so much so, they fail or become ineffective without a cooling solution. They include cooling engines in vehicles used to transport people and goods, electrical motors used to drive conveyors and computers using specialized heat sink plates. Some of the common cooling components used throughout current industry are:

- Air/liquid radiators for moving stock
- Air/solid heat sinks, often in combination with a fan
- Cooling Towers
- Heating, ventilation, and air conditioning (HVAC) environments
- Liquid/liquid or liquid/gas heat exchangers.

This study focuses on indirect type liquid/liquid heat exchangers. These are commonly used to cool industrial systems by cooling the equipment's oil or coolant using process water as a cooling liquid. A heat exchanger is used to transfer heat from a hot liquid or gas to a cool liquid or gas without mixing the fluids. To achieve this, the two fluids are run through a series of fluid paths separated by a highly conductive thin wall. The heat energy transfers very effectively through the thin wall conductive material exchanging from the hot fluid to the cold fluid.

An example of an industrial scenario, and the focus of this study, is the cooling of a stationary engine during dynamometer performance testing. An out-of-chassis engine connected to a dynamometer does not have the vehicle's radiator and fan system so the engine needs to be cooled by different means. To best represent the vehicle's radiation and fan system, and provide corrosion protection to the engine, a closed loop cooling system (CLCS) is often used. A CLCS runs a circuit of coolant/water mixture through the engine which transfers the heat generated to process water through a heat exchanger. The process water is subsequently cooled by cooling towers. If the process water side is simplified and considered a constant low temperature source, the cooling system can be represented with a simple system diagram as shown in Figure 1-1 below.

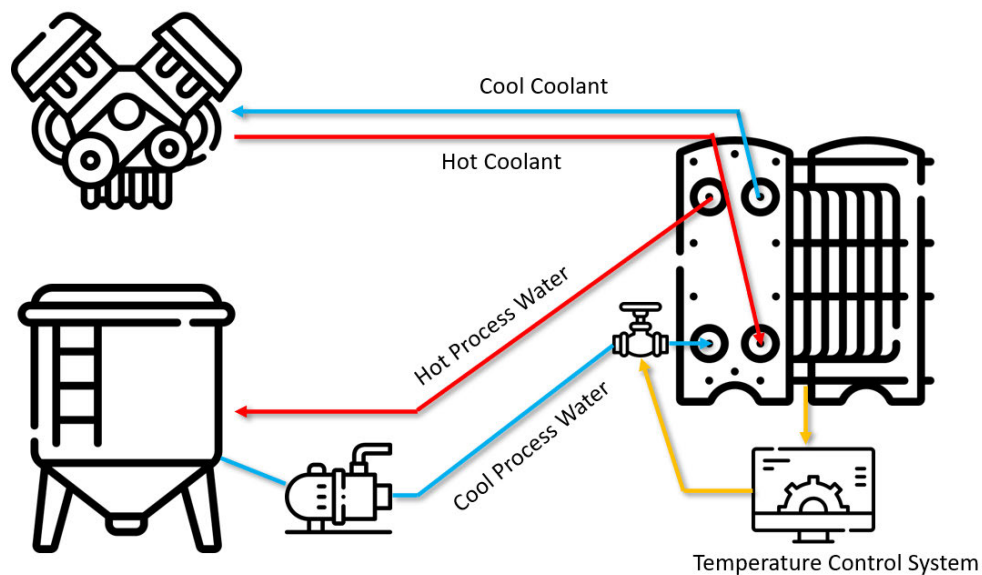


*Figure 1-1: Engine dynamometer cooling system (Icons made by Freepik from [www.flaticon.com](http://www.flaticon.com)).*

For the engine to operate within its normal operating temperature range, the cooling process water flow rate needs to be controlled to prevent over cooling. Traditionally this has been achieved by using a simple temperature control system closing and opening a valve on the heat exchanger process water inlet connection.

## 1.2 Idea Generation

The author of this study works for a business which carries out dynamometer testing of large engines to validate their performance against published performance ratings as a critical part of the overall testing regime. Recently the business has been looking at replacing an aging, inefficient system with a modern system. A specialist equipment supplier has provided sales material claiming their product is superior to their competitors. They advise their product uses a control system which utilises a variable speed pump instead of the traditional approach of using a fixed output pump with the flow throttled using a control valve. The anecdotal advantages advised by the sales team were as follows:

- Improved efficiency as the variable speed pump uses less power
- Longer pump life by reducing cavitation from throttling
- Longer life and efficiency out of the heat exchanger core due to less ‘hot-spots’ resulting in fouling.

The first two advantages are intuitively correct. However, the third effect is not something that has been revealed by the authors career experience or undergraduate studies. This intriguing claim is the subject of the authors final year dissertation.

## 1.3 Expected Outcomes

It is hypothesized that the use of a control valve at the heat exchanger process water entry could create turbulence and other entry conditions impacting on both the global temperature distribution and localised heat distribution in the entry region transfer wall.

The aim of this dissertation is to simulate the entry effects of a control valve in the entry region of heat exchanger using computation fluid dynamics (CFD) software to validate if the entry affects will produce a temperature distribution different to a variable speed pump. This will be tested at both a global and local sense within the heat exchanger in experiments that can be verified with physical experiments and scaled experiments to replicate real industrial conditions.

## 2.0 Chapter 2: Literature Review and Knowledge Gap

An extensive literature review was undertaken to understand existing knowledge surrounding heat exchanger modelling and verify that a knowledge gap exists. This dissertation will provide a valuable content to fill some of that gap. The concepts reviewed are:

- Heat exchanger technologies
- Heat exchange efficiency improvements
- Inefficiencies within heat exchangers, especially around fouling and flow distribution
- Existing studies on the entry region of heat exchangers
- Previous CFD modelling of heat exchangers
- Control valve types
- Butterfly valve modelling
- Any existing similar studies available.

### 2.1 Heat Exchanger Technologies

Three common types of heat exchangers are used in industry today:

- Direct-contact heat exchangers
- Storage-type heat exchangers
- Indirect-contact heat exchangers.

#### 2.1.1 Direct Contact Heat Exchangers

Direct-contact heat exchangers transfer heat by direct mixing of two fluids. Direct-contact heat exchangers produce much higher transfer rates, are less expensive and reduce fouling rates (Shah & Sekulic 2003). Examples of these methods in industry are direct water mixing chambers and water/air cooling towers.

Where flow rates of fluids cannot be changed (fixed pumps or controlled by up/down stream process) a common method of controlling the desired temperature is by means of 'bypassing' (Luyben 2011). Bypassing involves taking a portion of the fluid stream and routing around the heat exchanger. The control speed can be accelerated by mixing both control and process bypass streams rather than routing through the heat exchanger (Luyben 2011). This method is known as steam-blending and is only practical if both the control and process fluid are the same fluid.

The methods of direct mixing or bypass mixing would not be applicable in the application of this study as two different fluids are used and mixing is undesirable.

#### 2.1.2 Storage-Type Exchanger

In a storage-type heat exchanger, the fluids flow through the same passage at alternate times. Heat is transferred from the hot fluid and stored in the heat exchanger material walls. The cold fluid then flows through the exchanger and the heat transfer from the material walls to the cold fluid (Shah & Sekulic 2003). In this type of exchanger, there will always be some fluid transfer due to flowing through the same passages.

### 2.1.3 Indirect-Contact Heat Exchangers

Indirect-contact heat exchangers are devices designed to allow heat transfer between two fluids without allowing the fluids to mix (Cengel, Ghajar 2015). Two fluids flow through the heat exchanger in two different passages and heat is continually transferred from the hot to cold fluid through a thin conductive metal wall (Shah & Sekulic 2003). These heat exchangers come in several arrangements depending on applications. The common construction types are:

- Tubular – shell and tube
- Extended surface
- Regenerative
- Plate.

**Tubular:** Tubes, usually circular, of high conductive metal are bent in various shapes and configurations to meet the performance, fluid properties and sizing constraints. Tubular exchangers are very common in industry for liquid-to-liquid applications. Tubular construction exchangers can be further broken down into:

*Shell and Tube:* A bundle of round tubes in a cylindrical shell parallel to the tubes. One fluid flows through the tubes and one through the shell. This is the most common liquid/liquid type exchanger found in industry (Cengel, Ghajar 2015). Baffles are often used to ensure the shell fluid flows where desired and support the tubes.

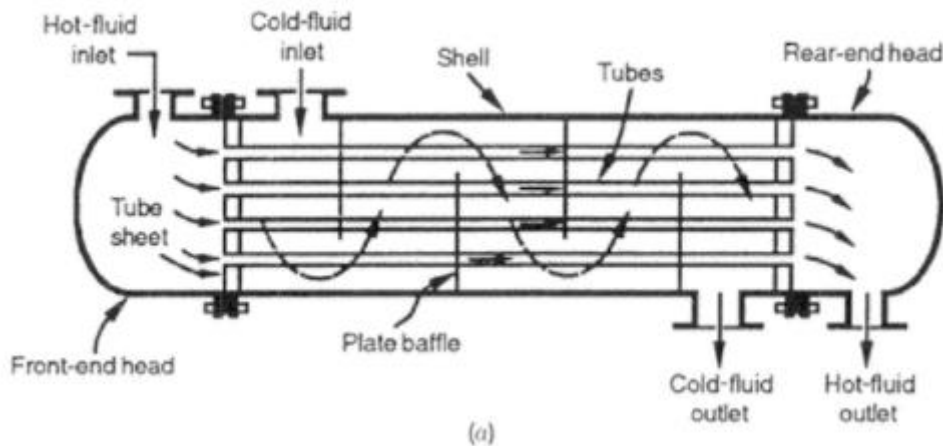


*Figure 2-1: A typical single pass tube and shell heat exchanger arrangement (Shah & Sekulic 2003).*

*Double-Pipe:* This is the simplest design of heat exchanger with two concentric round tubes separated by thin wall of conductive metal material. One fluid flows through the inner tube and one fluid through the outer tube.

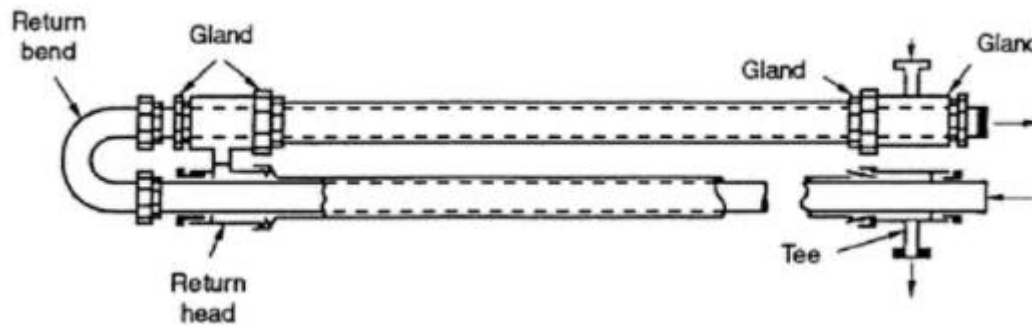


Figure 2-2: A typical double pipe heat exchanger arrangement (Shah & Sekulic 2003).

*Plate-type:* These heat exchanger systems are built of a series of plates with hot and cold circuits through them. The thin plates can then be joined together (with gaskets, weld or braising) in an enclosure/frame. The two fluids then flow through main galleries and in/out of each plate. There are many different plate designs in the industry with different performance characteristics for different fluids and applications. These plate-type exchangers are considered much more efficient as the transfer wall has much more surface area for the fluid to be exposed to (Aghayari et al 2015).

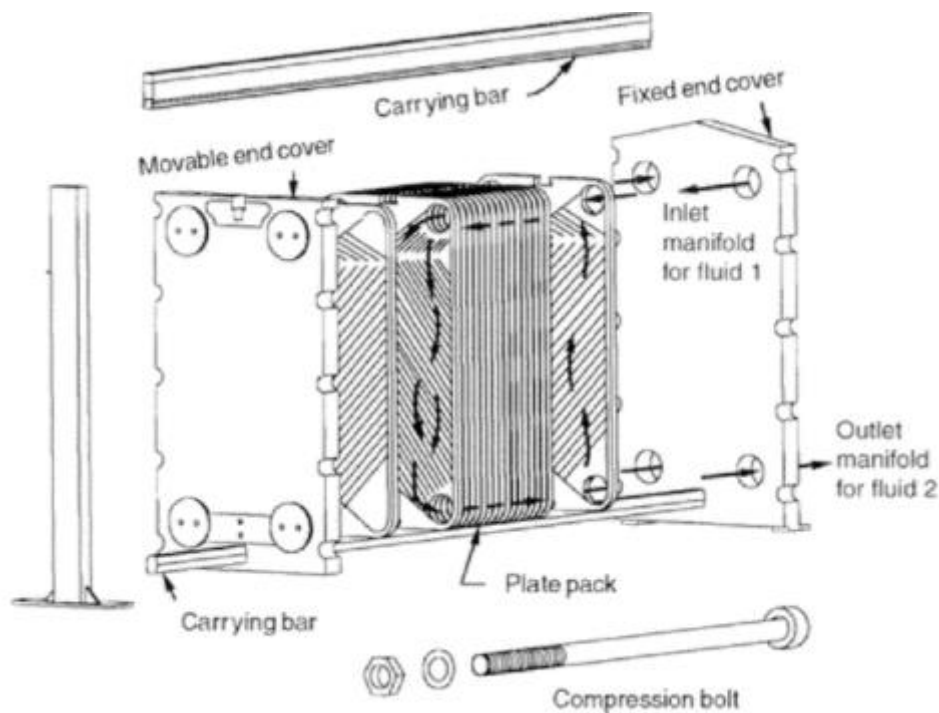


Figure 2-3: A typical gasketed plate-type heat exchanger arrangement (Shah & Sekulic 2003).

In all construction types, there are three common flow configurations (Ahmed, Mesalhy & Abdelatif 2015):

- Parallel flow – both fluids flow in the same directions through the heat exchanger
- Counter flow – the two fluids flow in opposite directions through the heat exchanger
- Cross-flow – fluids cross perpendicularly through the exchanger.

In a parallel flow arrangement, the hot and cold entry points are at the same end of the heat exchanger. The counter-flow arrangement is the opposite with the entry points of the fluids on opposite ends of the exchanger

core. The parallel arrangement is rarely used in industry as the counter-flow arrangement reduces thermal stresses, can transfer more heat, and produce a more uniform transfer rate through the exchanger (Engineers Edge 2021). Cross flow exchangers are used mostly in fluid to air coolers where gases (usually air) flow over the fluid domain. A common example of this is a car radiator.

## **2.2 Heat Exchanger Efficiency and Optimisation**

With any technology, manufactures are always trying to make efficiency improvements to increased performance whilst minimizing the volumetric footprint and weight of the hardware. There are two methods of doing this (Sharifi et al 2018):

- Passive methods: improving the material or geometry of the exchangers to improve performance; for example, adding fins or coiled wire inserts.
- Active methods: adding energy to improve performance; for example, adding vibrational flow.

Some examples of these improvement are also mentioned in a study by Ahmed, Mesalhy & Abdelatief (2015), and include:

- Passive methods of improving fin surface area designs and adding vortex generating geometry to the fins such as slits, louvers, and serrations
- Active methods of adding electric or acoustic fields, moving mechanical devices and/or adding vibration to the surfaces.

The literature review found studies on improving heat exchanger design through these methods, however they add little value to the interest of this study so are not being pursued further.

## **2.3 Heat Exchanger Inefficiencies**

### **2.3.1 Heat Exchanger Flow Maldistribution**

Flow maldistribution occurs where the fluids are not uniformly distributed at the heat exchanger inlets and/or throughout the heat exchanger core (Shah & Sekulic 2003). The term maldistribution is not to be misunderstood with one of the key concepts being investigated in this study – temperature maldistribution. Flow maldistribution of fluids most commonly occurs in multi-channel heat exchangers like plate or fin crossflow exchangers. Flow maldistribution can be induced by:

- Geometry
- Operating conditions
- Poor design.

A recent study by Denkenberger et al. (2021), compared mathematical models of heat exchangers to CFD models to investigate the flow maldistribution effects on the performance of the exchangers. This study produced many datasets and plots that can help determine the effects of maldistribution at different flow rates and geometries including the different effectiveness of each channel. This study was however researching the

effects in multi-channel exchangers which is likely relevant to the application plate-style exchanges, but not so much the dual-wall type in this dissertation.

Similarly, another recent study by Zang et al (2021), performs some mathematical modeling of cross flow heat exchangers to analyse the effects of maldistribution to the performance of the heat exchanger. This study concluded that for several key regions of the heat exchanger the maldistribution of the fluids can have significant influence of the performance of the system.

The findings of this literature are not directly valuable to the case in this dissertation, but they do show that flow behaviour does affect the performance of the heat exchanger. This could possibly result in temperature maldistribution throughout the heat exchanger core.

### **2.3.2 Heat Exchanger Fouling**

Fouling of heat exchangers is the accumulation of undesirable material in the heat exchanger core resulting in poor performance of the heat exchanger (Shah & Sekulic 2003). This fouling is usually a deterioration of the heat transfer surface performance over time (Cengel & Ghajar 2015). The effects of fouling can be:

- Reduction in heat transfer
- Increased pressure drop
- Increase corrosion of the core

As a result of these affects, or in preventative attempts to mitigate these affects, fouling of heat exchangers can be expensive. Some examples of the costs of fouling include:

- Increases in component cost to ensure the heat exchanger serviceability
- Increases in maintenance costs – cleaning, additives, etc.
- Loss of production from unexpected failures
- Energy loss from inefficiencies.

In mathematical modelling, the fouling effects are considered in calculations by adding the fouling factor ( $R_f$ ) to the overall transfer coefficient (Cengel & Ghajar 2015). When designing an appropriate heat exchanger for an application that is likely to operate in conditions that could cause these fouling factors to occur, a larger heat exchanger would be required to account for the performance loss with time.

#### ***Fouling Mechanisms***

There are three primary fouling mechanisms relevant to liquid\liquid heat exchangers (Shah & Sekulic 2003):

- Precipitation or crystallisation
- Corrosion
- Biological.

**Precipitation or crystallisation:** This phenomenon is the precipitation of dissolved salts on to the heat transfer surface when the surface concentration exceeds the solubility limit. This can occur both in the process and

controlled fluids and can occur both when fluids are being heated or cooled. This is the same kind of fouling noticed on everyday appliances like the inside of a kettle.

**Corrosion:** In some application chemical fouling can occur from corrosion of the transfer wall or outside wall surfaces. This corrosion can affect the transfer and flow performances.

**Biological:** Certain conditions can also cause algae growth and are considered a form of biological fouling.

It is noted in Cengel & Ghajar (2015), that fouling increases with increases in temperature and decreasing velocity.

### 2.3.3 Heat Exchanger Nucleate Boiling

Nucleate boiling is a very complex chaotic phenomenon that occurs when there is a temperature difference between the transfer wall and fluid of between 5 and 30 degrees (Cengel & Ghajar 2015). Nucleate boiling is where bubbles and possible vapour voids occur near the surface and in the fluid. These bubbles can affect the heat transfer rate of the heat exchanger.

An example investigating how nucleate boiling can affect heat exchanger transfer rate can be seen in a study by Chun & Kang (1996). In this study, vertical and horizontal tube arrangements of varying diameters were tested to investigate the nucleate affect. One of the key outcomes of their study was an improved heat transfer rate from the bubbles and turbulence caused by the nucleate boiling. Contrary to this it was found the large vapour voids caused by nucleate boiling cause a reduction in heat transfer.

Due to the complex nature of this phenonomen, and the difficulty in modeling it, it is being omitted from the study. It is worth noting that this phenonmen could possibly be an area of extra study to see if the temperature in the localised temperature spikes could cause excessive nucleate boiling.

## 2.4 Heat Exchanger CFD modelling

### 2.4.1 Mathematical Modelling

There are three common methods of mathematically modelling heat exchangers (Lazarevic et al 2019):

- Basic energy balance formulation
- Log mean temperature difference (LMTD)
- Effectiveness number of transfer units ( $\epsilon - NTU$ ).

The log mean temperature method is the primarily used in European regions and the ( $\epsilon - NTU$  method is mainly used in the USA. Both methods are valid and can both be useful depending on the known values of the application. The LMTD is valuable if the inlet and outlet temperatures are known and can be difficult to use in finding missing temperature values, though not impossible. The NTU method is good if the cooling specifications of the heat exchanger are given and the inlet or outlet temperatures need to be calculated.

From these methods, and using other fluid dynamic and thermodynamic principles, problem specific computations can be performed. A very thorough book was found explaining many of these methods in depth

(Taler 2019). This book firstly explains the fundamental heat transfer theories including the mass, energy and momentum equations, and explanations of both laminar and turbulent fluid flow through ducts. In the next section the mathematical models are explained in detail. Regarding indirect heat exchangers, in the counter-flow arrangement, the following equations models are of interest. All these formulae were verified through Cengel & Ghajar (2015), and found to be verified with different variables in some cases. When referencing temperatures in the formula below, refer to diagrams in figure 2-4.

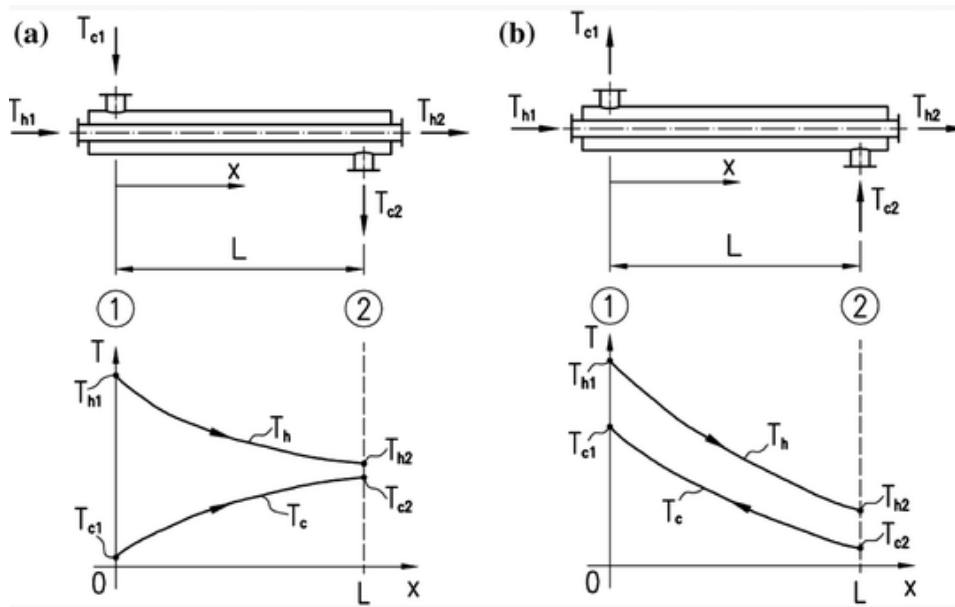


Figure 2-4: Cocurrent flow (a) and Countercurrent flow (b) (Taler 2019).

### Heat Transfer

Assuming that mass flow rates are constant, the outside is insulated and there are no external or internal heat sources there are two fundamental equations for the heat transfer:

$$\dot{Q}_h = \dot{m}_h c_h (T_{h1} - T_{h2})$$

$$\dot{Q}_c = \dot{m}_c c_c (T_{c1} - T_{c2})$$

This formula is showing that the heat transfer can be calculated from the mass flow rate, specific heat capacity and temperature difference from either the cold or hot fluid. Temperature lost from the hot fluid is gained by the cold fluid.

### LMTD Method

The formula for finding the logarithmic mean temperature between the two fluids is fully derived in the source and can be shown as:

$$\Delta T_m = \frac{\Delta T_2 - \Delta T_1}{\ln \left( \frac{\Delta T_2}{\Delta T_1} \right)}$$

From this log mean temperature value, the heat transfer can be calculated using:

$$\dot{Q} = \Delta T_m A k_A$$

where  $k_A$  is the overall heat transfer rate of the exchanger and A is the surface area of the transfer wall.

### NTU Method

To calculate the NTU's, which are heat transfer units:

$$NTU = \frac{(k_A A)}{\dot{C}_{min}}$$

where  $\dot{C}_{min}$  is the smaller of the two fluid's specific heat capacity rates. The specific capacity rates are the specific heat values multiplied by the mass flow rate.

$\varepsilon$  is the heat exchanger effectiveness and described as the ratio between the real thermal power and the maximum power from the exchanger:

$$\varepsilon = \frac{\dot{Q}_{rz}}{\dot{Q}_{max}} = \frac{\dot{Q}_{rz}}{\dot{C}_{min} (T_{h,wlot} - T_{c,wlot})}$$

For counter-current flow heat exchangers,  $T_{h,wlot} - T_{c,wlot} = T_{h1} - T_{c2}$  (Hot inlet – cold inlet)

Rearranging, the main equations used to find unknowns are:

$$\varepsilon = \frac{\dot{C}_h (T_{h1} - T_{h2})}{\dot{C}_{min} (T_{h1} - T_{h2})} = \frac{\dot{C}_c (T_{c1} - T_{c2})}{\dot{C}_{min} (T_{c1} - T_{c2})}$$

$$\varepsilon = \frac{1 - \exp \left[ -NTU \left( 1 - \frac{\dot{C}_{min}}{\dot{C}_{max}} \right) \right]}{1 - \frac{\dot{C}_{min}}{\dot{C}_{max}} \exp \left[ -NTU \left( 1 - \frac{\dot{C}_{min}}{\dot{C}_{max}} \right) \right]}$$

### Temperature at a point

The temperature in the cold or hot fluid can be calculated at any distance along the heat exchanger using two equations:

$$T_h = T_{h1} - \frac{(T_{h1} - T_{c2}) \{ 1 - \exp \left[ -k_A U_A \left( \frac{1}{\dot{m}_h c_h} - \frac{1}{\dot{m}_c c_c} \right) x \right] \}}{1 - \frac{\dot{m}_h c_h}{\dot{m}_c c_c} \exp \left[ -k_A U_A \left( \frac{1}{\dot{m}_h c_h} - \frac{1}{\dot{m}_c c_c} \right) \right]}$$

$$T_c = T_{h1} - \frac{(T_{h1} - T_{c2}) \{ 1 - \frac{\dot{m}_h c_h}{\dot{m}_c c_c} \exp \left[ -k_A U_A \left( \frac{1}{\dot{m}_h c_h} - \frac{1}{\dot{m}_c c_c} \right) x \right] \}}{1 - \frac{\dot{m}_h c_h}{\dot{m}_c c_c} \exp \left[ -k_A U_A \left( \frac{1}{\dot{m}_h c_h} - \frac{1}{\dot{m}_c c_c} \right) \right]}$$

Where x is the distance from the hot inlet,  $\alpha_c$  &  $\alpha_h$  are the heat transfer coefficients of the cold and hot fluids, and  $U_A$  is the transfer wall circumference.

## 2.4.2 Computation Fluid Dynamic (CFD) Modelling

A study by Sharifi et al (2018), used a computation fluid dynamic method to model the heat transfer improvements of a horizontal heat exchanger with helical wire inserts. These inserts produce a spiral flow

through the core improving efficiency. To confirm the accuracy of the model, Sharifi et al (2018) compared initial results with a previous study with numerical results. The software package “Fluent” was used for CFD computation. Sharifi et al used a highly refined mesh around the tube walls and wire areas with a course mesh through the rest of the domain. The resultant mesh densities tested were 400,000, 1,200,000, 2,000,000 and 3,200,000 elements.

A similar study by Rajeshkumar et al. (2021), created a CFD model in ANSYS to analyse the improvements of changing the geometry of a heat exchanger to have fins added. The model created in this article only included one fluid domain but shows the general setup of a heat exchanger fluid domain. The study showed how the results were interpreted to see the model was realistic. This model used over 3 million elements for the single domain.

To test if corrugated tubing is more efficive in a douple pipe heat exchanger than a simple wall, a study was peformed by Bashtani & Esfahani (2019). This study created CFD models in ANSYS of a section of heat exchanger with both simple wall and corrigated wall. The same boundary conditions were used on both experiements and the results compared to each other. The SST turbulence model was used and mesh independence study was completed to ensure the results were valid. The results were also validated using mathematical models. An element count of 4,000,000 elements was required for the corrugated model.

These studies show that CFD can be used to model heat exchangers though the studies references found good results with many more elements that the ANSYS student version have available.

### **2.4.3 Physical Experiments**

There have been recent studies into heat exchanger performance using physical experiments, though none can be found in relations to the use of a valve in the entry region of the exchanger.

An experiment by Aghayari et al (2015), used an experimental jig, like the Armfield HT36, in a study to test the effects of nanoparticles within a fluid on the overall heat transfer. For this study a dual-wall exchanger was fabricated, and the experimental results considered applicable to plate style (and other) heat exchangers.

Amanowicz (2018), is another example of a great heat exchanger experiment where an experimental jig was created with various sensor test points to perform physical experiments. This study was performed on multi-channel earth-air exchanger but showed very thorough physical and CFD testing.

A book by Fridman & Mahajan (2014), was studied as is discussed techniques to completed physcial experiements around heat exchangers in the virtual environment. It was noted in this book that they used the Armfield HT36 experiemental equipment which is the same equipment used in the USQ laboratory.

## **2.5 Heat Exchanger Entry Conditions**

The primary focus of this dissertation is at the entry condition of the heat exchanger and how a control valve may affect the flow in this region. There does not seem to be any studies directly investigating this for simple dual-wall type heat exchangers.

An example of a study that focuses on a similar scenario is by Iqbal and Syed (2011), where different finned-type heat exchanger in entry region geometry was investigated to find the best performing geometry. This study found that the different geometry and fin arrangements did produce different heat transfer rates in the entry region that fully developed flow areas. The study indicated the heat transfer rate could possibly be influenced by the valve causing a different effective geometry.

## 2.6 Control Valve Types

Heat exchanger control systems adjust the desired output temperature by using control valves on the process water side of the system. The common effective valve types used to regulate of the flow are (Kapustenko, et al 2009):

- Globe
- Angle
- Ball
- Plug
- Needle
- Butterfly.

The most effective of these is noted to be the globe or saddle valves, however due to their complexity and expense, butterfly valves were noted to be the most common control valve used in industry. With the Author's understanding of the industry, it is assumed butterfly valves will be used in our application.

A good resource explaining the differences in valve technologies and verifying that the butterfly design is ideal for control applications is the valve datasheet by Tomovalve (n.d.). This technical datasheet shows the different valve types and explains their strengths and weaknesses. The data sheet shows that each valve is sold with a known Cv value which specifies the relationship between the flow rate and pressure drop of a valve.

## 2.7 Butterfly Valve Modelling

Butterfly valves have been identified to be the most common valve type used in industry. Butterfly valves are a mechanical device used to restrict the flow of liquid through their cross-sectional area by rotation of a round disk. When rotated  $90^\circ$ , the valve is fully open, and the design offers very little restriction. When fully closed the disk seals on a sealing surface in the valve body allowing no flow of fluids (Song, Wang, Park 2009).

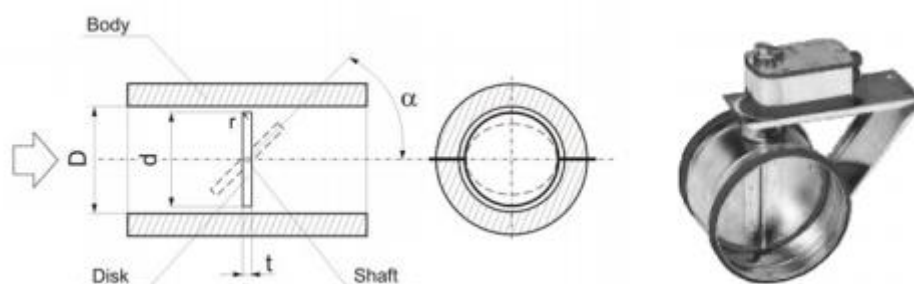


*Figure 2-5: Butterfly valve simplified model and example from industry (Janusz 2006).*

## 2.7.1 Mathematical Modelling

The Cv value of a valve is often provided with a valve in the form of a datasheet for example of the dataset provided by Sure Flow Equipment Inc in figure 2-7 below.

Cv Values - Valve Sizing Coefficients (US - GPM @ 1 PSI Δ P)									
Size	Flow in GPM @ 1 PSI Δ P @ Various Disc Angles								Full 90° Open
	10°	20°	30°	40°	50°	60°	70°	80°	
2	0.1	5	12	24	45	64	90	125	115
2 1/2	0.2	8	20	37	65	98	144	204	196
3	0.3	12	22	39	70	116	183	275	302
4	0.5	17	36	78	139	230	364	546	600
5	0.8	29	61	133	237	392	620	930	1,022
6	2	45	95	205	366	605	958	1,437	1,579
8	3	89	188	408	727	1,202	1,903	2,854	3,136
10	4	151	320	694	1,237	2,047	3,240	4,859	5,340
12	5	234	495	1,072	1,911	3,162	5,005	7,507	8,250
14	6	338	715	1,549	2,761	4,568	7,230	10,844	11,917
16	8	464	983	2,130	3,797	6,282	9,942	14,913	16,388
18	11	615	1,302	2,822	5,028	8,320	13,168	19,752	21,705
20	14	791	1,674	3,628	6,465	10,698	16,931	25,396	27,908
24	22	1,222	2,587	5,605	9,989	16,528	26,157	39,236	43,116

Figure 2-6: Butterfly valve advertised Cv values.

These Cv value gives the ratio of the flow rate to the pressure drop across the valve at various valve angles. They are used by system designers to choose the appropriate valve for a particular application. This Cv value is an imperial ratio which has the equivalent metric ratio which is the Kv value. The relevant equations are:

$$K_V = Q \frac{\sqrt{SG}}{\Delta P}$$

$$K_V = 0.865 C_V$$

where  $K_V$  is the flow factor ( $\frac{m^3}{h}$ ),  $Q$  is the flowrate ( $\frac{m^3}{h}$ ),  $SG$  is the fluid's specific gravity and  $\Delta P$  is the pressure difference in bar (Fisher 2001). These equations show that with a known valve, flow rate can be calculated if the pressure difference is known, or the pressure difference can be calculated if the flow rate is known. If the Cv value is not known, proper sizing of the valve can be calculated using (Song, Wang, Park 2009):

$$K_1 = \left( \frac{V_1^2}{2} + \frac{P_1 - P_2}{\rho} \right) * \frac{2}{v_2^2} - \left( 1 + \frac{f * L}{D} \right)$$

where  $K_1$  is the valve coefficient value provided by the manufacturer,  $P_1$  and  $P_2$  are the static pressures upstream and downstream of the valve,  $v_1$  and  $v_2$  are the upstream and downstream velocities,  $L$  is the distance between  $P_1$  and  $P_2$ ,  $D$  is the hydraulic diameter of the valve and  $f$  is circular friction factor.

## 2.7.2 Computational Fluid Dynamic Modelling

In an article explaining the methods of optimisation of a butterfly valve (Song, Wang, Park 2009) a combination of FEA and CFD were performed on a valve. In this article, CFD was completed on a butterfly valve within a pipe domain to optimise the design a valve for optimal strength to weight ratio. Some parameters of note here were the upstream length of 8x the valve diameter and downstream length of 10x the valve diameter in respect to the valve.

Janusz and Czeslaw (2016), performed a physical and CFD experiment on butterfly valves to determine the flow characteristics, pattern and pressure changes caused by a butterfly valve in with water flow for both laminar and turbulent flows. The study reveals recirculation is non-existent at shallow valve angles behind the valve disk. Some parameters of note here were the upstream length of 2.5x the valve diameter and downstream length of 15.5x the valve diameter in respect to the valve.

A study by Del Toro, Johnson, and Spall (2015), performed a comprehensive dataset to measure the pressure drop, hydrodynamic torque, flow coefficient, loss coefficient, and torque coefficient on a specific valve under different opening angle positions. This study found that the CFD results varied from actual in the low and high angle cases. Physical experiments were conducted for the mid-open ranges of 30-60 degrees. The study concluded velocity and turbulence could create temperature differences within a heat exchanger.

It can be seen from these studies that the butterfly valve causes turbulence to the fluid around the valve and can affect the flow for some distance past the valve. In all cases the effect of the valve is seen to only influence the flow for a short distance. This aligns with general flow thermal entry lengths with are assumed to be 10D (Cengel & Ghajar 2015).

## 2.8 Turbulence Modelling

When fluid is travelling through the inside of a tube and reaches a certain speed relative to the fluid density and geometry of the tube, the flow will lose stability and transition to turbulent flow (Rao 2017).

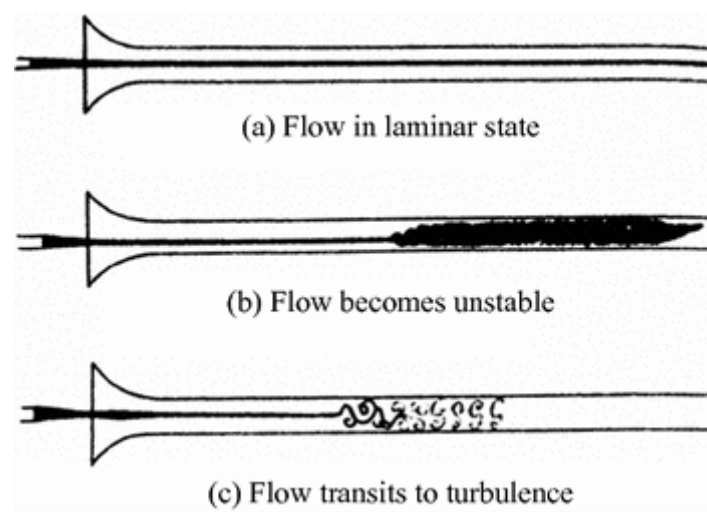


*Figure 2-7: Flow transition from laminar to turbulent flow (Rao 2017).*

Turbulence produces less predictable and unstable velocities through the fluid including eddies. There are several models used within CFD software suited to modelling turbulent flow with the main two being variants (Wasserman 2016), of:

- Standard k- $\epsilon$
- Standard k- $\omega$
- SST k- $\omega$ .

There are more complex models, for example direct numerical simulation (DNS) available requiring much more computational power, however these three and variants of them are the most used (Andersson 2012). These models all use a method of simplifying the Reynolds averaged Navier stokes equations by assuming statistical averaging for unknown values. Some of the models work better for different applications due to the assumptions made.

### ***k- $\epsilon$ Model***

The standard k- $\epsilon$  model is the most widely used model and is computationally efficient (Andersson 2012). This model is strong for flows within pipes, however, has some weaknesses around the wall area. It is also known to be weak when simulating swirling flows, streamline curvature and axisymmetric jets. To improve on the standard model, RNG and realizable variants have been developed and commonly used in place of the standard model. The RNG variant was made to better model swirling type flow and the realizable model has been developed to handle cases with large mean strain rates. Near wall modelling effects can also be added to the k- $\epsilon$  model to improve performance of the standard k- $\epsilon$  wall modelling.

### ***k- $\omega$ Model***

The k- $\omega$  differs from the k- $\epsilon$  model in that it can manage wall boundary layers with high pressure gradients. This is particularly useful in the high flow near a wall – for example flow over a wing. A very fine mesh is required around the wall for this model. Variants of the k- $\omega$  also exist, however do not add value to this project, other than the SST variant discussed below.

### ***SST Model***

The SST model uses both the k- $\epsilon$  and k- $\omega$  model. It uses the k- $\omega$  close to the wall regions and transitions to the k- $\epsilon$  in regions of less shear stress (ANSYS 2009).

In the modelling of heat exchangers with control valves the choice of turbulence model to use is not clear. A recent study was found by Sung-Woong et al. (2021), compared three models with control valves of various diameters. This study found no conclusion in their attempt to define a best model for simulating the turbulence around a control valve. The study suggests all models should be tried and analysed case by case.

## **2.9 Similar CFP and Physical experimental Studies**

In 2009 a study was completed by the National Technical University (Kharkiv Polytechnic Institute) to improve the flow quality of a butterfly valve (Kapustenko, et al 2009). In this study both computer and physical modelling were performed on a heat exchanger and butterfly valve system. The study found that they could

better control the temperature using the parametric predictive control technique with less oscillation and quicker response. These results are of little impact to this dissertation, but the methodology is of interest.

A study of a corrugated double pipe heat exchanger by Bashtani & Esfahani (2019), although not modelling butterfly valves, is a great example of where a CFD model was built and compared to a mathematical model, producing a very robust experiment.

In 2011, a study was completed by the Department of Chemical Engineering, Lehigh University (Luyben 2011), with physical experiments to test the design of heat exchanger system when bypassing is used. The results of this study found an increased area of the heat exchanger and more bypassing improves the ratio of maximum-to-design heat transfer rates. Bypassing is not an applicable option for our purpose as the two fluids used are different.

After extensive literature review no studies could be found investigating the influence of a butterfly control valve on the flow or heat distribution within a heat exchanger.

## **2.10 Knowledge Gap**

There is a wealth of knowledge available on heat exchanger technologies, control valve technology, heat exchanger efficiency, control valve efficiency and modelling of these individual systems. Unfortunately, there are no studies on how the use of a control valve at the heat exchanger process water entry point would affect the heat exchanger performance compared to a heat exchanger using a variable speed control pump with a control valve.

It is hypothesized that the use of a control valve at the heat exchanger process water entry point could create turbulence and other entry conditions that could affect the heat distribution in the heat exchanger.

## 3.0 Chapter 3: Study Methodology

### 3.1 Experimental Methodology

The following step-wise phases were completed in succession and form the structure of this investigation. Completion of all phases is necessary before conclusions can be formulated:

**Phase 1:** Conduct physical experiments of a simple heat exchanger arrangement and gather experimental data

**Phase 2:** Undertake computational fluid dynamics (CFD) simulation of a heat exchanger modelled on the physical experiment

**Phase 3:** Compare the results of the experimental and simulation studies. Refine the CFD model until the results are within an acceptable error range

**Phase 4:** Conduct a physical experiment and CFD model of a simple heat exchanger using a control valve at the process water entry point and analyse the temperature distribution at a global level

**Phase 5:** Analyse the temperature distribution at the entry of the heat exchanger for localized hot spots on the transfer wall

**Phase 6:** Scale the CFD model to the size and boundary conditions of the real-life application and repeat global and localized analysis.

### 3.2 Limitations

#### 3.2.1 Student

The limiting factor of this project is the student's time. The timeframe to complete the project was 7-8 months with the student completing this course part time alongside work and family commitments.

The student is an undergraduate and unfamiliar with ANSYS software, and CFD methodologies. The CFD course (MEC5100) was not available for undergraduate students and the student's electives have already been exhausted.

#### 3.2.2 Heat Exchanger Technology

The large plate-type heat exchanger used in large dyno engine applications has driven the student's interest in this project. Modelling of this type of heat exchanger is more complex as the fluid may behave as though it were in an open channel. The complexity increases even more as it is likely to exceed limitations of the ANSYS student version.

A more detailed analysis could be performed using the actual geometry of an industrial plate-type exchanger; however, it would be unlikely that most manufactures' would share the detailed drawings of their heat exchanger parts to model in a CFD suite.

This study was completed on dual-tube type exchanger design and reveals the effects of a butterfly valve in the entry region considering global and local heat distribution. As discussed further in section 6, a study should be completed on a plate-type exchanger with appropriate geometry before making conclusions on the true industrial application.

### **3.2.3 ANSYS Student Edition**

Experiments performed in the writing of this dissertation were performed on the ANSYS student edition which has mesh limitations of 512,000 elements. As discussed in the literature review, in section 2.4.2, similar available studies have required over 3 million elements. It is likely the results of this study could have errors due to these mesh element limits.

## **3.3 Scope**

For this study, a dual-wall type exchanger will be used as this is the simplest exchanger that can be created within the computational and experimental environment available at the University of Southern Queensland Toowoomba campus laboratory.

## **3.4 Methodology Used and Expected Outcomes**

It is hypothesized that the use of a control valve at the heat exchanger process water entry point could create turbulence and other undesirable entry conditions affecting the global and local entry region transfer wall heat distribution within the heat exchanger. It is not possible to measure the temperature distribution through the entry region of the heat exchanger accurately, or completely, under the conditions of this physical experiment as the flow turbulence is very complex and any physical measurement devices will affect the flow of water in this area. Computational Fluid Dynamic (CFD) modelling will be the primary method used to analyse this the fluid behaviour.

The CFD models will be validated with physical and mathematical where possible before conclusions are formulated.

It is expected the modelling will show no significant global change in heat exchanger performance, with or without a valve. However, it is anticipated the modelling will show significant local temperature distribution difference due to turbulence created from the valve.

## **3.5 Study Planning/Timeline**

A project plan was initially completed with various key components timelines and milestone key dates and can be seen in appendix B. The scope has changed with the initial literature review and experimental data and a summary of the adjusted major project milestones can be seen in table 3-1 below:

*Table 3-1: Major project milestones.*

<b>Item</b>	<b>Original Due Date</b>	<b>Actual Completion Date</b>	<b>Notes</b>
Literature Review	30 Apr 2021	08-Aug-2021	Timeline priority changed to the ANSYS learning and experimental work to ensure risk mitigated as shown in section 3.7. Completed 50% by May, remainder in Aug.
Research HT36 Jig	30 Apr 2021	13 Apr 2021	
Complete initial CFD Model	30 Apr 2021	30 Apr 2021	
Complete initial physical experiment	25 Jun 2021	24 May 2021	
Compare results and optimise CFD	10 Jul 2021	25 May 2021	
Compile and lodge progress report	26 May 2021	26 May 2021	
Complete CFD and physical experiment with valve entry condition.	N/A	18 Jul 2021	Was not in initial scope but critical to find results to meet aim. New Goal 15-Jul-2021
Scale CFD models to real-life boundary conditions	21 Aug 2021	01 Sep 2021	
Analyse data and generate conclusions	01 Sep 2021	05 Sep 2021	
Compile and lodge partial dissertation	08 Sep 2021	07 Sep 2021	
Compile and present presentation	24 Sep 2021	23 Sep 2021	
Compile and lodge final dissertation	13 Oct 2021	13 Oct 2021	

## **3.6 Resource Planning**

The planning of this project identified several items of equipment that would be required to complete the experiments and perform the analysis required to meet the objectives of this dissertation.

### **3.6.1 Physical Experimental Jig**

The University of Southern Queensland has an experimental heat exchanger used for educational purposes. Access to this equipment was required to establish baseline data for comparison to computational models. Access to the USQ laboratory and technical staff was negotiated with the project supervisor.

The equipment which the student required access to was, the Armfield HT36 heat exchanger and computer program located in the Toowoomba campus Z-block. All experiments within the scope of this project were completed without purchasing additional equipment by the University or the student.

### **3.6.2 Software**

Various software applications were required to complete the analytical computations and compile the dissertation report. Modelling was performed on a combination of the student's personal computer and USQ computer lab resources. The software used were:

- Microsoft Office package
- ANSYS 2021 R1 – Student version
- ANSYS 2020 R2 – Student version

### **3.6.3 Computer Lab Access**

Computational modelling required access to the USQ computer laboratories to gain increased processing ability.

### **3.6.4 Confidentiality of Proprietary Information**

On initial launch of the study, it was thought that proprietary information might be needed to accurately model scenarios, however it was found all the required information to get acceptable results was publicly available. This negated the need to include confidentiality restrictions to this dissertation.

#### ***Armfield HT36 Test Equipment***

To accurately model the Armfield HT36 test equipment, correct dimensions and material properties were required. The student was able to source this information through combining information from the Armfield instruction booklet with actual measurements of components.

#### ***Application Heat Data***

The heat generation and operating temperatures of an industrial High Horse-power engine was found publicly available through search engine search. The information was found to be sufficient to scale the model to represent an industrial application.

### 3.7 Project Risk

Risks to the success of this project were identified and documented. A simple risk matrix was developed as seen in figure 3-2 below. Where possible, controls were put in place to lower the risk as much as possible. As seen in the table the biggest risk to the success of the dissertation is other commitments in the student’s life, including work and family. The author’s work stretched to many hours of over-time implementing a new Manufacturing Execution System (MES) where he was the main resource. Item 6 also proved true as the author spent a few key study weekends in hospital with my young baby. Planning, mitigating the risk and getting ahead of deadlines allowed this dissertation to be completed by the deadlines required.

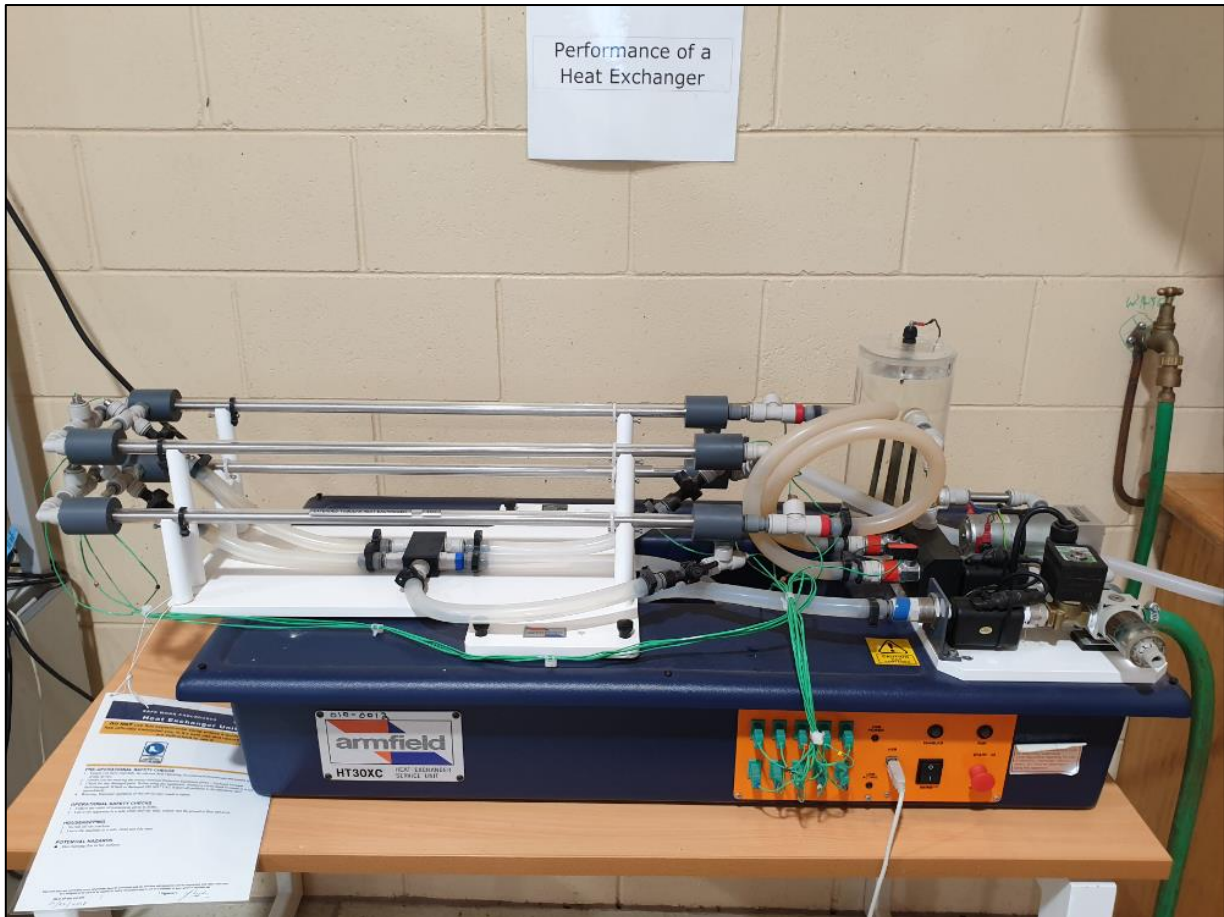
ID #	Description of Risk	Likelihood	Consequence	Risk Score	Controls	Residual Risk
1	File corruption / Data loss	Unlikely	Extreme	High	- Save file on OneDrive for cloud backup. - Regular Manual Backup of Files on cloud and USB stick	Low
2	Scope Creep	Likely	Medium	Medium	- Stick to Project Specification and discuss with Supervisor if project creep is identified.	Low
3	Physical Experiment Equipment Failure	Unlikely	Medium	Low	- Perform physical experiment as earlier as possible in case alternate options need pursuing	Low
4	Software/Hardware Failure	Unlikely	Medium	Low	- Backup software is available on the Student's work computer as well as University Labs. - Ensure money available if required to replace failed student hardware	Low
5	Lack of time to complete dissertation - work commitments	Likely	Medium	Medium	- Discuss with work, keep annual leave available in case required. - Ensure significant progress so unplanned unavailability will not leave in Failing position	Medium
6	Lack of time to complete dissertation - family and personal health/commitments	Likely	Medium	Medium	- Leverage assistance with family to look after child during wife's nursing placement periods - Ensure significant progress so unplanned unavailability will not leave in Failing position	Medium
7	Unable to continue dissertation due to lack of available information	Unlikely	Low	Low	- Complete literature review as soon as possible and discuss with sponsor.	Low

Figure 3-1: Project risk matrix.

## 4.0 Chapter 4: Physical and Computer Modelling

### 4.1 Phase 1: Verification Physical Modelling

The test equipment being modelled in the physical experiments to validate the computational model is the Armfield HT36 Extended Tubular Head Exchanger located in the University of Southern Queensland Toowoomba campus.



*Figure 4-1: Armfield HT36 extended heat exchanger experiment in USQ laboratory.*

#### 4.1.1 Experiment Equipment

The Armfield HT36 heat exchanger was built to support educational courses. The system contains four major sub-systems as well as auxiliary plumbing not described:

- Heat Exchanger Core
- Control System
- Heating System
- Computer System.

## **Heat Exchanger System**

The heat exchanger core comprises four dual tube lengths with the internal walls of 0.6mm stainless steel. The core of the system has ten thermocouples throughout to measure and record the temperature at various points through both the hot and cold sections of the exchanger.

## **Control System**

The control system comprises a series of valves allowing switching between parallel and counter-flow. It has control valves enabling adjustment of the fluid flow throughout circuits. Valves are also included to isolate lengths of the heat exchanger core so that experiments can be performed on one, two, three or four lengths. The valves used to change the direction of flow and tube lengths are manually controlled however the flow rates are controlled through a computerised control system.

## **Heating System**

The heating system can control the temperature of the hot circuit simulating a heat source in industry. The temperature is set on the Armfield software, and a heater/thermocouple is used to maintain a consistent hot water temperature. The heating system also contains a fluid sensor, so the pump does not run dry.

## **Computer System**

The computer software and hardware controls the flow rate valves and monitors/records the temperatures in the ten (10) thermocouples. The computer can control the control system by the changing PID controller parameters.

### **4.1.2 Design of Experiment**

The experiment performed for validation of the ANSYS model was in accordance with the Armfield HT36 Instruction Manual Issue 7 (Armfield 2014). The test equipment was set up in counter-flow arrangement using all four (4) tubes. Once turned on, hot water was allowed to heat and circulate to purge air bubbles. The cold-water side was also allowed to flow and clear out any air bubbles.

Once setup was completed, the entry conditions were set to pre-determined flow rates and temperatures given in the manual as can be seen in table 4-1 below. The flow rates and temperatures throughout the experimental rig are logged using the Armfield HT36 software. These logs were exported for data analysis and comparison to the ANSYS model.

Two tests with varying test conditions were completed and compared with two CFD models. This was done over a single experiment to increase confidence the ANSYS modelling matches the physical experiment. A single experiment could be likely modelled to match, however, the second data point verified the model with more confidence.

**Table 4-1:** Physical experiment test conditions.

Test Case	Parameter	Value
1	Hot Water In	30°C above cold water temperature
	Hot Water Flow	3 lpm
	Cold Water In	Temperature of the tap water
	Cold Water Flow	1 lpm
2	Hot Water In	30°C above cold water temperature
	Hot Water Flow	3 lpm
	Cold Water In	Temperature of the tap water
	Cold Water Flow	2 lpm

### 4.1.3 Experimental HSE Risk

This experiment comes with risk to the student and possibly other bystanders. A risk assessment was performed, and controls put in place, until all risks were as low as reasonably possible. With all the identified controls implemented, all risks were classed as ‘low’. The risk assessment was then approved by the supervising staff. The full risk assessment can be seen in appendix C.

A site safety induction was completed on the day of the experiment to make the student aware of local layout, staff, procedures, and equipment.

### 4.1.4 Experiment Details

The experiment was performed in the University of Southern Queensland labs on the morning of 24<sup>th</sup> of May 2021. The ambient temperature was 17°C during the experiment. The experiments were undertaken and in accordance with procedures other than the following:

- The heating elements were not able to reach the inputted temperature (48.6° C) when the cold-water flow rate was set at 2 lpm. The values were recorded and will still be suitable for validation purposes. These can be seen in the T1 values in table 4-3 below
- Readings were not as stable as expected, however several data points were captured for each experiment to enable averaging of the values

The full set of results can be seen in table 4-2 and table 4-3 below.

## 4.1.5 Results

Table 4-2: Table of results from experiment 1.

Sample Number	Elapsed Time [mm:ss]	Temp T1 [°C]	Temp T2 [°C]	Temp T3 [°C]	Temp T4 [°C]	Temp T5 [°C]	Temp T6 [°C]	Temp T7 [°C]	Temp T8 [°C]	Temp T9 [°C]	Temp T10 [°C]	Hot Water Pump Setting [%]	Hot Water Flowrate Fhot [l/min]	Cold Water Valve Setting [%]	Cold Water Flowrate Fcold [l/min]	Flow Orientation
1	00:01	48.4	47.0	44.9	43.3	41.3	18.5	24.0	27.8	32.2	35.4	46	3.1	53	1.04	Countercurrent
2	00:06	48.4	47.0	44.9	43.2	41.4	18.5	23.9	27.8	32.0	35.3	46	3.1	53	1.01	Countercurrent
3	00:11	48.4	46.9	44.8	43.2	41.3	18.5	24.0	27.4	32.2	35.4	46	3.0	53	0.92	Countercurrent
4	00:16	48.5	47.0	44.9	43.2	41.3	18.5	23.8	28.0	32.3	35.5	46	3.0	53	0.99	Countercurrent
5	00:20	48.6	47.0	44.9	43.3	41.4	18.5	24.0	28.0	32.0	35.5	46	3.0	53	1.06	Countercurrent
6	00:25	48.6	47.0	44.8	43.2	41.5	18.5	23.9	27.9	32.2	35.3	46	3.1	53	0.98	Countercurrent
7	00:30	48.6	47.1	44.9	43.2	41.5	18.5	23.9	28.0	32.1	35.6	46	3.0	53	0.95	Countercurrent
8	00:35	48.7	47.2	45.2	43.3	41.4	18.5	24.0	27.9	32.1	35.5	46	3.0	53	1.03	Countercurrent
9	00:40	48.6	47.1	45.1	43.5	41.5	18.5	23.8	27.6	32.3	35.6	46	3.0	53	0.94	Countercurrent

Table 4-3: Table of results from experiment 2.

Sample Number	Elapsed Time [mm:ss]	Temp T1 [°C]	Temp T2 [°C]	Temp T3 [°C]	Temp T4 [°C]	Temp T5 [°C]	Temp T6 [°C]	Temp T7 [°C]	Temp T8 [°C]	Temp T9 [°C]	Temp T10 [°C]	Hot Water Pump Setting [%]	Hot Water Flowrate Fhot [l/min]	Cold Water Valve Setting [%]	Cold Water Flowrate Fcold [l/min]	Flow Orientation
1	00:00	44.0	42.2	39.7	37.7	35.7	18.6	22.1	24.9	28.2	30.6	46	3.0	100	1.83	Countercurrent
2	00:05	44.0	42.2	39.8	37.7	35.7	18.6	22.1	24.9	28.1	30.6	47	2.6	100	1.87	Countercurrent
3	00:10	44.1	42.2	39.8	37.7	35.6	18.6	22.1	24.9	28.1	30.5	47	3.1	100	1.86	Countercurrent
4	00:15	44.0	42.2	39.9	37.9	35.7	18.6	22.1	25.0	28.1	30.6	46	3.1	100	1.83	Countercurrent
5	00:20	43.8	42.0	39.6	37.5	35.5	18.6	22.1	24.9	28.0	30.4	47	3.0	100	2.04	Countercurrent
6	00:25	43.9	42.0	39.5	37.5	35.5	18.6	22.1	24.9	28.0	30.4	46	3.0	100	1.97	Countercurrent
7	00:30	43.7	41.8	39.5	37.5	35.5	18.6	22.1	24.8	28.0	30.3	46	3.1	100	1.97	Countercurrent
8	00:36	43.4	41.6	39.1	37.3	35.3	18.6	22.0	24.8	27.9	30.2	46	2.9	100	1.93	Countercurrent
9	00:41	43.3	41.5	39.2	37.2	35.2	18.6	22.0	24.7	27.8	30.2	46	2.9	100	1.89	Countercurrent

These values were averaged and plotted to visualise the data as seen in figure 4-2 and 4-3 below. The curves are the temperature distributions expected with counter-flow heat exchangers.

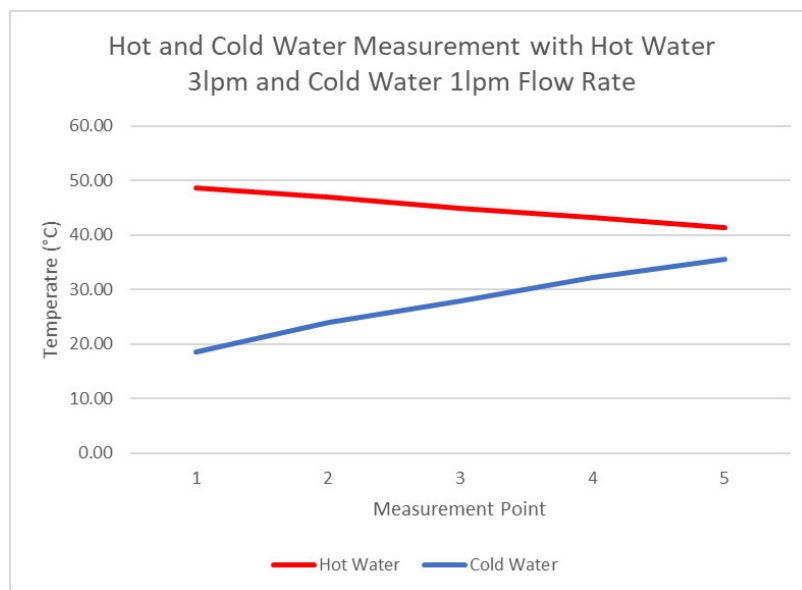
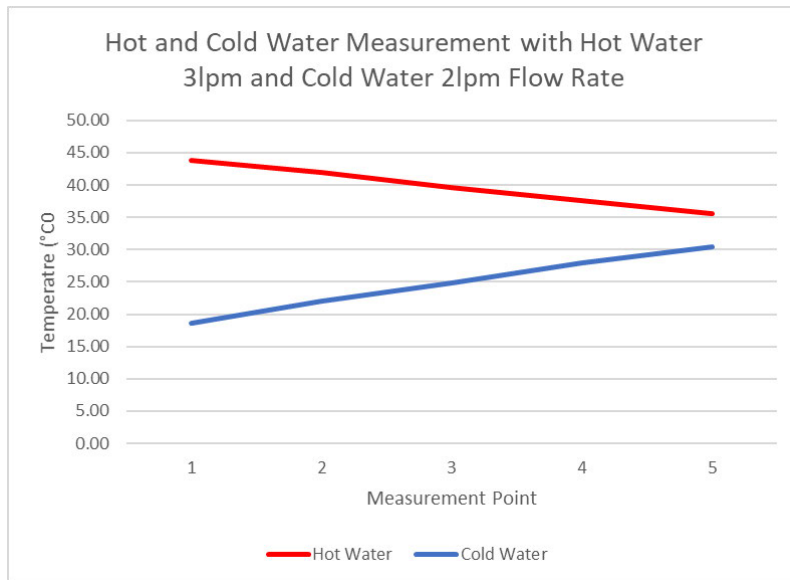


Figure 4-2: Hot and cold-water measurements with hot water 3lpm and cold water 1lpm flow rate.



*Figure 4-3: Hot and cold-water measurements with hot water 3lpm and cold water 2lpm flow rate.*

## 4.2 Phase 2: Verification ANSYS Modelling

The test equipment being modelled in the CFD model is the Armfield HT36 Extended Tubular Head Exchanger, identical as used in section 4.1.

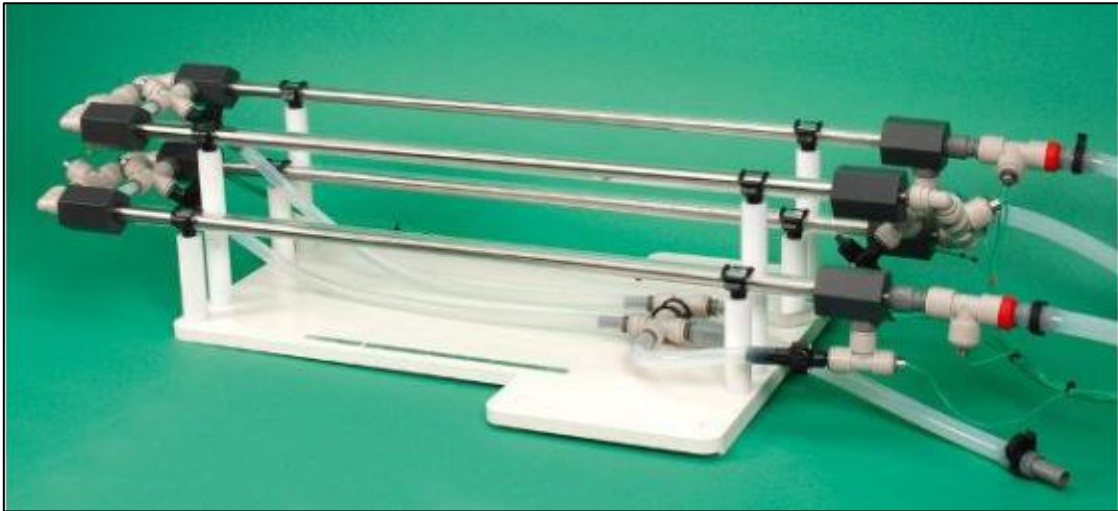


*Figure 4-4: Armfield HT36 extended heat exchanger (Armfield 2015).*

To create the 3D model, the available information was used from the supplier manual (Armfield Ltd). Where data was not available, the test rig was reversed engineered, and measurements taken. Information gathered from the supplier identified the inner tube was 3/8" stainless steel tube with 0.6mm wall thickness and length of 760mm. The outer tube is 16mm acrylic tube with 2mm wall thickness and length of 670mm. This gives a nominal OD of the annulus fluid 14mm cross section and a nominal OD of the inner tube as 8.925mm.

### 4.2.1 Assumptions Made

#### Base and Stand

The Armfield HT36 is mounted on a stand which holds the experimental hardware in place. The stand does not affect the experiment and has been omitted in the 3D model

#### 'O'-Ring Seals

The Armfield HT36 is designed with 'o'-ring seals to allow for expansion and contraction of the joints. The model does not simulate this behaviour and assumes a simplified solid sized joint.

The Armfield HT36 uses 3/8" push connect fittings. These fittings are not required for modelling and the model was simplified with solid size on size joints assuming the fluid flows through a continual 9.825mm cross section. The elbow is simplified as a 15mm radius.

The elbow fittings, large 'tee' unions and thermocouple adapter 'tee' unions are noted to be made of acrylic material and considered to be adiabatic.

The outer annulus of the heat exchanger is manufactured from acrylic material and considered to be adiabatic.

In between the acrylic fittings each end connection has sections of 3/8" stainless steel exposed to the air. Heat loss through these joints cannot be ignored and are included in the CFD model. Where the tube is offset as shown in the "Jumper Tube" callout in figure 4-5 below, is it simplified in the model to be symmetric with equal halves of the total tube length either side of the thermocouple.

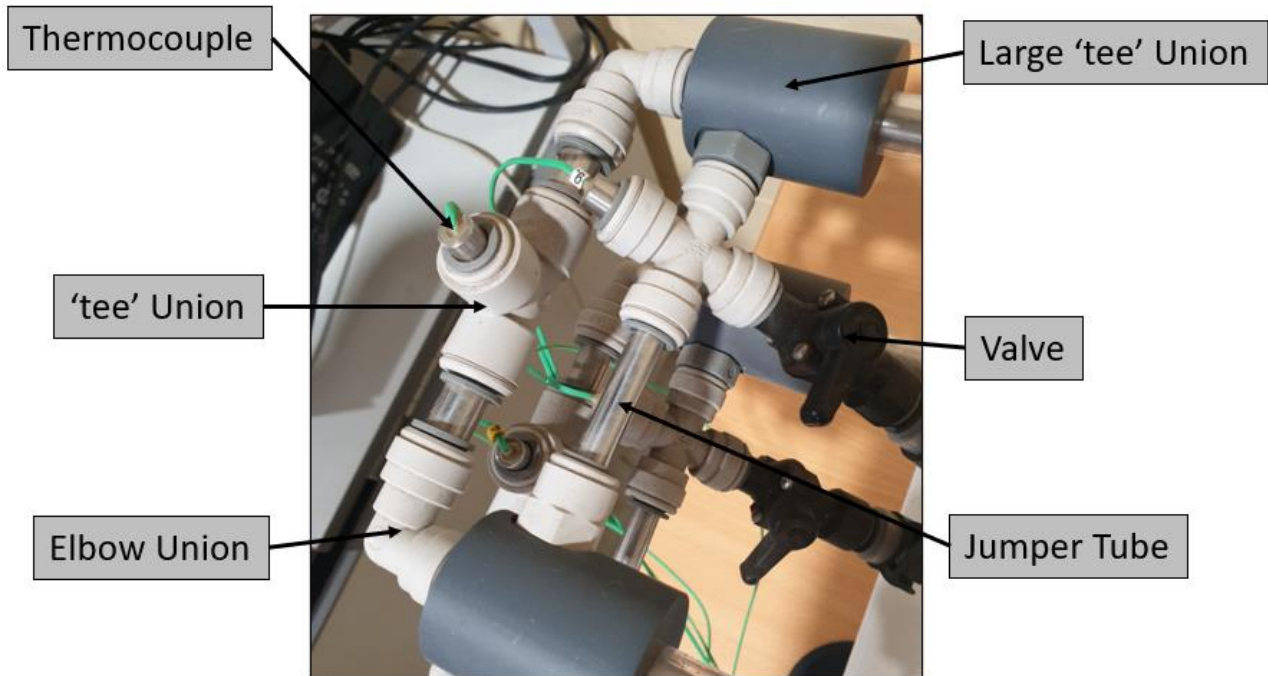


*Figure 4-5: Photo and nomenclature of Armfield HT36 heat exchanger end transfer arrangement.*

### **Layout**

The actual experimental device is laid out such that it takes as little bench space as possible. Our model however assumes a flat orientation and was chosen because it will not affect the results of the experiment, however, will present that data in a neater way. This layout is like the flow diagrams from the Armfield Teaching Extracts Manual shown in figure 4-6.

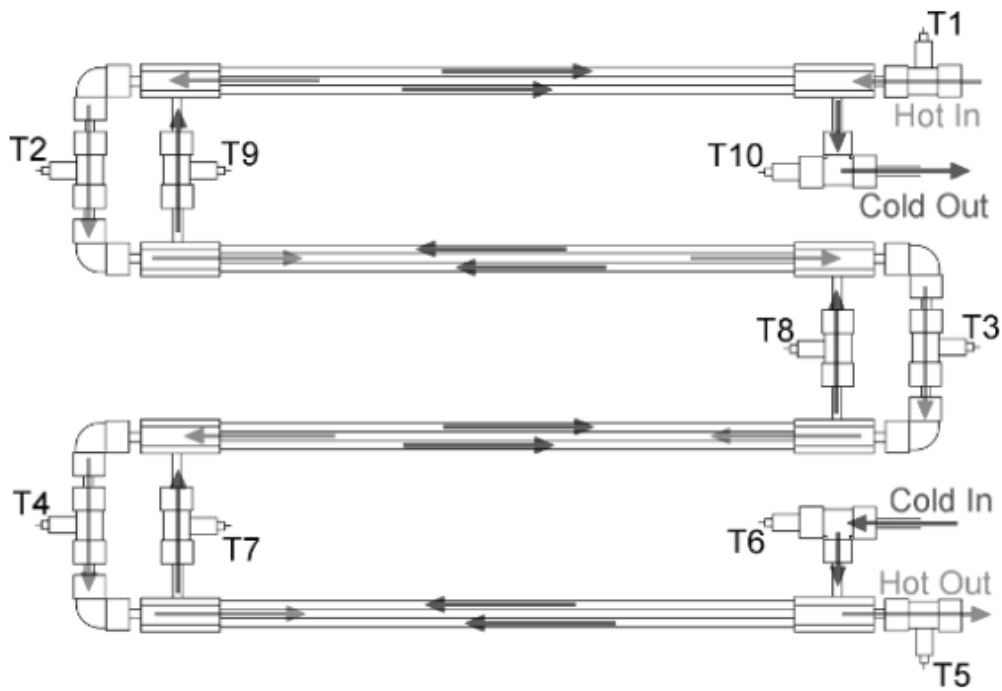


*Figure 4-6: Counter-current flow diagram (Armfield 2015).*

#### 4.2.2 Model Creation

The 3D model of the fluid path was created in ANSYS DesignModeler using a combination of extruded and swept frozen volumes. Booleans were then created removing the hot section volume from the cold section volume. No physical wall was modelled between the two fluid domains, instead the Fluent “shell conduction” mode was used alongside zero-transfer wall boundary conditions.

Segments in the sweep path were made to create segments for applying boundary conditions for areas where stainless steel were exposed to the air. These locations will have heat loss from convection and were modelled accordingly.

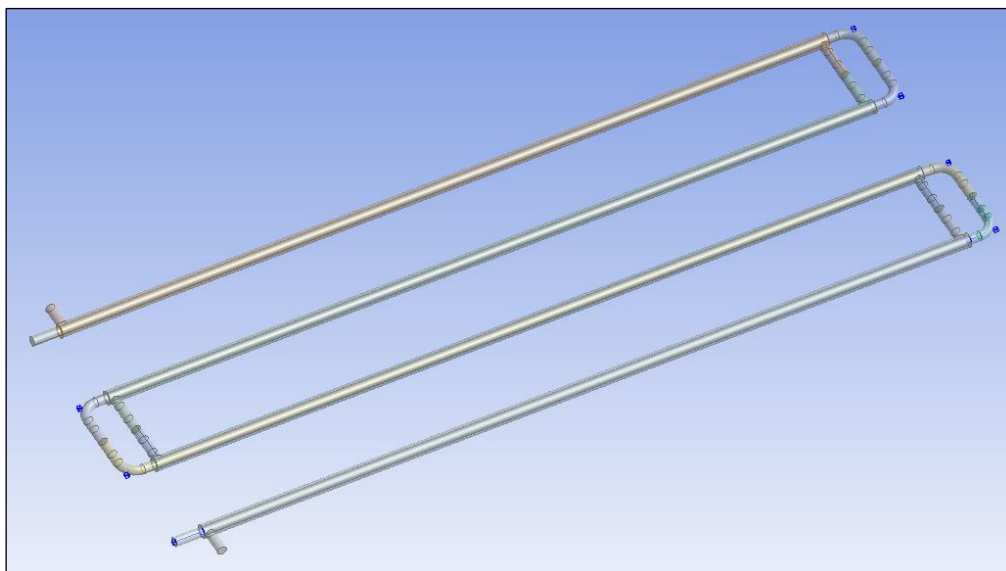


*Figure 4-7: The Armfield HT36 fluid path 3D model.*

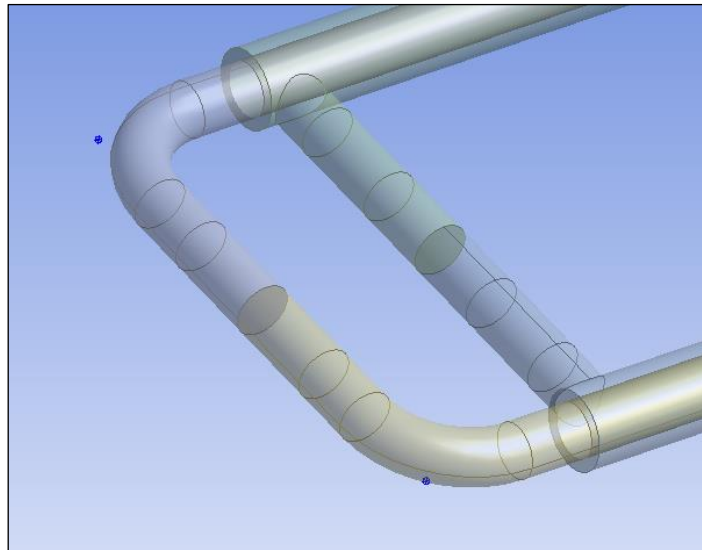


*Figure 4-8: Segments for heat loss through convection.*

### **Meshing**

To setup the initial model a mesh size was chosen to achieve as accurate results as possible, whilst staying within the limits of ANSYS Student version which is limited to 512,000 elements. Once a working model was produced a mesh analysis was completed to find an appropriate mesh size to achieve accurate results whilst minimizing the calculations required.

A combination of different meshes were chosen to achieve accuracy in the complex areas of geometry whilst keeping mesh in the simpler regions less dense. Whilst the element limit is 512,000, ANSYS was found to require a lower limit of about 450,000, otherwise it failed during the Fluent modelling stage with an element limit warning. This was likely due to the use of the “shell conduction” feature for the transfer and convection walls as Fluent will automatically create a layer of elements for the wall calculations.

**Hot water domain:** The hot water domain has a very simple geometry; it mainly comprises a straight pipe with simple radius bends on the ends. A sweep mesh method was chosen as it gave the best shaped mesh for accuracy around the transfer wall whilst giving neat mesh on the corners. For this domain, the following mesh parameters were used:

- **Method:** Sweep mesh, using hot water entry face as source and outlet as the target
- **Mesh Type:** All Quad
- **Divisions:** 2200
- **Edge Divisions:** 28
- **Bias:** No Bias.

**Cold Water Domain:** The cold-water domain has a more complex geometry with sharp corners between the transfer ends. To get accurate results whilst minimizing the elements used, the mesh around the corners was refined whilst keeping the linear areas relatively coarse. For this domain, the following mesh parameters were used:

- **Method:** Tetrahedrons
- **Body Sizing:** 0.0026m
- **Face Sizing:** Around the corner areas 0.0008.

The total elements with this setup equates to 443,487 elements. A graphical representation of the resulting mesh can be seen in figure 4-9 and 4-10 below.

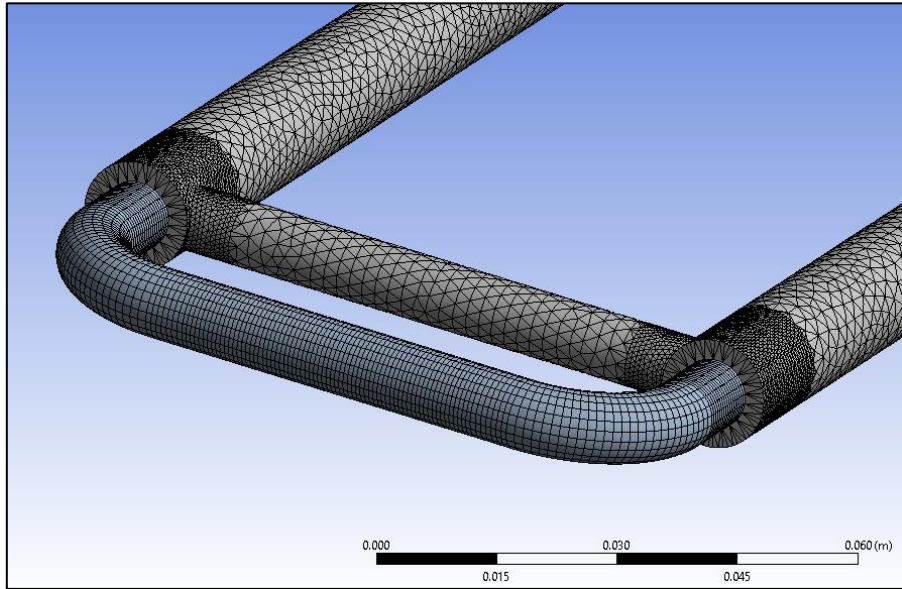


*Figure 4-9: Resulting mesh for initial verification.*

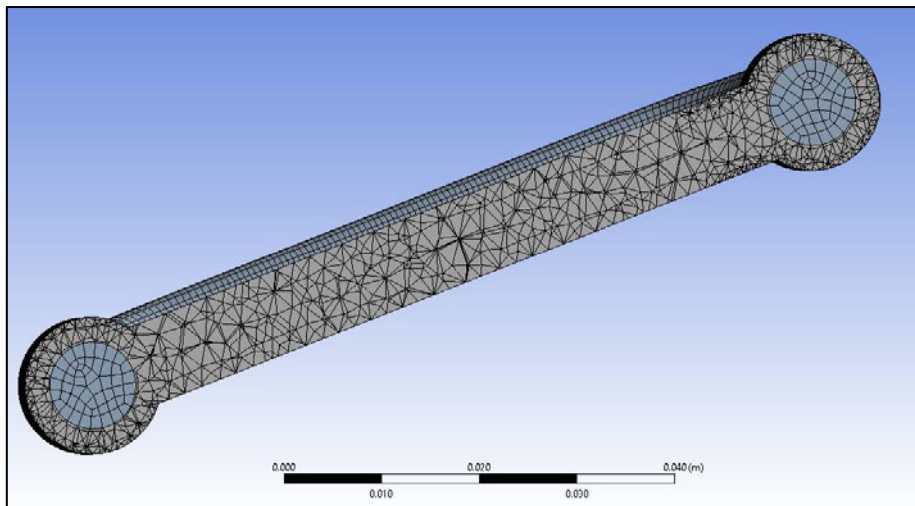


*Figure 4-10: Resulting mesh for initial verification – sectioned through the centre of cold-water corner.*

### **Governing Equations**

The Fluent software was chosen to perform the calculations and three fundamental equations will be solved across the system:

Continuity Equation (conservation of mass) (Pedlosky 1987):

$$\frac{\partial \rho}{\partial t} + \nabla(\rho \cdot \mathbf{u}) = 0$$

Which in our case of incompressible fluid, can be simplified as:

$$\nabla \cdot \mathbf{u} = 0$$

Momentum Equation (Sharifi et al 2018):

$$\frac{\partial}{\partial t}(\rho \cdot \mathbf{u}) + \nabla(\rho \cdot \mathbf{u} \cdot \mathbf{u}) = -\nabla p + \rho \cdot \mathbf{g} + \vec{f}$$

Energy Equation (Sharifi et al 2018):

$$\frac{\partial}{\partial t}(\rho \cdot e) + \nabla[(\rho \cdot e + p) \mathbf{u}] = \nabla(k_{\text{eff}} \nabla T - \sum h_j \cdot \vec{J}_j + (\bar{\tau}_{\text{eff}} \cdot \mathbf{u}))$$

Where  $\rho$  is the mass density,  $T$  is time,  $e$  is the energy per unit mass,  $p$  is the fluid pressure,  $k_{\text{eff}}$  is the thermal conductivity,  $h_j$  is the enthalpy of species  $j$ ,  $J_j$  is the diffusion flux of species  $j$ ,  $\bar{\tau}_{\text{eff}}$  is the stress tensor,  $\mathbf{u}$  is flow velocity vector and  $\vec{f}$  is the volumetric force.

### Setup

Named Selections: All the key bodies, faces and walls were named so the correct boundary conditions and material properties could be added in the Fluent setup.

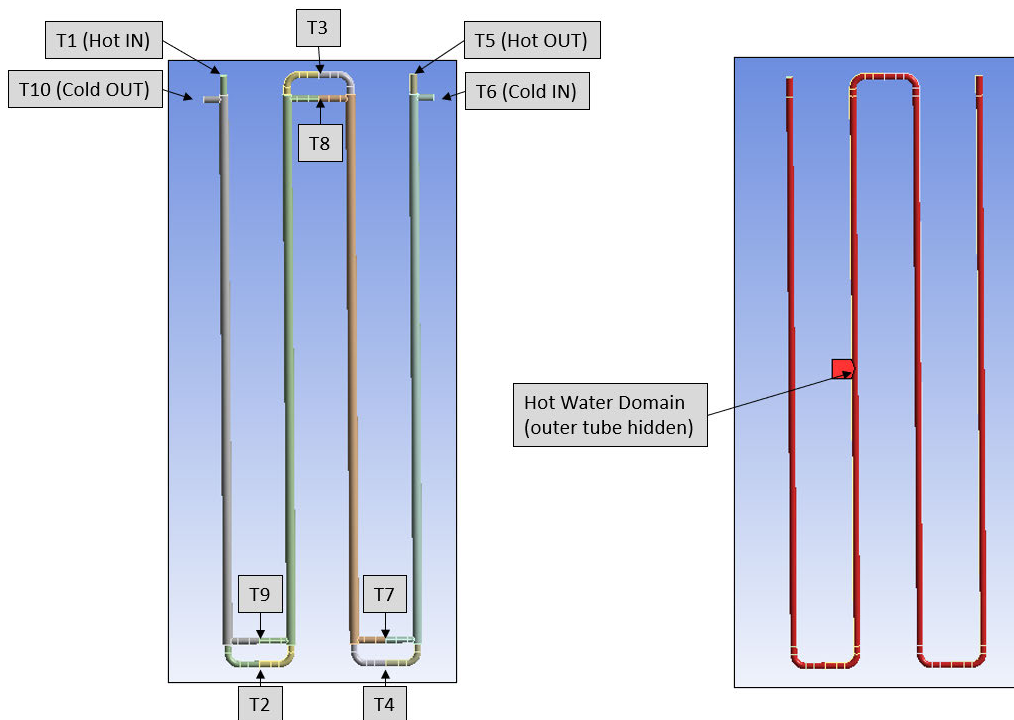
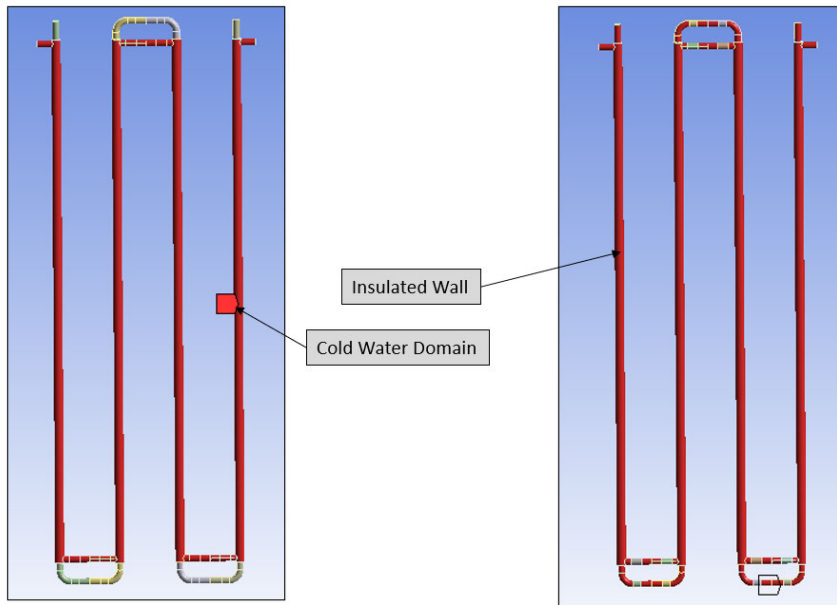
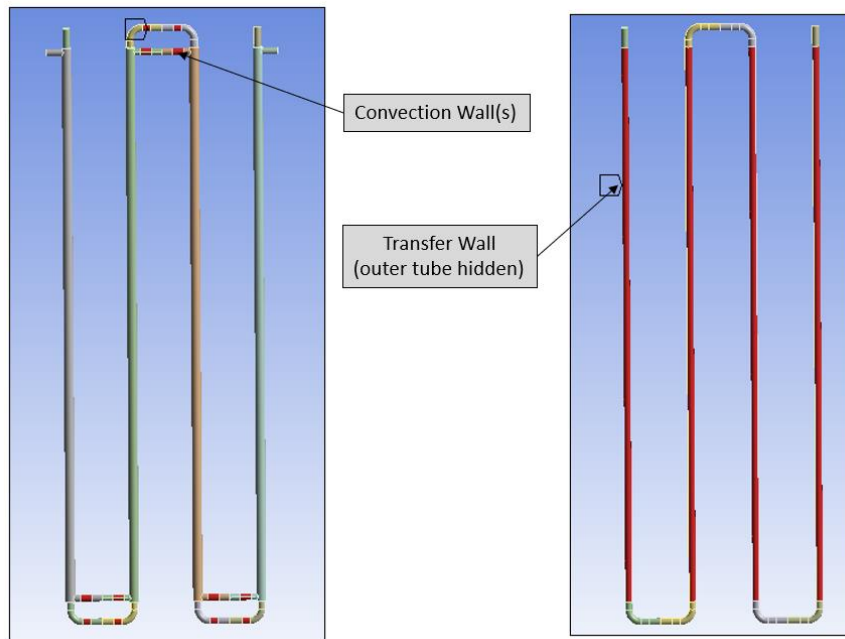


Figure 4-11: Model naming – Thermocouple location and hot water domain.



*Figure 4-12: Model naming – Cold water domain and insulated wall.*



*Figure 4-13: Model naming – Convection wall and Transfer wall*

**Material Properties**

Material properties required were sourced from several locations for use in the CFD model as shown in table 4-4 below.

\

*Table 4-4: ANSYS verification model material properties.*

Material	Density (kg/m <sup>3</sup> )	Specific Heat (J/(kg K))	Thermal Conducti vity (W/(m K))	Viscosity (kg/(m s))	Heat Transfer Coefficient (W/m <sup>2</sup> .K)	Source
Water @ 20°C	998.2	4182	0.6	0.001003	N/A	ANSYS Library
Stainless Steel	7900	477	14.9	N/A	N/A	(Cengel & Ghajar 2015)
Insulation (acrylic)	1410	1395	0.2	N/A	N/A	(Dielectric Manufacturing 2020) / (Energy Education 2020)
Still Air	N/A	N/A	N/A	N/A	25	

### **Boundary Conditions**

To be able to validate the physical experimental data to the ANSYS model, the CFD model was setup with boundary conditions matching those recorded from the physical experiment in section 4.1.

*Table 4-5: ANSYS verification model boundary conditions.*

Test Case	Parameter	Value
1	Hot Water In	48.53°C = 321.53 K
	Hot Water Flow	3.02 lpm
	Hot Water Mass Flow (calculated)	0.05024 kg/s
	Hot Water Volumetric Flow Rate (calculated)	5e-5 m <sup>3</sup> /s
	Cold Water In	18.59°C = 291.59 K
	Cold Water Out	0.99 lpm
	Cold Water Mass Flow (calculated)	0.01647 kg/s
	Cold Water Volumetric Flow Rate (calculated)	1.667e-5 m <sup>3</sup> /s
	Ambient Temperature	17°C = 290 K
2	Hot Water In	43.80°C = 316.8 K
	Hot Water Flow	2.96 lpm
	Hot Water Mass Flow (calculated)	0.04924 kg/s
	Hot Water Volumetric Flow Rate (calculated)	5e-5 m <sup>3</sup> /s
	Cold Water In	18.59°C = 291.95 K
	Cold Water Out	1.91 lpm
	Cold Water Mass Flow (calculated)	0.03178 kg/s
	Cold Water Volumetric Flow Rate (calculated)	3.333e-5 m <sup>3</sup> /s
	Ambient Temperature	17°C = 290 K

### **Laminar vs Turbulent Flow Model**

Flow could be either laminar or turbulent depending on the speeds of the flow and the area through which the flow is passing, and this affects the choice of modelling processes in ANSYS Fluent. To determine if the flow is turbulent or laminar the Reynolds number will be calculated:

For Flow in a pipe:

$$Re = \frac{\rho Q D_H}{\mu A}$$

Where,

$D_H$  is the hydraulic diameter of the pipe (ID) (m)

$Q$  is the volumetric flow rate (m<sup>3</sup>/s)

$\rho$  is the density of the fluid (kg/m<sup>3</sup>)

$\mu$  is the viscosity of the fluid kg/(m.s)

$A$  is the cross-sectional area (m<sup>2</sup>)

In the case of an annulus the hydraulic diameter becomes the difference between the hole diameter (ID of outside tube) and the pipe diameter (OD of the internal tube) (Ramsey 2019).

Viscosity of a fluid changes with temperature, therefore:

$$\mu_{inner} = 0.547 * 10^{-3} \text{ (water @50°C, Table A-15 (Cengel, Turner, Cimbala 2016))}$$

$$\mu_{outer} = 1.002 * 10^{-3} \text{ (water @20°C, Table A-15 (Cengel, Turner, Cimbala 2016))}$$

To find the Areas:

$$A_{inner} = \frac{\pi * D^2}{4} = \frac{\pi * 0.008925^2}{4} = 62.6 * 10^{-6} \text{ m}^2$$

$$A_{outer} = \frac{\pi * D_{hole}^2}{4} - \frac{\pi * D_{pipe}^2}{4} = \frac{\pi * 0.014^2}{4} - \frac{\pi * 0.008925^2}{4} = 91.4 * 10^{-6} \text{ m}^2$$

To simply for this case with known constants:

$$Re = \frac{\rho Q D_H}{\mu A}$$

$$Re_{inner} = \frac{998.2 * 8.925 * 10^{-3} * Q}{0.547 * 10^{-3} * 62.6 * 10^{-6}}$$

$$Re_{inner} = 260 * 10^6 * Q$$

$$Re = \frac{\rho Q D_H}{\mu A}$$

$$Re_{outer} = \frac{998.2 * (14 - 8.925) * 10^{-3} * Q}{0.001002 * 91.4 * 10^{-6}}$$

$$Re_{outer} = 55.3 * 10^6 * Q$$

Inputting known flow rates:

Test Case 1:

$$Re_{inner} = 260 * 10^6 * 5 * 10^{-5} = 13000$$

$$Re_{outer} = 55.3 * 10^6 * 1.667 * 10^{-5} = 922$$

Test Case 2:

$$Re_{inner} = 260 * 10^6 * 5 * 10^{-5} = 13000$$

$$Re_{outer} = 33.5 * 10^6 * 3.333 * 10^{-5} = 1843$$

Rao (2017), states “For water the flow is laminar when  $R < 2300$ , transient when  $2300 < R < 4000$  and turbulent when  $R > 4000$ ”. Since our hot water path (inner tube) has Reynolds values  $>2000$ , the flow can be considered fully turbulent and appropriate turbulent modelling mode will have to be used. This is also appropriate due to the complex and sharp bends required in cold water pipe.

Because of turbulence the k- $\epsilon$  model was chosen for the initial modelling as it best suits internal flow as shown in section 2.5.3. Wall treatment was enhanced using the ANSYS option of ‘Realisable’ and ‘Enhanced Wall Treatment’ to better model the flow near the walls where the heat transfer will occur. This is suitable for the global model, however alternative methods will be tested during the modelling of the entry region with the valve in section 4.5 and section 5.

### ***Fluent Setup Parameters***

The following settings were configured in the Fluent Setup. Parameters not mentioned have been left as the Fluent 2021 R1 student version default values.

**Table 4-6: ANSYS verification model Fluent parameter setup**

<b>Area</b>	<b>Parameter</b>	<b>Comments</b>
Setup - Models	Energy Equation	Turned on
Setup - Models	Viscous Model	k-epsilon Realizable Enhanced Wall Treatment
Setup - Materials	Fluids	Water-liquid setup
Setup - Materials	Solids	Steel-stainless setup Acrylic setup
Setup - Cell Zone Conditions	Cold water domain Hot water domain	Setup as fluid – water-liquid
Setup - Boundary Conditions	T5 – Hot water out T10 – Cold water out	Setup as mass flow outlet with flow rate matched to the inlet. Pressure outlet was tested with same results
Setup - Boundary Conditions	T1 – Hot water in T6 – cold water in	Setup as mass flow inlet Setup flow rate as normal to boundary with flow rate and temperature as per actual results in 4.1.5
Setup - Boundary Conditions	Insulated Wall – Cold water domain Insulated Wall – Hot water domain	Setup heat transfer coefficient to 0
Setup - Boundary Conditions	Convection wall	Setup convection heat transfer with stainless steel material value and single layer shell conduction of thickness 0.0006m, ambient temperature of 300K
Setup - Boundary Conditions	Transfer wall	Setup as coupled transfer with the shadow equivalent. Setup as single layer steel-stainless shell conduction with wall thickness of 0.0006m
Solution - Method	Scheme	Coupled
Solution - Monitors	Residuals	All changed to 1E-06
Solution - Initialization	Method	Hybrid Initialization
Run Calculation	Number of Iterations	500

### 4.2.3 Results

#### Convergence of Calculations

After 500 iterations, the approximate average residual values were obtained:

- X, Y Velocities:  $5e-6$
- Z velocity:  $6e-6$
- Continuity equation:  $2E-3$
- Energy equation:  $1.4E-7$
- Epsilon:  $2.3e-5$
- k:  $8.5e-6$ .

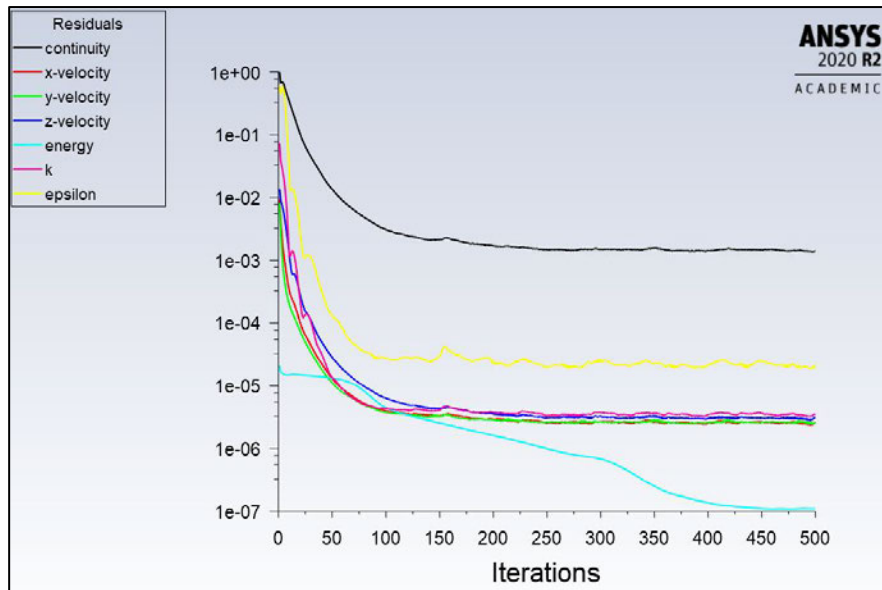


Figure 4-14: Residuals of test case 1.

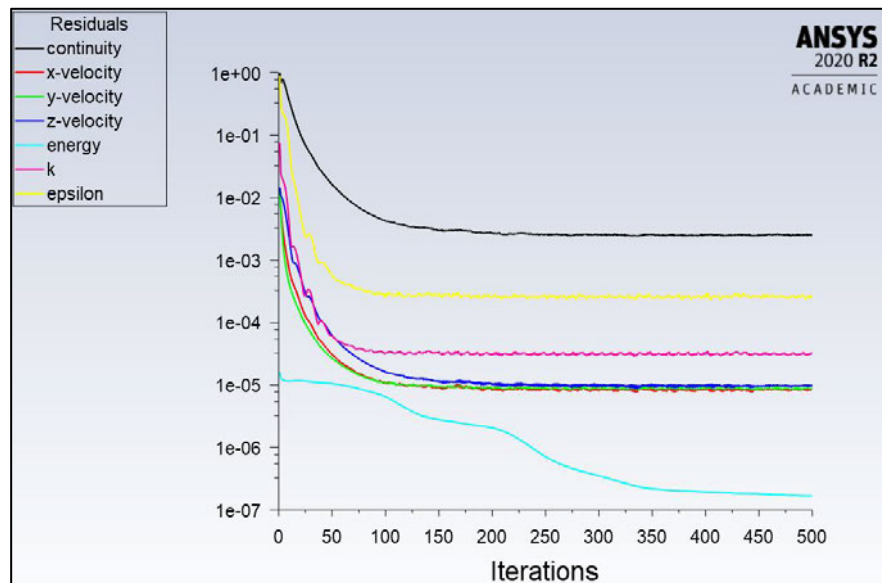


Figure 4-15: Residuals of test case 2.

**Temperature distribution values**

The temperature distribution values were extracted from ANSYS Results model as shown in table 4-22. The temperatures at each location were calculated using a function of Mass Flow Average across a cross-sectional cut.

*Table 4-7: Temperature distribution reported at fixed locations throughout the heat exchanger.*

Test Case	Parameter	Result
1	T1 (Hot In)	321.53 K
	T2 (Hot – bend 1)	320.46 K
	T3 (Hot – bend 2)	318.93 K
	T4 (Hot – bend 3)	316.85 K
	T5 (Hot Out)	313.90 K
	T6 (Cold In)	291.53 K
	T7 (Cold – bend 3)	300.05 K
	T8 (Cold – bend 2)	306.53 K
	T9 (Cold – bend 1)	311.30 K
	T10 (Cold Out)	314.84 K
2	T1 (Hot In)	316.80 K
	T2 (Hot – bend 1)	314.89 K
	T3 (Hot – bend 2)	312.68 K
	T4 (Hot – bend 3)	310.22 K
	T5 (Hot Out)	307.38 K
	T6 (Cold In)	291.95 K
	T7 (Cold – bend 3)	295.67 K
	T8 (Cold – bend 2)	299.53 K
	T9 (Cold – bend 1)	302.99 K
	T10 (Cold Out)	306.17 K

**Mass flow rate**

To validate there are no problems with modelling, mass flow at the outlets was checked against the mass flow at the inlets as shown in figure 4-16 and 4-17. The change in mass was negligible in both cases.

Mass Flow Rate	[kg/s]
t10_cold_out	-0.01664
t1_hot_in	0.04991
t5_hot_out	-0.04991
t6_cold_in	0.01664
Net	-1.3877788e-17

*Figure 4-16: Mass flow rate at inlet and outlet for Test Case 1.*

Mass Flow Rate	[kg/s]
t10_cold_out	-0.03327
t1_hot_in	0.04991
t5_hot_out	-0.04991
t6_cold_in	0.03327
Net	2.7755576e-17

Figure 4-17: Mass flow rate at inlet and outlet for Test Case 2.

### Temperature Distribution Contours

A plane cut was made through the X-Z axis, and a temperature contour plot made as shown in figure 4-18 and 4-19. The temperature contours show the continual cooling of the hot water and heating of the cold water as would be expected to be seen in this arrangement. The contour was inspected for any unintentional mixing of the two fluids or any other unusual or unexpected results.

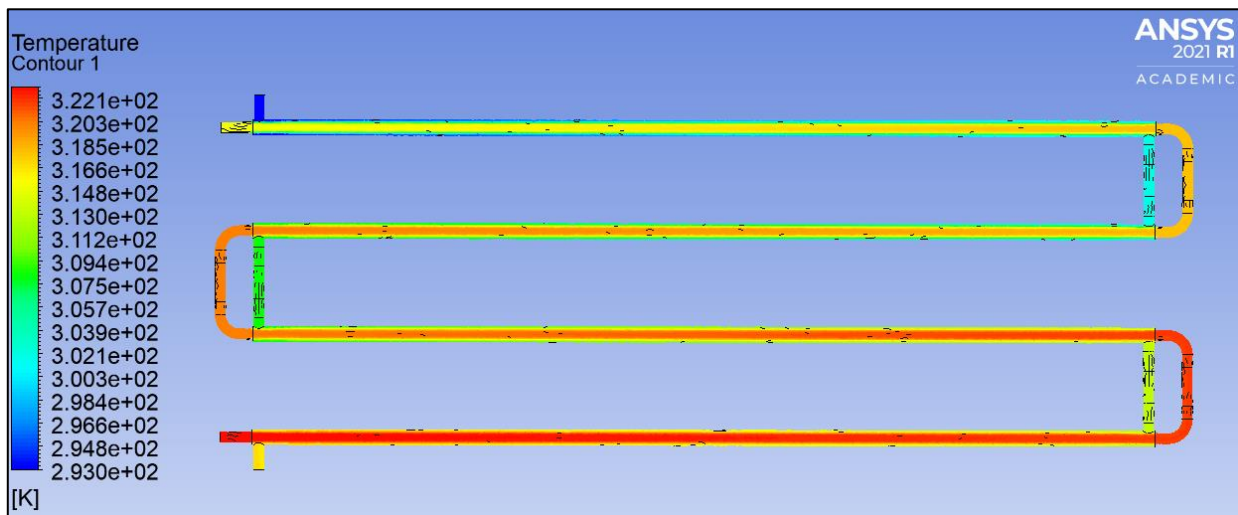


Figure 4-18: Temperature contour through the X-Z plane for Test Case 1.

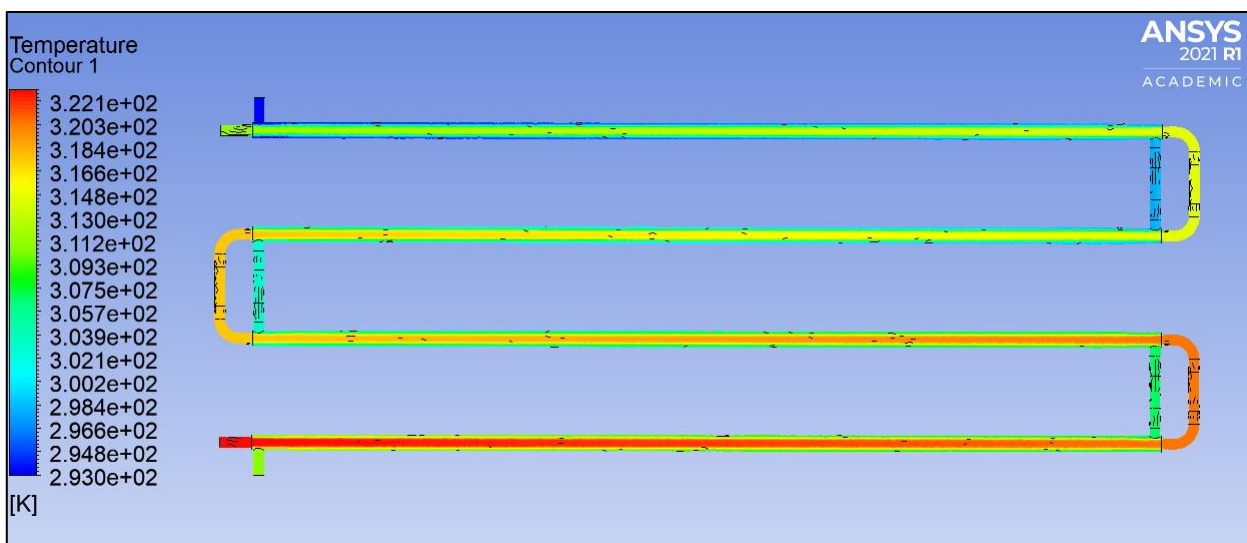


Figure 4-19: Temperature contour through the X-Z plane for Test Case 2.

#### 4.2.4 Mesh Independence Study

A mesh independence study was performed to ensure that the results being obtained were stable and correct. Many computations were completed to find a mesh size suitable to achieve accurate calculations whilst minimizing computation time to complete the study. This mesh study was important to reduce calculation times for the bulk computations required in the rest of the dissertation. This study has required additional mesh elements for the modelling of the butterfly valve entry conditions in section 4.4, so minimising elements used that this stage is important to free these elements up.

To complete this study, 16 fluent simulations were run with various mesh sizing and the results tabulated. For the mesh independency study, an ideal set of boundary conditions, as shown in table 4-8 were used, and results compared to check what mesh setup obtained accurate results.

*Table 4-8: Ideal boundary conditions for mesh independence study.*

Test Case	Parameter	Value
Mesh Study	Hot Water In	50°C = 323 K
	Hot Water Flow	3.00 lpm
	Hot Water Mass Flow (calculated)	0.04991 kg/s
	Cold Water In	20°C = 293 K
	Cold Water Out	1.00 lpm
	Cold Water Mass Flow (calculated)	0.01664 kg/s
	Ambient Temperature	20°C = 293 K

Five resulting categories were reviewed and compared.

- Convergence Error Representation: Each study was compared to the baseline for the X,Y&Z velocity, continuity equation and energy equation residuals. To compare to the baseline, any value larger than the baseline was averaged and compared to the baseline in percentage error
- Temperature Error: Each study was compared to the baseline for the outlet and mid-core temperatures. Any deviation from the baseline was averaged across the four temperatures and compared to the baseline as an average
- Wall Pressure: The wall pressure in the centre of the core was compared to the baseline as a percentage error
- Mass Flow Rate: Each study was compared to the baseline for the outlet and mid-core mass flow rates. Any deviation from the baseline was compared to the baseline as percentage error
- Element Reduction: Each study was compared to the based for the total elements generated through the mesh setup. The mesh was compared to the baseline using a percentage.

The full results of the mesh independence study can be found in Appendix D. The resulting elements were plotted against the dependant variables to determine if the study was mesh dependant. Analysis of the results

in figure 4-20 below shows that the results are mesh dependant and stability is achieved with a mesh count of approximately 275,000 elements.



Figure 4-20: Mesh Independence Study results showing stability after approximately 275,000 elements.

The study found the optimal settings for the mesh to minimize elements whilst reducing the temperature error, pressure error and residuals are:

- Hot Water Sweep Divisions: 1700
- Hot Water Edge Divisions: 22
- Cold Water Body Sizing: 0.0035m
- Cold Water Corner Face Sizing: 0.0015m
- Cold Water Transfer Face Sizing: 0.0025m.

This setup resulted in:

- Reduction of elements of 32% from 443,487 to 300,306
- Residual increase of 9% from the baseline
- Temperature difference of 0.04% from the baseline
- Mass flow difference of 0.26% from the baseline
- Pressure difference of 6.15% from the baseline.

### 4.3 Phase 3: Verify and Optimize the Model

To validate the CFD model, the temperature distribution across the thermocouple locations in the physical and computational models was compared.

#### 4.3.1 Expected Errors

It is expected the physical and CFD results will have some level of error due to:

- Material property assumptions
- Geometry differences due to simplifications
- Acrylic not being truly adiabatic like modelled
- Accuracy and calibration of thermocouples
- Accuracy and calibration of the flow meters
- The turbulence model k-ε was used though some of the flow regions have laminar flow.

The flow meter used on the Armfield HT36 is the Sensata UF25B Ultrasonic Flow Meter which has an accuracy of ±3% of the reading when used in the range of the experiments performed (Sensata 2021). The thermocouples used on the Armfield HT36 were noted to be K-type thermocouples. The accuracy of K-type thermocouples are generally accepted to be ±2.2°C which is about ±5% in the range we are measuring.

#### 4.3.2 Results

The physical vs CFD results for both flow rate experiments were tabulated and compared as shown in table 4-9 below.

*Table 4-9: Results comparing physical model vs CFD results.*

Comparison of Physical and CFD modelling after optimisation		Hot Water Flowrate Fhot [l/min]	Cold Water Flowrate Fcold [l/min]	Temp T1 [°C]	Temp T2 [°C]	Temp T3 [°C]	Temp T4 [°C]	Temp T5 [°C]	Temp T6 [°C]	Temp T7 [°C]	Temp T8 [°C]	Temp T9 [°C]	Temp T10 [°C]
Experiment 1	Physical Model	3.02	0.99	48.53	47.03	44.94	43.27	41.41	18.53	23.92	27.81	32.16	35.47
	CFD (Fluent) Model	3.02	0.99	48.53	47.402	46.04	44.372	42.285	18.53	24.841	29.73	33.614	36.74
	Error (%)	0.00%	0.00%	0.00%	0.79%	2.45%	2.55%	2.11%	0.00%	3.85%	6.90%	4.52%	3.58%
Experiment 2	Physical Model	2.96	1.91	43.8	41.94	39.56	37.56	35.52	18.59	22.09	24.88	28.02	30.4
	CFD (Fluent) Model	2.96	1.91	43.8	42.193	40.466	38.603	36.58	18.59	22.037	24.852	27.432	29.827
	Error (%)	0.00%	0.00%	0.00%	0.60%	2.29%	2.78%	2.98%	0.00%	0.24%	0.11%	2.10%	1.88%

This data was then plotted to better visualise the data as shown in figure 4-21 and 4-22 below.

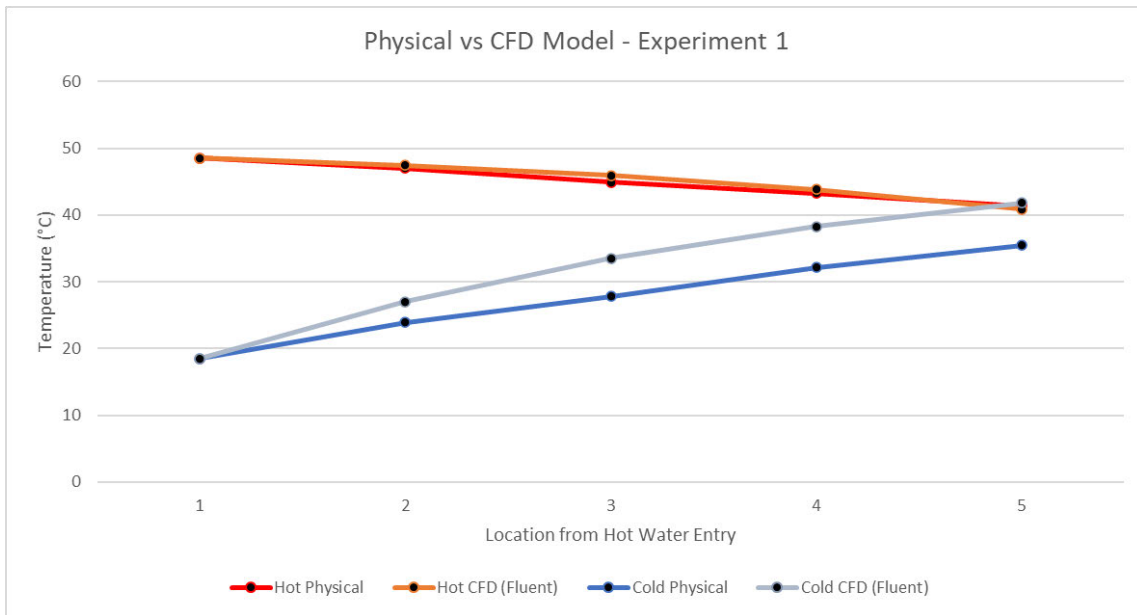


Figure 4-21: Chart showing physical vs CFD results – experiment 1 (1 lpm).

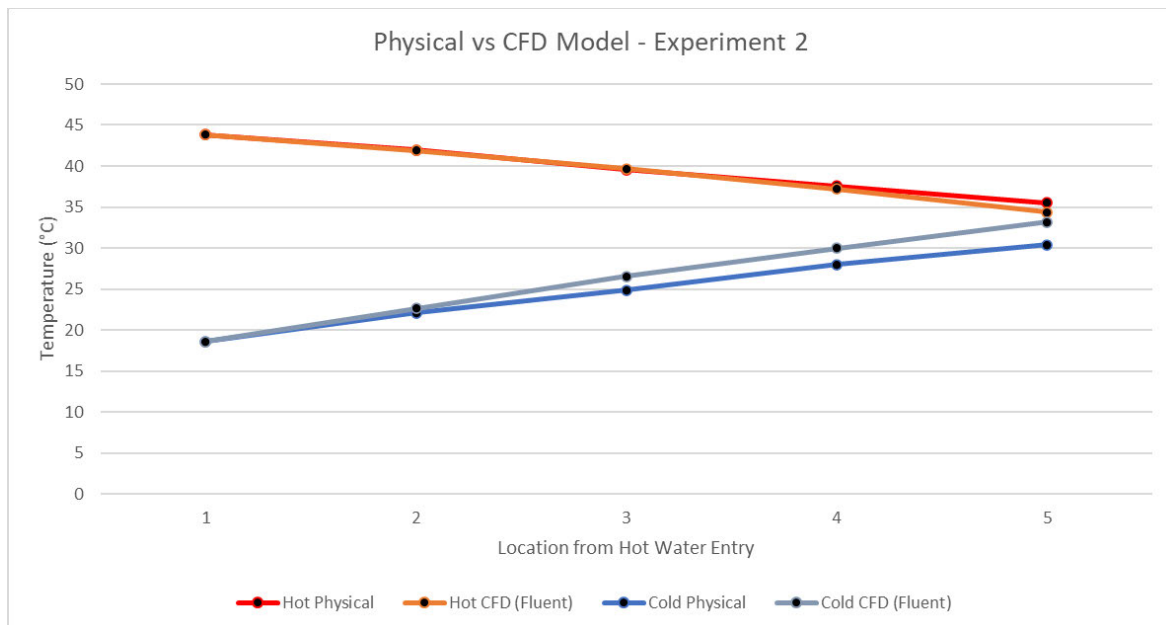


Figure 4-22: Chart showing physical vs CFD results – experiment 2 (2 lpm).

These results give an average error of 1.28% on the hot water system, but 12.02% on the cold-water system. Since the physical system contains less heat overall, it is hypothesized the main difference in these results is due to the assumption the acrylic walls are adiabatic and not suitable. The error was noted to be considerably less in the higher flow experiment, and it is hypothesised this is due to less time for heat losses with the higher flow than in the lower flow experiment.

### 4.3.3 Model Optimisation

To reduce the error between the CFD and physical model, the CFD boundary conditions were updated to include convection losses through the long sections of acrylic wall. In the Fluent module, the “insulated wall” selection boundary condition setup was changed from adiabatic to convection with heat transfer coefficient of

25 W/m<sup>2</sup>.K, ambient temperature of 290K and shell conduction with settings of 0.002m thickness of acrylic material.

Due to the addition shell conduction, which adds elements, the mesh was changed to the setting found optimal in section 4.2.4. The calculations were completed again for both experiment 1 and 2 and compared to the physical models. The results converged with residuals slightly lower than the original models. The results were still not within acceptable error tolerance to verify the model.

During the physical experiment the test equipment was observed to be aged and the hot water circuit was discoloured, indicating surface rust and scale present within the system. The setup procedure of the Armfield instruction manual discussed flowing 80°C water through the system to remove any air bubbles. The experimental jig used could only achieve about 50°C. It is possible air bubbles remained trapped in the system.

The Fluent model was however modelling perfect conditions. This scale, corrosion and fouling would reduce the effectiveness of the heat exchanger as shown in section 2.3, so the thermal conductivity of the stainless steel was lowered to a final value 6 W/(m K). The thickness of the transfer wall was slightly increased and the convection transfer coefficient updated to 50W/m<sup>2</sup>.K. With these changes the CFD model now appeared to better represent the physical experiment.

#### 4.3.4 Results after Optimisation

The results after the optimisation from section 4.3.4 was tabulated to compare to the original physical models as shown in table 4-10 below. For better visualisation they were also plotted as seen in figure 4-23 and 4-24 below.

*Table 4-10: Tabular results comparing physical model vs CFD results after optimisation.*

Comparisen of Physical and CFD modelling after optimisation		Hot Water Flowrate Fhot [l/min]	Cold Water Flowrate Fcold [l/min]	Temp T1 [°C]	Temp T2 [°C]	Temp T3 [°C]	Temp T4 [°C]	Temp T5 [°C]	Temp T6 [°C]	Temp T7 [°C]	Temp T8 [°C]	Temp T9 [°C]	Temp T10 [°C]
Experiment 1	Physical Model	3.02	0.99	48.53	47.03	44.94	43.27	41.41	18.53	23.92	27.81	32.16	35.47
	CFD (Fluent) Model	3.02	0.99	48.53	47.402	46.04	44.372	42.285	18.53	24.841	29.73	33.614	36.74
	Error (%)	0.00%	0.00%	0.00%	0.79%	2.45%	2.55%	2.11%	0.00%	3.85%	6.90%	4.52%	3.58%
Experiment 2	Physical Model	2.96	1.91	43.8	41.94	39.56	37.56	35.52	18.59	22.09	24.88	28.02	30.4
	CFD (Fluent) Model	2.96	1.91	43.8	42.193	40.466	38.603	36.58	18.59	22.037	24.852	27.432	29.827
	Error (%)	0.00%	0.00%	0.00%	0.60%	2.29%	2.78%	2.98%	0.00%	0.24%	0.11%	2.10%	1.88%

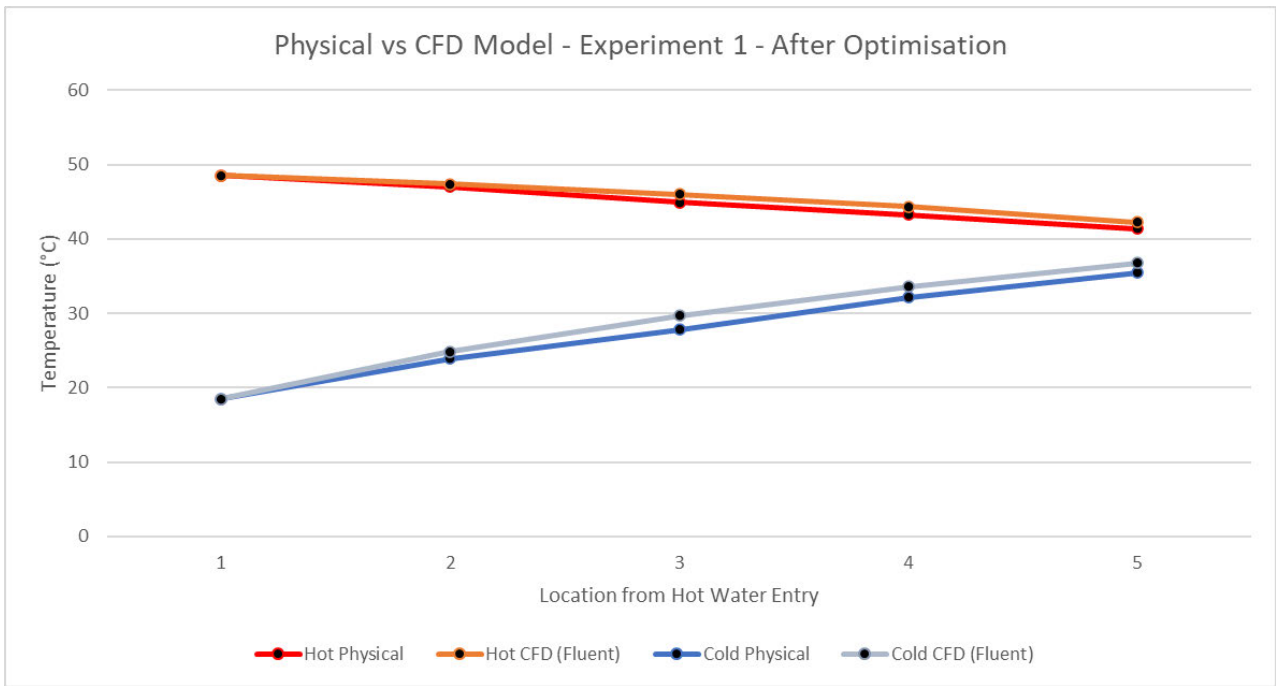


Figure 4-23: Chart showing physical vs CFD results – experiment 1 (1 lpm).

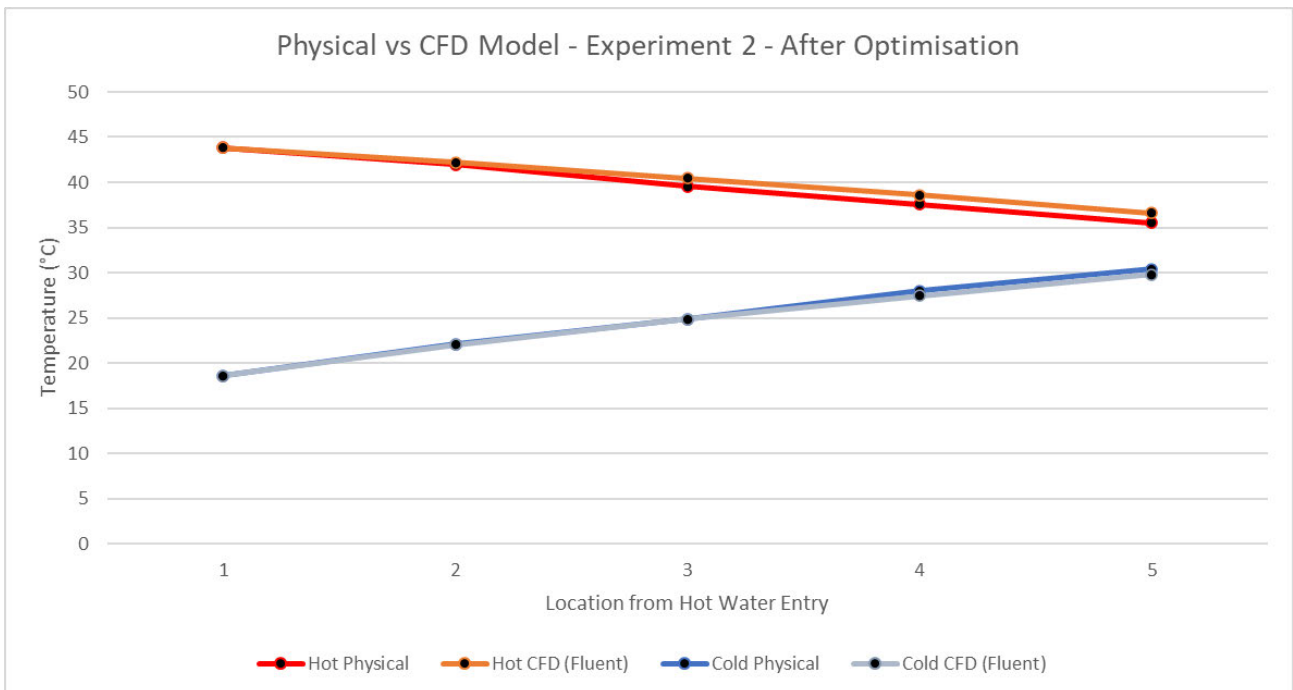


Figure 4-24: Chart showing physical vs CFD results – experiment 2 (2 lpm).

These results give an average error of 2.07% on the hot water system, 2.90% on the cold-water system and 2.48% overall. This is considered acceptable, and the model was validated as these values fall within the accuracy of the equipment used within the Armfield HT36 experiments shown in section 4.3.1.

## 4.4 Phase 4: Global Temperature Distribution with Control Valve

To investigate the control valve impacts on the global temperature distribution throughout the heat exchanger, both physical and CFD experiments were compared and analysed.

### 4.4.1 Physical Model with Control Valve

#### *Design of Experiment*

The test equipment being modelled in the physical experiments with the control valve is the same as used to validate the computational model in section 4.1. Initially physical experimental data was gathered to analyse the effect of the control valve on the global temperature distribution through the heat exchanger.

The test equipment was set up in counter-flow arrangement using all four tubes. The equipment was turned on and the hot water allowed to heat and circulate to purge out any air bubbles. The cold-water side was also allowed to flow and clear out any air bubbles.

Once the setup was complete, the entry conditions were set to pre-determined flow rates and temperatures given in the manual. The flow rates and temperatures throughout the experimental rig were logged using the Armfield HT36 software. These logs were exported for data analysis and compared to the ANSYS model.

The flow rate for the cold water was set to maximum (built in control valve fully open). The butterfly valve at the entry region of the heat exchanger tubes, shown in figure 4-25, was then used to throttle the cold-water flow rate until it reached the test values shown in table 4-11 below.

*Table 4-11: Physical experiment boundary conditions with valve.*

Test Case	Parameter	Value
1	Hot Water In	30°C above cold water temperature
	Hot Water Flow	3 lpm
	Cold Water In	Temperature of the tap water
	Cold Water Flow	1 lpm (manually throttled)

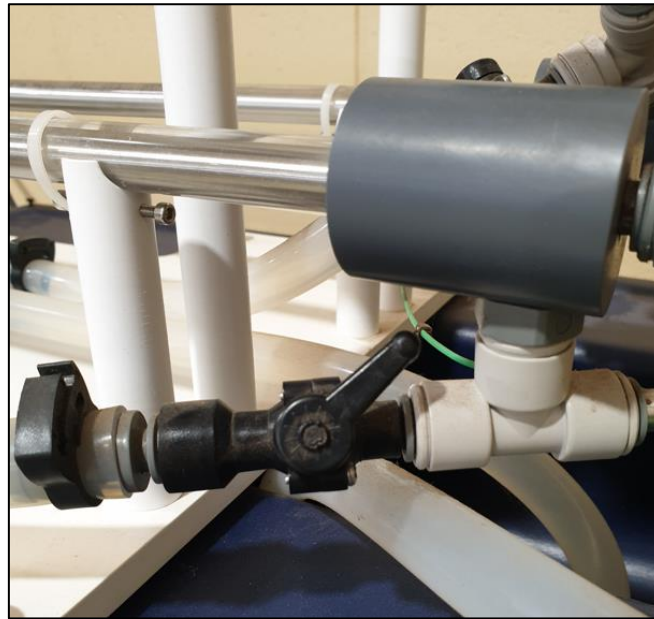


*Figure 4-25: The manual control valve at the heat exchanger entry point.*

### **Experimental HSE Risk**

The experiment for phase 4 was completed on the same day as the experiment in section 4.1. All the same risks and controls were applicable and considered during this experiment. See appendix C for the full risk assessment.

### **Experiment Details**

The experiment was performed in the University of Southern Queensland labs on the morning of 24<sup>th</sup> of May 2021. The ambient temperature was 17°C during the experiment. The experiments were undertaken and completed in accordance with the experiment design. There were no concerns.

### **Results**

The results were recorded using the Armfield software and exported to excel. The tabulated values from the nine records can be seen in figure 4-12 below.

*Table 4-12: Results from physical experiment with the valve.*

Sample Number	Elapsed Time [mm:ss]	Temp T1 [°C]	Temp T2 [°C]	Temp T3 [°C]	Temp T4 [°C]	Temp T5 [°C]	Temp T6 [°C]	Temp T7 [°C]	Temp T8 [°C]	Temp T9 [°C]	Temp T10 [°C]	Hot Water Pump Setting [%]	Hot Water Flowrate Fhot [l/min]	Cold Water Valve Setting [%]	Cold Water Flowrate Fcold [l/min]
1	00:00	48.5	46.8	44.7	43.0	41.0	18.5	23.8	27.8	32.0	35.2	46	2.9	100	0.94
2	00:05	48.5	46.8	44.8	43.1	41.2	18.5	23.9	27.7	31.9	35.2	46	3.0	100	0.95
3	00:10	48.7	47.0	44.8	43.1	41.1	18.5	23.8	28.0	32.0	35.2	46	3.0	100	1.06
4	00:15	48.7	47.1	45.0	43.1	41.2	18.5	23.9	27.7	32.0	35.4	46	3.0	100	0.93
5	00:20	48.5	47.1	45.1	43.3	41.3	18.5	24.2	27.4	32.0	35.4	47	3.1	100	0.95
6	00:26	48.7	47.1	45.0	43.2	41.2	18.5	24.0	27.6	32.2	35.2	46	3.0	100	0.95
7	00:31	48.5	47.1	45.0	43.2	41.2	18.5	24.0	27.6	32.0	35.4	46	3.1	100	0.93
8	00:36	48.7	47.1	45.0	43.2	41.2	18.5	23.8	27.8	32.0	35.4	46	3.0	100	1.04
9	00:41	48.8	47.1	45.0	43.3	41.2	18.5	24.1	27.8	32.1	35.3	46	3.1	100	1.05

These results can be seen to look very similar to the results from physical experiment 1 using the system control valve rather than the manual valve near the entry condition. This was investigated in more depth in section 4.6.

## 4.4.2 CFD Model with Control Valve

### *Base Model*

The base model used was identical to the model optimised during section 4.2, however a control valve was added to the cold-water entry region of the model as described below.

### *Control Valve angle*

To make the comparison of the physical model to the CFD model, the butterfly valve angle needed to be as close as possible to the physical model. As there was no gauge on the valve, the image was loaded into an online protractor tool to measure the angle as shown in figure 4-26 below.

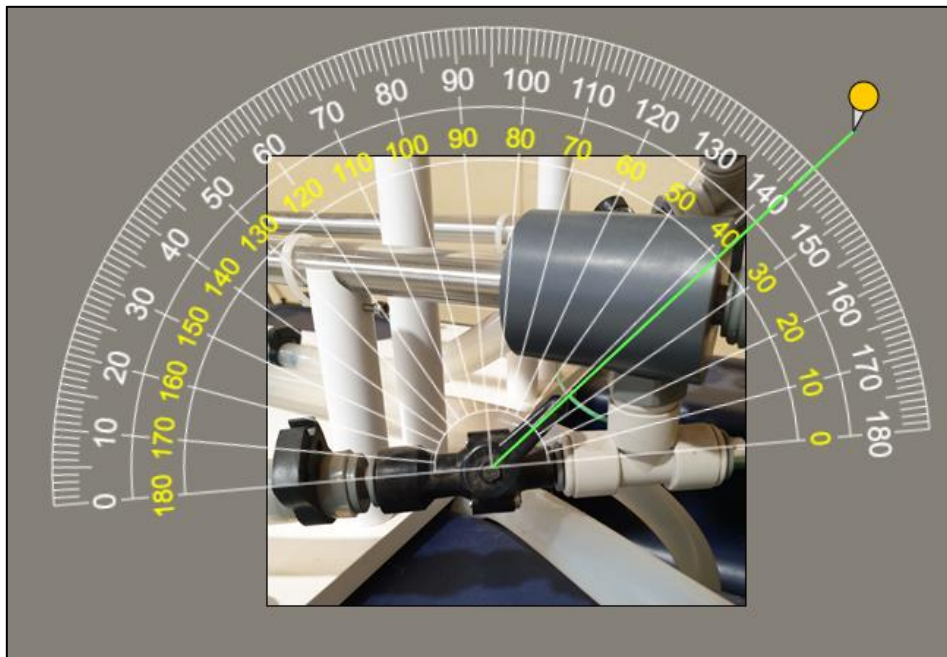


*Figure 4-26: Online protractor tool to measure the valve angle. ([https://www.ginifab.com/feeds/angle\\_measurement/](https://www.ginifab.com/feeds/angle_measurement/) 2021).*

The angle was measured at  $38^\circ$  from fully open or  $52^\circ$  from fully closed.

### *Control Valve Modelling*

The butterfly control valve was added as a simple circular disk and an angle of  $38^\circ$  from the open position. Butterfly valves come in many shapes and sizes with varying levels of complexity depending on their working environment. In the Armfield HT36 experimental jig, the valves are small and plastic so were assumed to be a very simple shape.

The valve was modelled as plane circular cross-sectional extrusion with 0.25mm radius on the edges. The outside diameter is 8.25mm to allow some clearance on the inside diameter of the cold-water fluid, as it was assumed when the valve was open, there would be water passing on all edges as it would be off the seal. The thickness has been selected as 1mm as most valves in industry have about 0.1-0.2 thickness relative to the diameter. The valve was inserted in the centre of the cold-water domain inlet 12mm from the centre of the main pipe.

This control valve body was then subtracted from the cold-water domain using a Boolean subtraction. To be able to add a finer mesh around the valve, the valve was also left in the model as a part. The new part was integrated into the main heat exchanger.

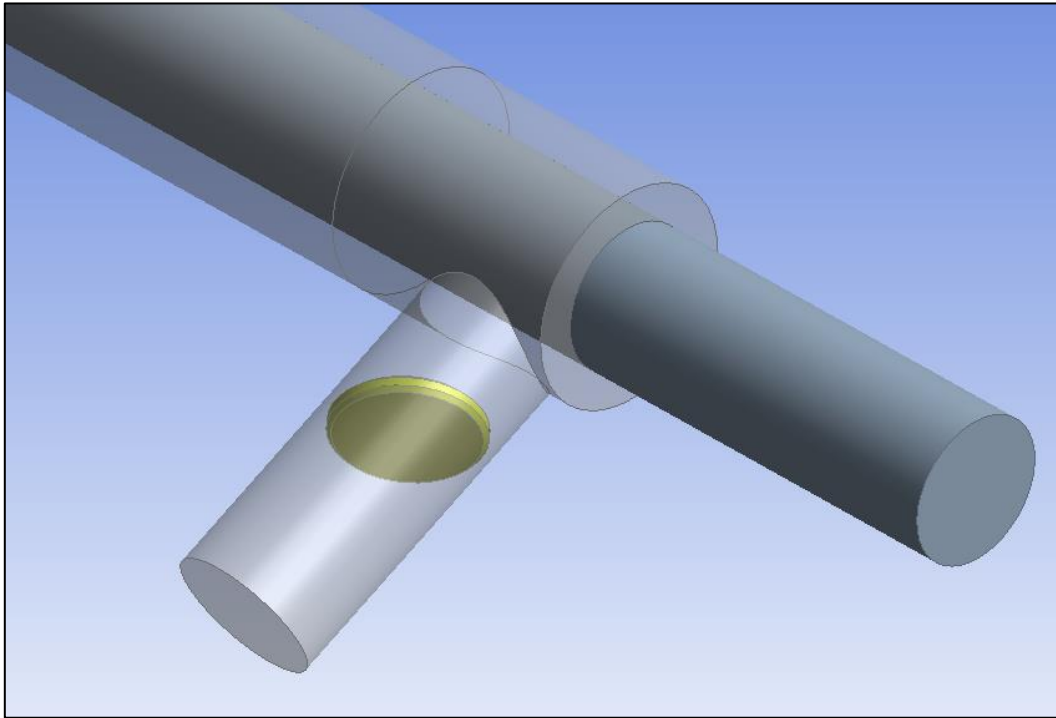


*Figure 4-27: Control valve created in CFD model.*

### **Mesh**

With the mesh left at the optimised values from section 4.3 the mesh can be seen to be inadequate around the valve feature.

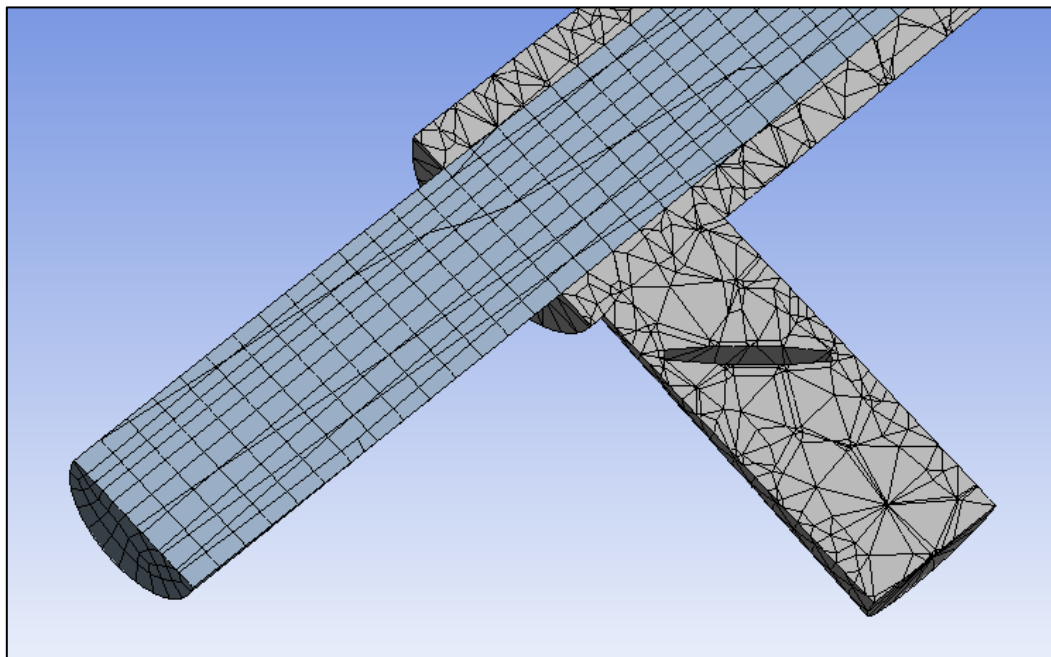


*Figure 4-28: Cross section of the mesh around the valve feature showing inadequate mesh.*

The mesh was refined by creating a 0.15mm face elements mesh feature for the faces of the cold-water domain which contacted the valve body and also on the edge of the cold-water domain in the entry region. After this refinement, the model had a total of 230,000 elements, leaving room for more refinement when we study this region in more detail in section 4.5.

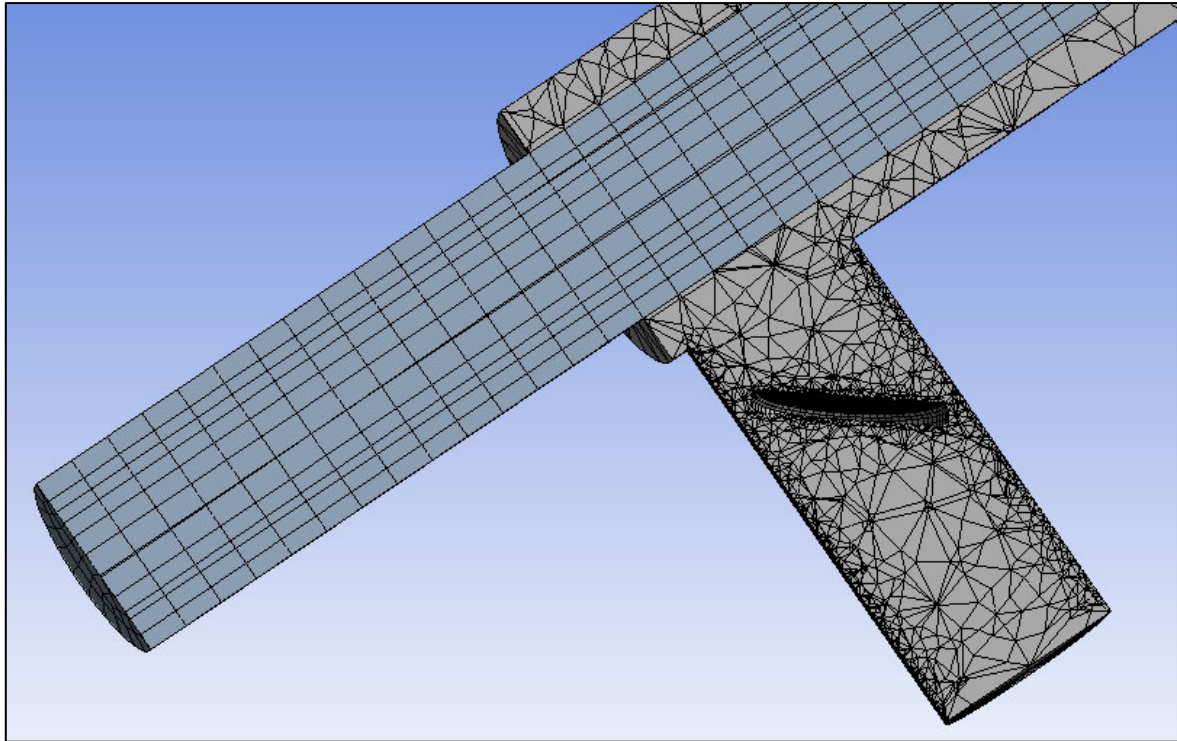


*Figure 4-29: Cross section of the mesh around the valve feature showing refined mesh.*

### **Fluent Setup**

The fluent setups were the same as the models from section 4.2 and 4.3 with some additional settings to the body and transfer wall where the valve has been added to the model. All the material properties from section 4.2.2 were replaced with the optimised values from section 4.3.4 to match the inefficient heat exchanger equipment.

*Table 4-13: ANSYS initial valve model material properties.*

<b>Material</b>	<b>Density (kg/m<sup>3</sup>)</b>	<b>Specific Heat (J/(kg K))</b>	<b>Thermal Conductivity (W/(m K))</b>	<b>Viscosity (kg/(m s))</b>	<b>Heat Transfer Coefficient (W/m<sup>2</sup>.K)</b>
Water @ 20°C	998.2	4182	0.6	0.001003	N/A
Stainless Steel	7900	477	5	N/A	N/A
Insulation (acrylic)	1410	1395	1.5	N/A	N/A
Still Air	N/A	N/A	N/A	N/A	50

The boundary conditions were matched to the physical experiment averaged readings from section 4.4.1 and can be seen in table 4-14 below.

*Table 4-14: ANSYS initial valve model boundary conditions.*

Test Case	Parameter	Value
1	Hot Water In	48.6°C = 321.6K
	Hot Water Flow	3.00 lpm
	Hot Water Mass Flow (calculated)	0.04991kg/s
	Cold Water In	18.50°C = 291.50 K
	Cold Water Out	0.98 lpm
	Cold Water Mass Flow (calculated)	0.01630 kg/s
	Ambient Temperature	17°C = 290 K

The Fluent parameters were setup with similar values/settings as the experiments from section 4.2.

*Table 4-15: ANSYS initial valve model fluent parameter setup.*

Area	Parameter	Comments
Setup – Models	Energy Equation	Turned on.
Setup – Models	Viscous Model	k-epsilon Realizable Enhanced Wall Treatment
Setup – Materials	Fluids	Water-liquid setup
Setup – Materials	Solids	Steel-stainless setup Acrylic setup
Setup - Cell Zone Conditions	Cold water domain Hot water domain	Setup as fluid – water-liquid
Setup - Boundary Conditions	T5 – Hot water out T10 – Cold water out	Setup as mass flow outlet with flow rate matched to the inlet. Pressure outlet was tested with same results
Setup - Boundary Conditions	T1 – Hot water in T6 – cold water in	Setup as mass flow inlet Setup flow rate as normal to boundary with flow rate and temperature as per actual results in 4.4.1
Setup - Boundary Conditions	Insulated Wall – Cold water domain Insulated Wall – Hot water domain	Setup convection heat transfer with acrylic material value and single layer shell conduction of thickness

		0.001m, ambient temperature of 290K
Setup - Boundary Conditions	Convection wall	Setup convection heat transfer with stainless steel material value and single layer shell conduction of thickness 0.0006m, ambient temperature of 290K
Setup - Boundary Conditions	Transfer wall	Setup as coupled transfer with the shadow equivalent. Setup as single layer steel-stainless shell conduction with wall thickness of 0.0013m
Setup - Boundary Conditions	Cold water domain to valve wall	Acrylic with no heat transfer
Solution – Method	Scheme	Coupled
Solution – Monitors	Residuals	All changed to 1E-06
Solution – Initialization	Method	Hybrid Initialization
Run Calculation	Number of Iterations	1000

### Results

The temperature distribution values were extracted from ANSYS Results model. The temperatures at each location were calculated using a function of Mass Flow Average across a cross-sectional cut as can be seen in table 4-16 below.

**Table 4-16:** Temperature distribution reported at fixed locations throughout the heat exchanger.

Test Case	Parameter	Result
<b>1</b>	T1 (Hot In)	321.60 K
	T2 (Hot – bend 1)	320.46K
	T3 (Hot – bend 2)	319.06 K
	T4 (Hot – bend 3)	317.35 K
	T5 (Hot Out)	315.18 K
	T6 (Cold In)	291.50 K
	T7 (Cold – bend 3)	298.01 K
	T8 (Cold – bend 2)	303.05 K
	T9 (Cold – bend 1)	307.02 K
	T10 (Cold Out)	310.22 K

To verify the valve was correctly modelled, the velocity profile was inspected around the valve using a velocity contour on a cut through the X-Y plane of the model. This showed results as expected with higher velocities around the edge of the valve and near-still stops near the centre of the valve and on the pipe edges. The results was noted to have some pixelisation and visible contours likely due to the course mesh.

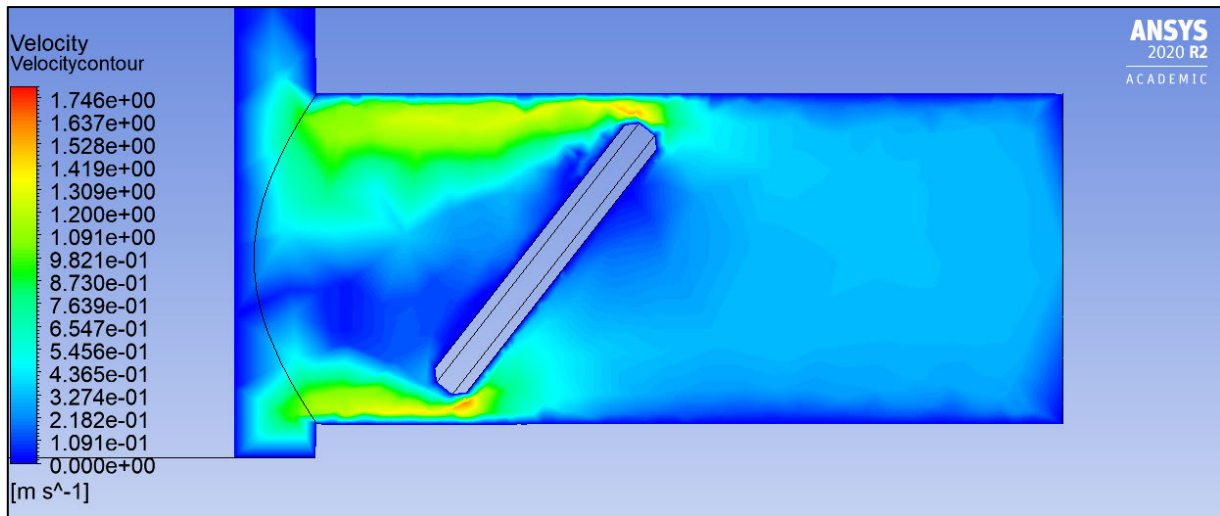


Figure 4-30: Velocity contour around throttling valve to verify modelling.

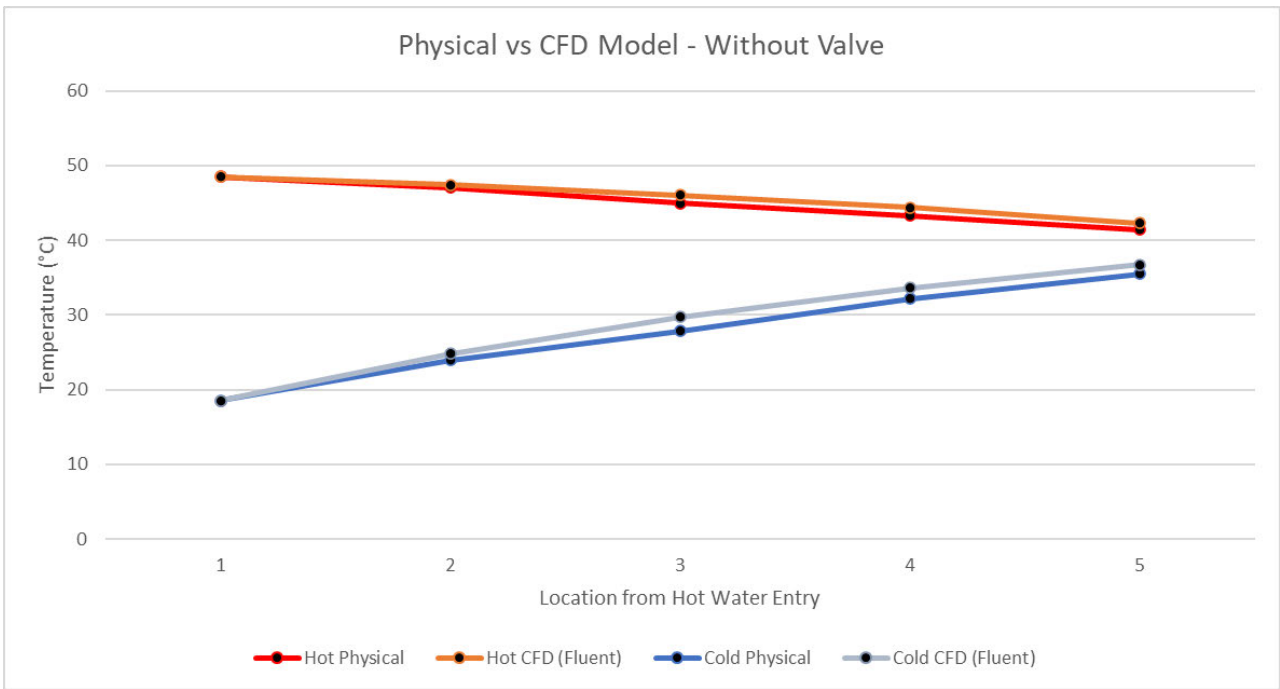
To discuss whether the valve has had any influence of the global temperature distribution throughout the heat exchanger, the results of both the physical experiments and the CFD models has been analysed.

**Physical to CFD Model error**

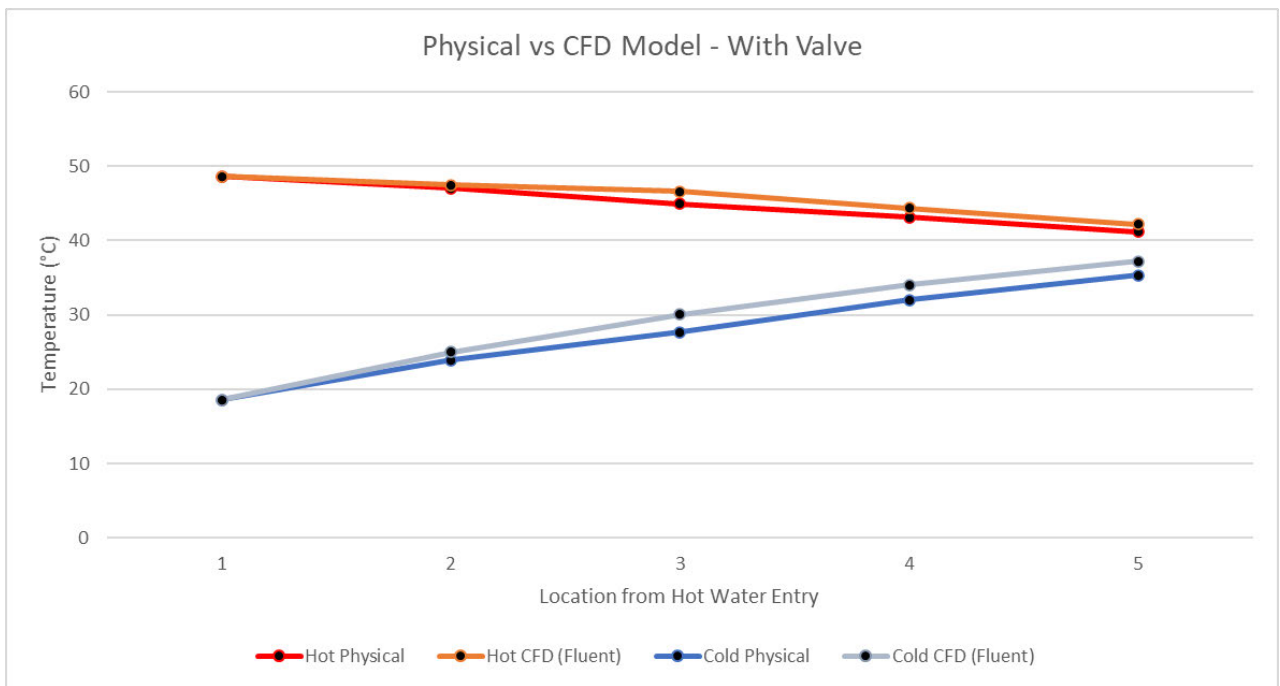
The physical results were tabulated as seen in table 4-17 below. To help visualise the results, the results of each set of experiments were plotted and can be seen in figures 4-31 and 4-32 below.

Table 4-17: Results of the physical and CFD experiment at 11pm with and without the valve.

Comparison of Physical and CFD models with and without valve		Hot Water Flowrate Fhot [l/min]	Cold Water Flowrate Fcold [l/min]	Temp T1 [°C]	Temp T2 [°C]	Temp T3 [°C]	Temp T4 [°C]	Temp T5 [°C]	Temp T6 [°C]	Temp T7 [°C]	Temp T8 [°C]	Temp T9 [°C]	Temp T10 [°C]
Without Valve (From 4.1 & 4.3)	Physical Model	3.02	0.99	48.53	47.03	44.94	43.27	41.41	18.53	23.92	27.81	32.16	35.47
	CFD (Fluent) Model	3.02	0.99	48.53	47.402	46.04	44.372	42.285	18.53	24.841	29.73	33.614	36.74
	Error (%)	0.00%	0.00%	0.00%	0.79%	2.45%	2.55%	2.11%	0.00%	3.85%	6.90%	4.52%	3.58%
With Valve (From 4.4.1 & 4.4.2)	Physical Model	3.00	0.98	48.6	47.0	44.9	43.1	41.2	18.6	23.9	27.7	32.0	35.3
	CFD (Fluent) Model	3.00	0.98	48.6	47.46	46.6	44.35	42.18	18.6	25.01	30.05	34.02	37.22
	Error (%)	0.00%	0.00%	0.00%	0.98%	3.79%	2.90%	2.38%	0.00%	4.64%	8.48%	6.31%	5.44%



**Figure 4-31:** Plot of the results of the physical and CFD experiment at 1lpm without the valve.



**Figure 4-32:** Plot of the results of the physical and CFD experiment at 1lpm with the valve.

The error between the physical and CFD models for the case without the valve was discussed in section 4.3. It was found the models matched within 3.34%. In the case with the valves, it was found that the physical and CFD models matched with an error of 4.37%. Both are accurate enough for this study and fall within the accuracy reliability of the thermocouples used within the physical experiment.

**Models With and Without Valve**

To understand if the valve had influenced the overall temperature distribution throughout the heat exchanger, the physical and CFD models, both with and without the valve, were analysed to see if there were notable differences.

The data was tabulated in a way to allow comparison of the four datasets and display the errors as shown in table 4-18. The physical experiments with and without the valve were compared to each other and this was duplicated for the CFD experiments.

**Table 4-18:** Data comparing the differences between experiments with and without the valve.

Comparisen of Physical and CFD models with and without valve		Hot Water Flowrate Fhot [l/min]	Cold Water Flowrate Fcold [l/min]	Temp T1 [°C]	Temp T2 [°C]	Temp T3 [°C]	Temp T4 [°C]	Temp T5 [°C]	Temp T6 [°C]	Temp T7 [°C]	Temp T8 [°C]	Temp T9 [°C]	Temp T10 [°C]
Physical Model	Without Valve	3.02	0.99	48.53	47.03	44.94	43.27	41.41	18.53	23.92	27.81	32.16	35.47
	With Valve	3	0.98	48.6	47	44.9	43.1	41.2	18.6	23.9	27.7	32	35.3
	Error (%)	0.66%	1.01%	0.14%	0.06%	0.09%	0.39%	0.51%	0.38%	0.08%	0.40%	0.50%	0.48%
	Average Error (entry conditions)	0.55%											
	Average Error (Dependants)	0.31%											
CFD Model	Without Valve	3.02	0.99	48.53	47.4	46.04	44.372	42.285	18.53	24.841	29.73	33.6	36.74
	With Valve	3.00	0.98	48.6	47	44.9	43.1	41.2	18.6	23.9	27.7	32	35.3
	Error (%)	0.66%	1.01%	0.14%	0.85%	2.48%	2.87%	2.57%	0.38%	3.79%	6.83%	4.80%	3.92%
	Average Error (entry conditions)	0.55%											
	Average Error (Dependants)	3.51%											

The physical model revealed the average differences between the temperature at the fixed measurements points was 0.31% and a difference of 0.55% in the entry temperatures and flow rates. In the CFD model it the average differences between the temperature at the fixed measurements points was 3.51% also and a difference of 0.55% in the entry temperatures and flow rates. It is hypothesised the higher percentage error in the CFD model is due to differences in meshing. The model was then optimised specifically for the valveless model rather than an actual effect of the valve in the entry region. This CFD model had slightly higher error compared to the physical model in the previous section.

This data can be visualised in the plots in figure 4-33 and 4-34.

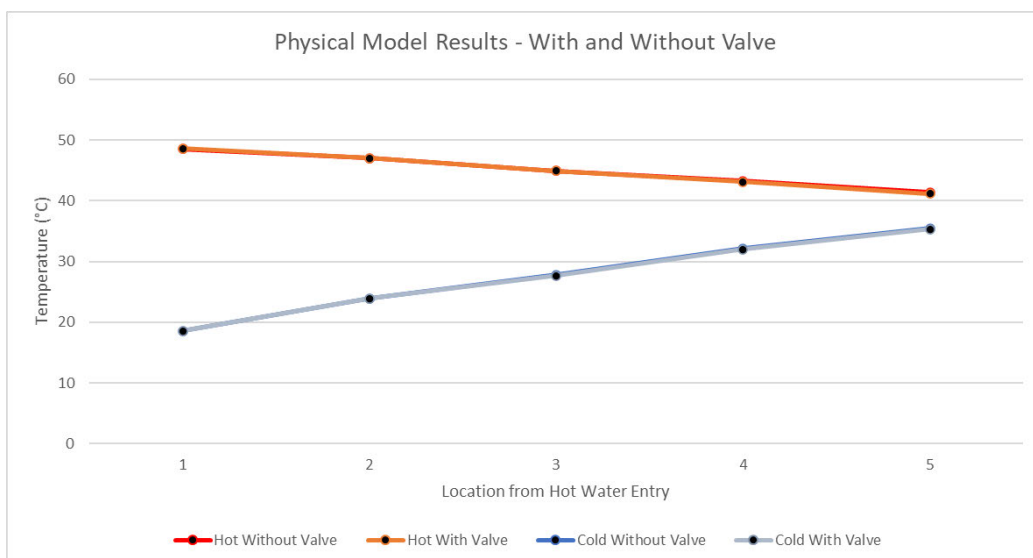


**Figure 4-33:** Plot of the physical experimental results with and without the valve.

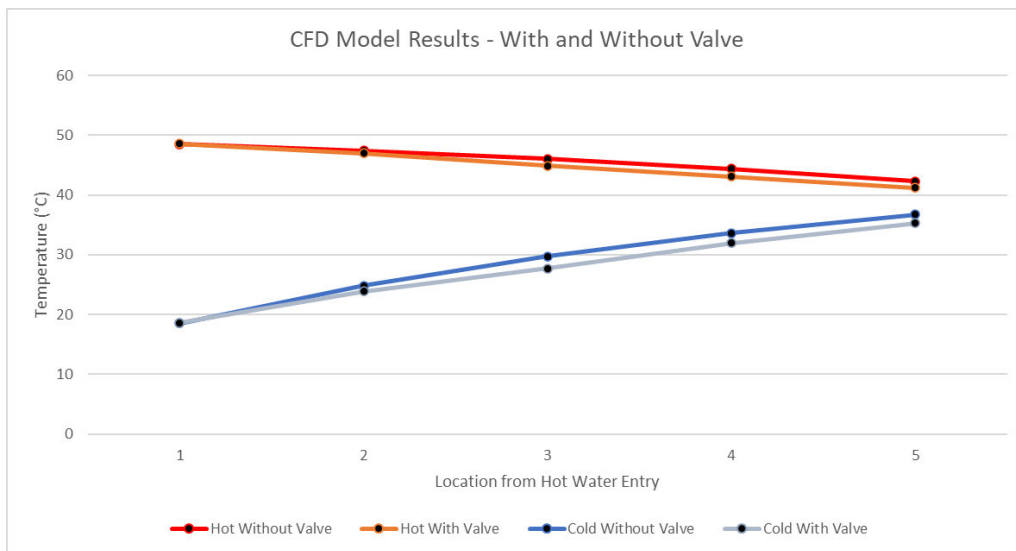


*Figure 4-34: Plot of the CFD experimental results with and without the valve.*

**Findings**

The percentages in temperature differences errors indicate that there is no effect to the global temperature distribution from the control valve in the entry region of the heat exchanger.

## 4.5 Phase 5: Analyse Cold Water Entry Region

In section 4.4 several physical and computational experiments were performed to investigate the effects of the control valve in the entry region of the heat exchanger. In section 4.5 these experiments were further refined with specific analysis around the entry region with and without a valve. Unlike the global level, these cannot be physically measured, so in this section only computational analysis is available. To get better mesh resolution in the areas around the valve and reduce unnecessary calculations in the remainder of the exchanger, a detailed local entry region model was created for the analysis.

### 4.5.1 Design of Experiment

This part of the study determines if the control valve will influence the local heat distribution within the entry region of the heat exchanger. To do this, a 4-stage process was used:

- Create a verified model
- Compare and choose turbulence model
- Completed a mesh independence study to determine suitable mesh to reduce processing time for multiple calculations
- Complete analysis for various valve open positions and compare to model without valve.

The control valve will be modelled at various openings. This is because, in industrial applications, the size of the pump could vary which would result in different valve open positions. The study will be done on the same boundary conditions as the physical experiment from section 4.1 with 11pm cold-water flow.

### 4.5.2 Verification Model Creation

The shape and sizing of the model was kept the same as the global exchanger modelling from section 4, however the model was reduced to a limited section containing the cold-water inlet, hot water outlet and 125mm of the main tube. 125mm was chosen to give adequate length for the turbulence effects of the valve to normalise as shown in the literature review (Song, Wang, Park 2009), (Janusz and Czeslaw 2016). The entrance region for internal turbulent flow is generally assumed to be 10x the tube diameter before the flow is considered fully developed (Cengel & Ghajar 2015), so after this region no further affects from the valve are expected.

#### *Assumptions*

All the material properties will be returned to the ideal values as the global inefficiencies are no longer required for analysis of the local effects of the valve. All external walls will now be considered fully insulated as the global heat losses through these sections are not required for analysis of the local effects of the valve.

### 3D Model

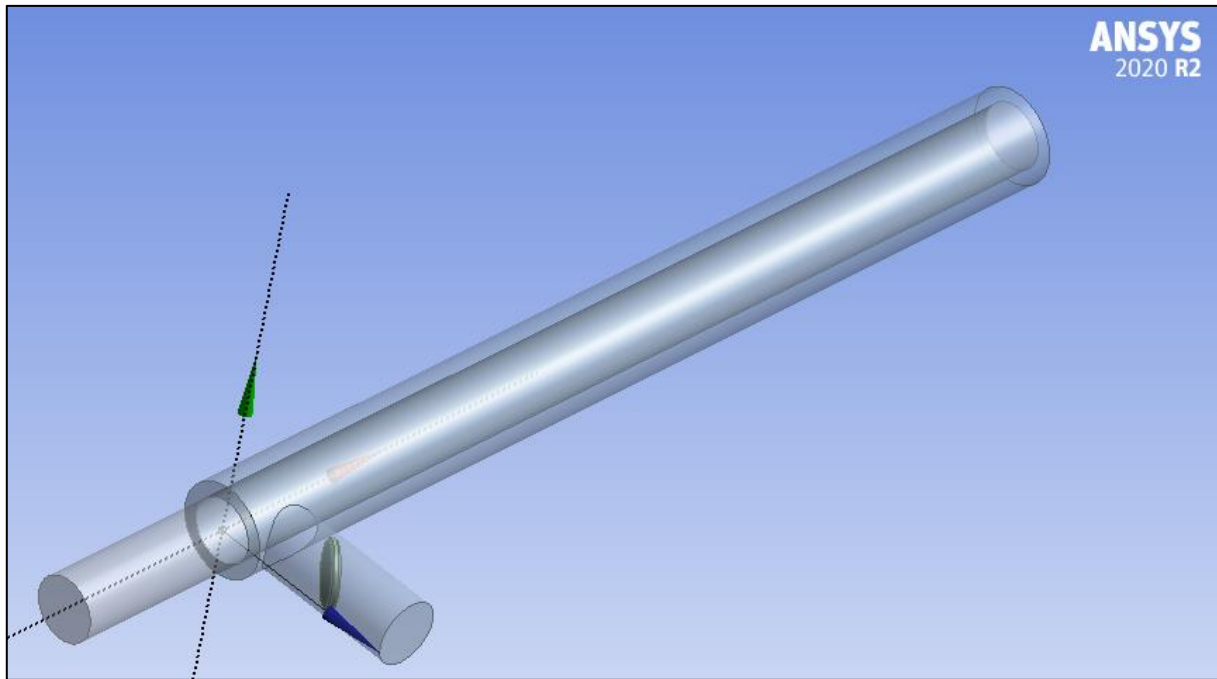


*Figure 4-35: ANSYS model of entry region of the heat exchanger.*

The heat exchanger entry region model is made of three parts:

- Hot water domain: Diameter of 8.325mm, 25mm length protruding past the start of the cold-water domain, 125mm long when aligned with the cold-water domain
- Cold water domain: Diameter of 12mm of the main 125mm length section, diameter of 8.325 feed in section with 5mm offset from the end of the tube
- Valve: 1mm width with 0.25mm chamfers, diameter of 8.25mm to give some clearance on OD to assume not sitting on seal, offset 12.5mm from the main tube centreline with an initial angle of 52°.

These parts were combined in DesignModeler to make a single part with three components.

### Mesh

A mesh was created to get good resolution through the cold-water domain and the transfer wall between the cold and hot water domains. The mesh was optimised to get the maximum number of elements without going over the allowable limit of 512,000 for ANSYS student edition, understanding that also some elements will be generated when using the shell conduction method.

Hot water Domain:

- **Method:** Sweep mesh, using hot water entry face as source and outlet as the target
- **Mesh Type:** All Quad
- **Divisions:** 60
- **Edge Divisions:** 52
- **Bias:** No Bias.

Hot water Domain:

- **Method:** Tetrahedrons
- **Body Sizing:** 0.0007m
- **Face Sizing:** Around the valve – 0.0002m.

Resulting Mesh: 465,279 elements.

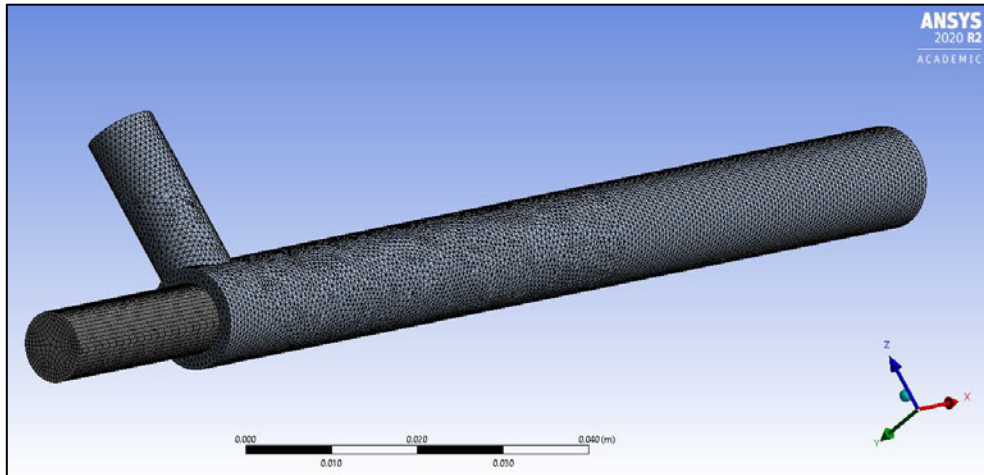


*Figure 4-36: External mesh in ANSYS model of entry region of the heat exchanger.*

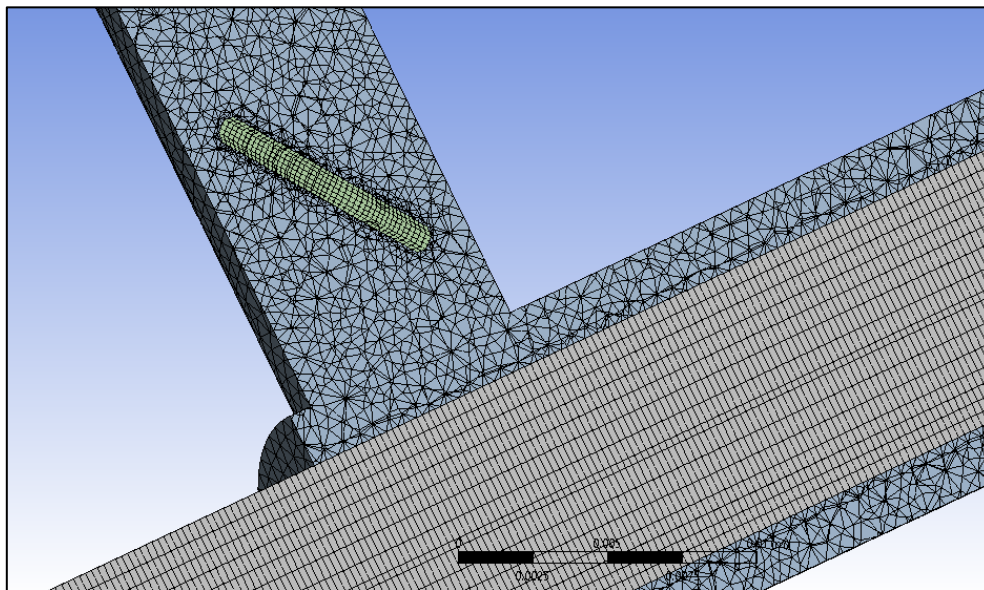


*Figure 4-37: Sectioned mesh of ANSYS model showing detail around valve.*

### Defining Region Names

The key features of the 3D model were named for correct allocation of boundary conditions in the ANSYS module.

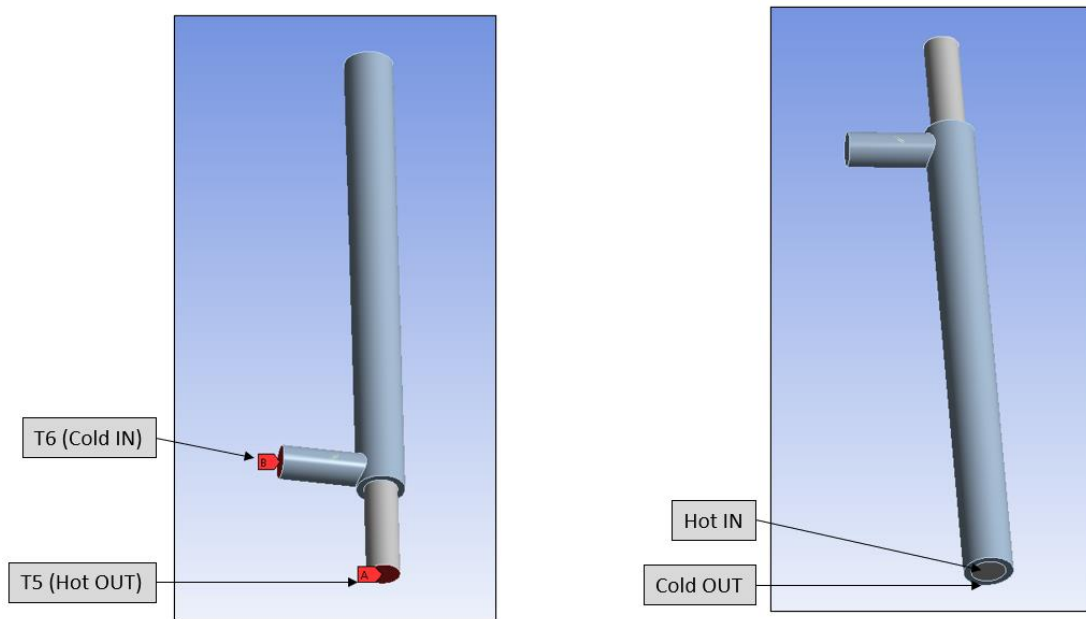


*Figure 4-38: Named sections: hot and cold inlets and outlets.*

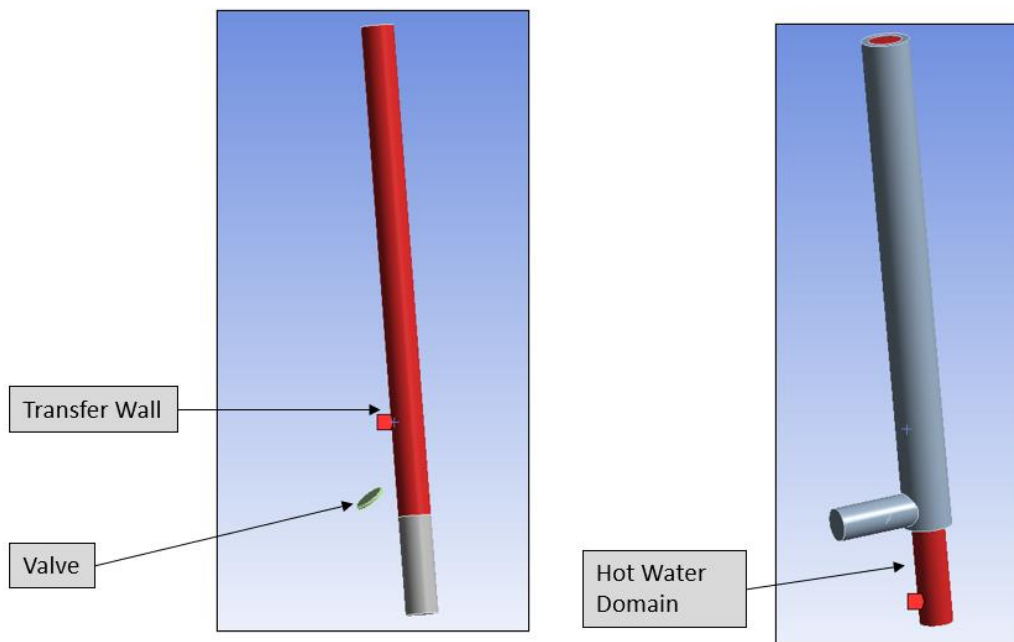


*Figure 4-39: Named sections: transfer wall, valve and hot water domain.*

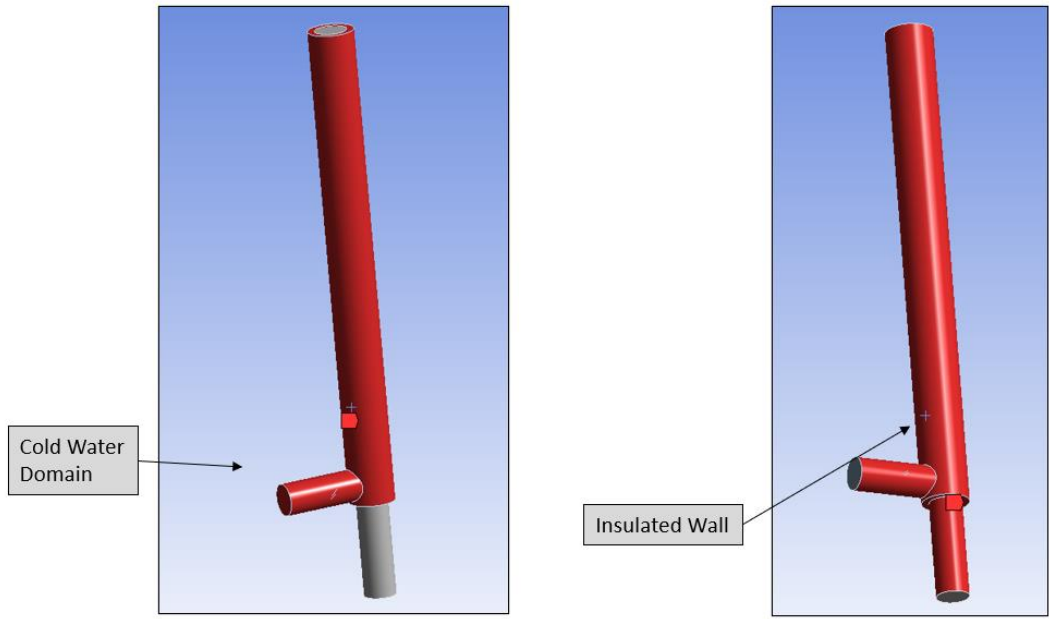


Figure 4-40: Named sections: cold water domain and insulated wall.

**Validation Data from Previous Models**

To get the hot water in temperatures at 125mm from the tube ends, the results from the section 4.3 were analysed.

Table 4-19: Entry region model material properties.

Cold Water Flow Rate	Hot Water IN @ 125mm	Cold Water OUT @ 125mm	Hot water OUT
1 lpm	315.9 K	293.5	315.29 K
2 lpm	310.1 K	292.9	309.58 K

**Material Properties and Boundary Conditions**

Table 4-20: Entry region model material properties.

Material	Density (kg/m <sup>3</sup> )	Specific Heat (J/(kg K))	Thermal Conductivity (W/(m K))	Viscosity (kg/(m s))	Heat Transfer Coefficient (W/m <sup>2</sup> .K)	Source
Water @ 20°C	998.2	4182	0.6	0.001003	N/A	ANSYS Library
Stainless Steel	7900	477	14.9	N/A	N/A	(Cengel & Ghajar 2015)
Insulation (acrylic)	1410	1395	0.2	N/A	N/A	(Dielectric Manufacturing 2020) / (Energy Education 2020)

**Table 4-21:** Entry region model boundary conditions.

<b>Parameter</b>	<b>Value</b>
Hot Water In @ 125mm from origin	315.9 K
Hot Water Flow	3.00 lpm
Hot Water Mass Flow (calculated)	0.04991kg/s
Cold Water In	291.50 K
Cold Water Out	0.98 lpm
Cold Water Mass Flow (calculated)	0.01630 kg/s

**Table 4-22:** ANSYS entry region model Fluent parameter setup.

<b>Area</b>	<b>Parameter</b>	<b>Comments</b>
Setup – Models	Energy Equation	Turned on
Setup – Models	Viscous Model	k-epsilon; Realizable Enhanced Wall Treatment
Setup – Materials	Fluids	Water-liquid setup
Setup – Materials	Solids	Steel-stainless setup Acrylic setup
Setup - Cell Zone Conditions	Cold water domain Hot water domain	Setup as fluid – water-liquid
Setup - Boundary Conditions	T5 – Hot water out Cold water out	Setup as mass flow outlet with flow rate matched to the inlet.
Setup - Boundary Conditions	Hot water in T6 – cold water in	Setup as mass flow inlet Setup flow rate as normal to boundary with flow rate and temperature as per table 4-21
Setup - Boundary Conditions	Insulated Wall – Cold water domain Insulated Wall – Hot water domain	Setup as not heat transfer
Setup - Boundary Conditions	Transfer wall	Setup as coupled transfer with the shadow equivalent. Setup as single layer steel-stainless shell conduction with wall thickness of 0.0006m
Setup - Boundary Conditions	Cold water domain to valve wall	Acrylic with no heat transfer
Solution – Method	Scheme	Coupled
Solution – Monitors	Residuals	All changed to 1E-06
Solution – Initialization	Method	Hybrid Initialization
Run Calculation	Number of Iterations	500

### Convergence of Calculations

After 500 iterations, the approximate average residual values were obtained:

- X, Y Velocities:  $6e-7$
- Z velocity:  $8e-7$
- Continuity equation:  $4E-4$
- Energy equation:  $1.4E-7$
- Epsilon:  $4e-5$
- k:  $4e-6$ .

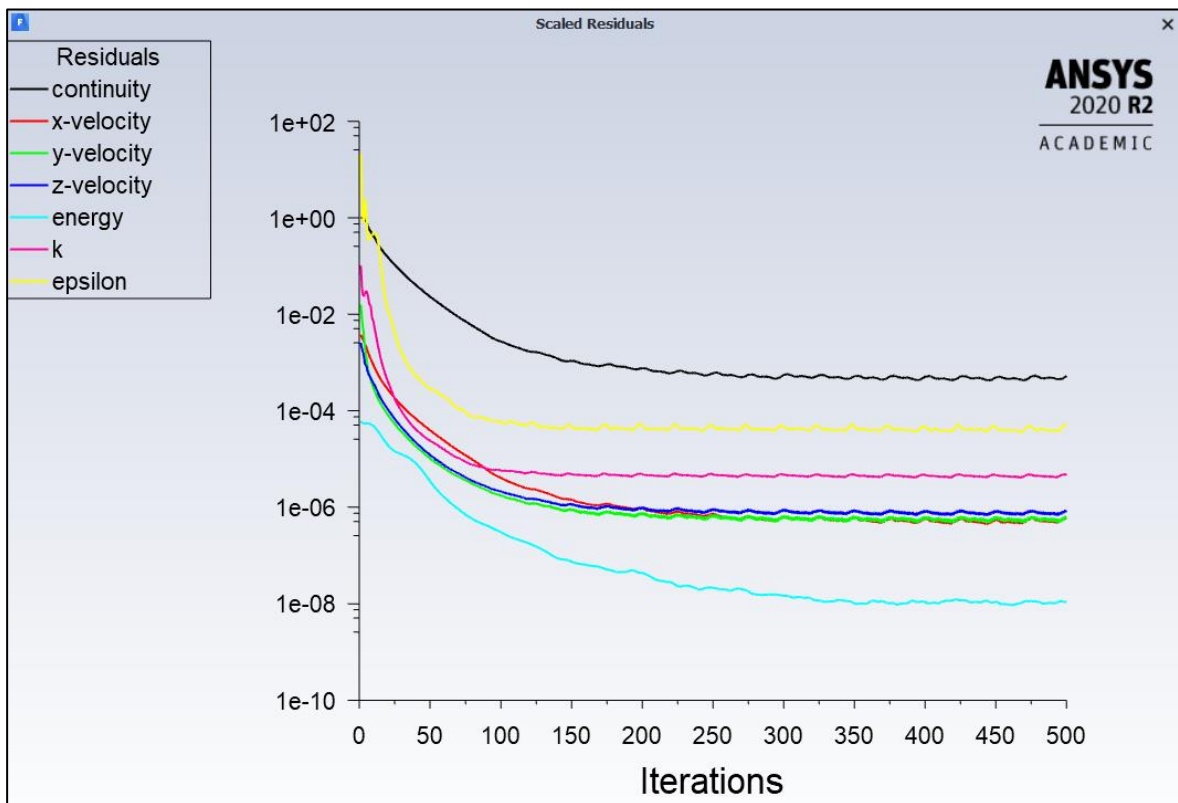


Figure 4-41: Residuals of entry region validation case

### Results

To validate the new entry region model, a few parameters and plots were checked. Firstly, the temperature outlets of the hot and cold temperature were validated against the values from the CFD model in section 4.2.

Table 4-23: Temperature validation of entry region CFD model.

	Data from 4.2	Entry Region Model	Error
Hot Water OUT	315.3 K	315.2 K	0.1 K (0.03%)
Cold Water OUT @ 125mm	293.5 K	293.8 K	0.3 K (0.10%)

Charts were created to validate that the temperature contour across the entry region section of the exchanger is correctly transferring heat from the hot to cold domains.

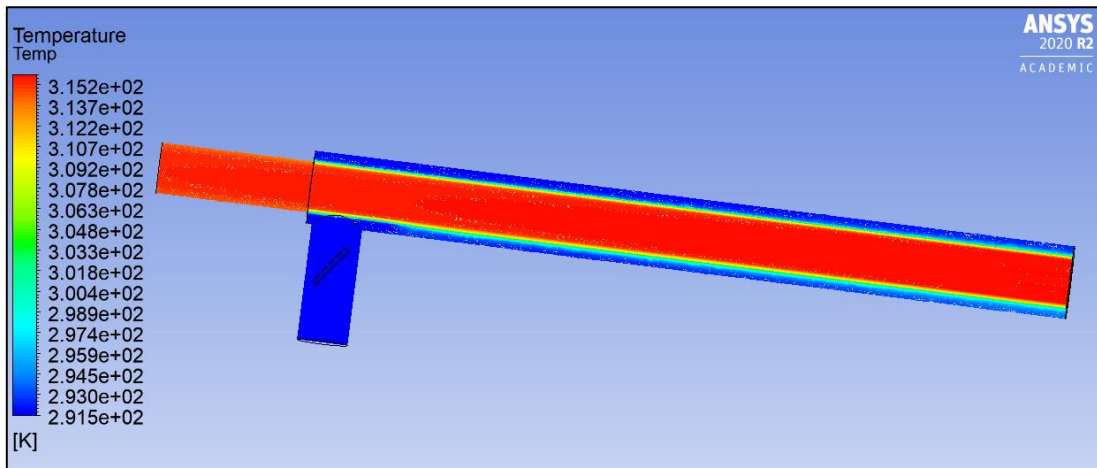


*Figure 4-42: Temperature contour showing correct transfer of heat.*

A velocity contour in the cold-water domain was created around the valve to ensure the model was correctly showing high velocity where the fluid needed to pass around the valve.

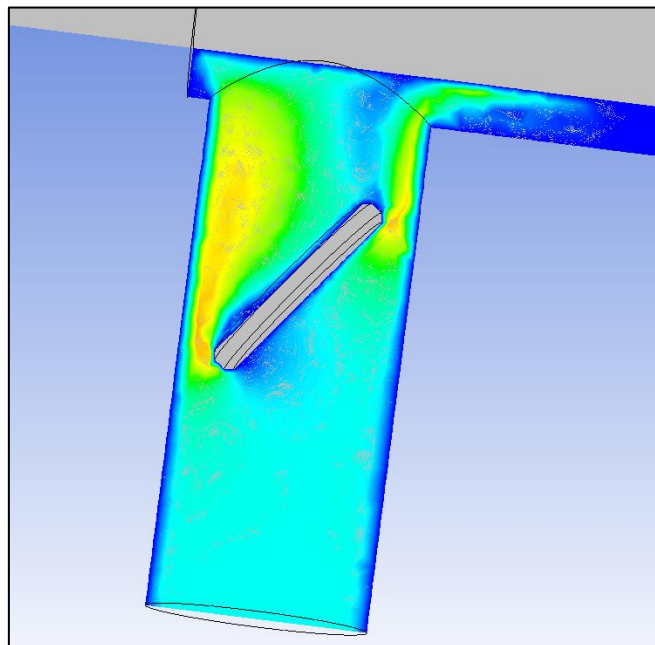


*Figure 4-43: Velocity contour showing expected velocity profile around valve.*

The mass flow rates at the entry and exits of each domain were checked to ensure segregation of the two fluids and ensure there was no gain or loss of mass.

Mass Flow Rate	(kg/s)
cold_outlet	-0.0163
hot_inlet	0.04991
t5_hot_outlet	-0.04991
t6_cold_inlet	0.0163
Net	-5.2041704e-17

*Figure 4-44: Image showing correct balance of mass flow.*

From this analysis, the model was considered to be verified as a working model.

### **4.5.3 Compare Turbulence Model**

As discussed in the literature review, there are various turbulent models within CFD software to model different fluent flows and interactions. Some models are better for modelling fluid flow over an object whilst others better for modelling fluid flow through a pipe. This study includes both flow around the valve object and flow through enclosed pipe, so an easy selection of the correct model cannot be made. Research showed that no single model is better for modelling around a butterfly valve but that each method should be tried and analysed to get the best results (Sung-Woong et al. 2021).

The models that will be considered are the three mainstream models:

- k- $\epsilon$  Model – Options: Realisable and Enhanced Wall Treatment
- k- $\omega$  Model – Default Fluent settings
- k- $\omega$  Model – SST

To see which model produces the results we would expect, the results were inspected for various phenomenon through several result reports:

- 2D streamline of the cold water around the valve
- 3D streamlines of the cold water
- 2D velocity contour
- 2D temperature distribution
- Residuals in the Fluent calculations.

## 2D Streamline

A cut was made on the X-Z plane in the cold-water domain. A surface streamline was created with 300 points.

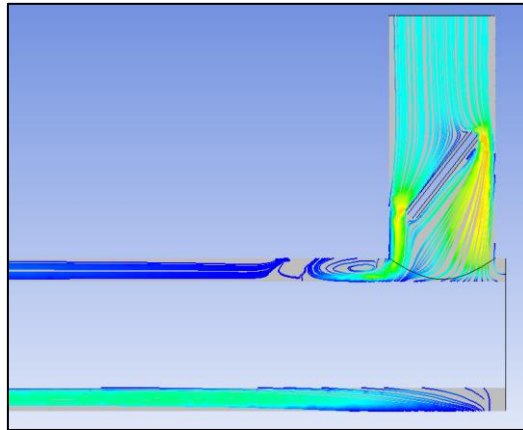


*Figure 4-45: 2D streamline on X-Z plane using  $k-\epsilon$  turbulence model.*

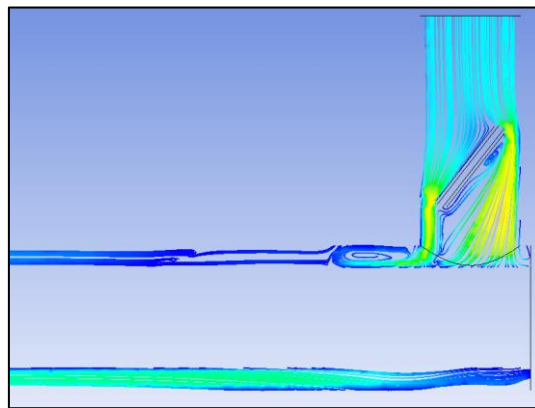


*Figure 4-46: 2D streamline on X-Z plane using  $k-\omega$  turbulence model.*

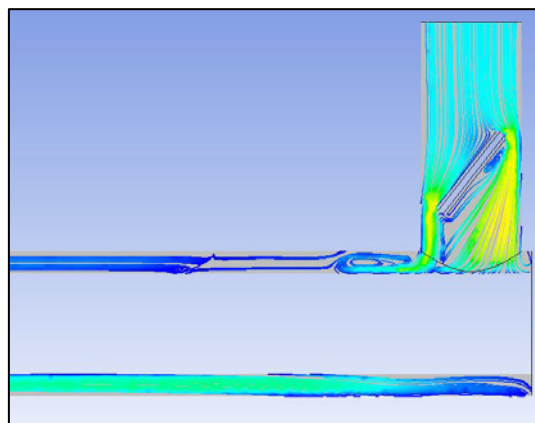


*Figure 4-47: 2D streamline on X-Z plane using SST turbulence model.*

All three models showed very similar results with streamlines around the valve representing expected profile. There were slight differences in the velocity profile after the sharp corner to the top of the main tube image. There were also differences in the velocity profile in the bottom corner of the main tube.

### 3D Streamlines

A 3D streamline was created with 300 points.

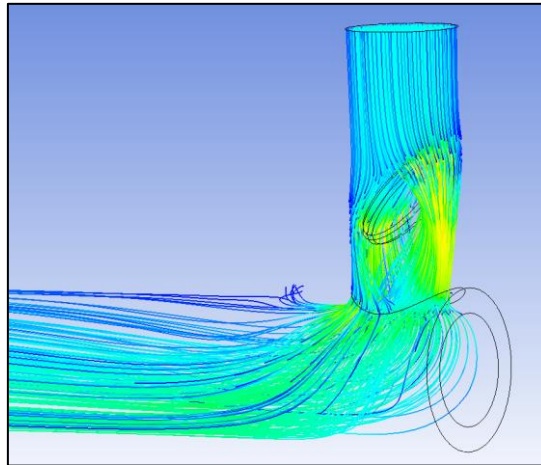


*Figure 4-48: 3D streamline using  $k-\epsilon$  turbulence model.*

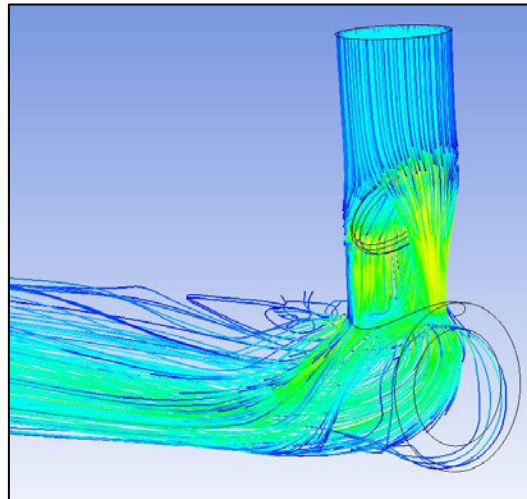


*Figure 4-49: 3D streamline using  $k-\omega$  turbulence model.*

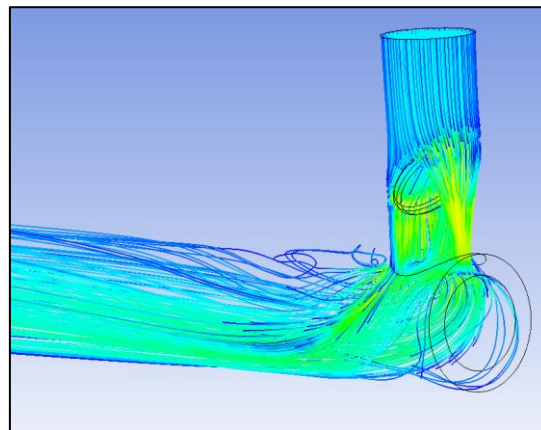


*Figure 4-50: 3D streamline using SST turbulence model.*

The 3D streamlines showed a much calmer velocity profile in the top of the main tube after the sharp corner with the  $k-\epsilon$  model. The two  $k-\omega$  models were similar with the standard model showing more turbulence.

## 2D Velocity Contour

A cut was made on the X-Z plane in the cold-water domain and a surface velocity contour was created with 100 contours.

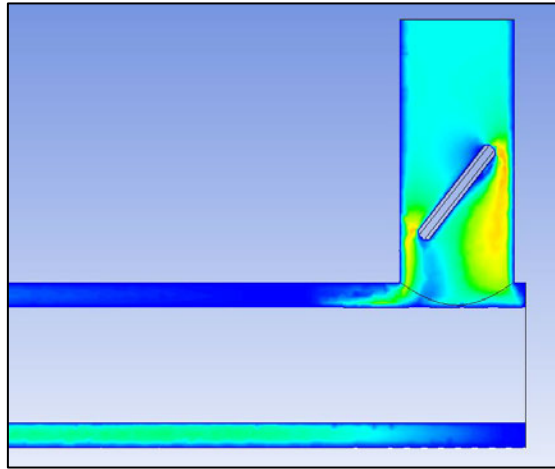


Figure 4-51: 2D velocity contour on X-Z plane using  $k-\epsilon$  turbulence model.

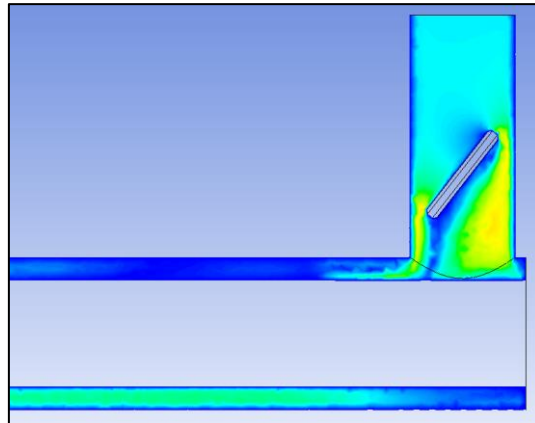


Figure 4-52: 2D velocity contour on X-Z plane using  $k-\omega$  turbulence model.

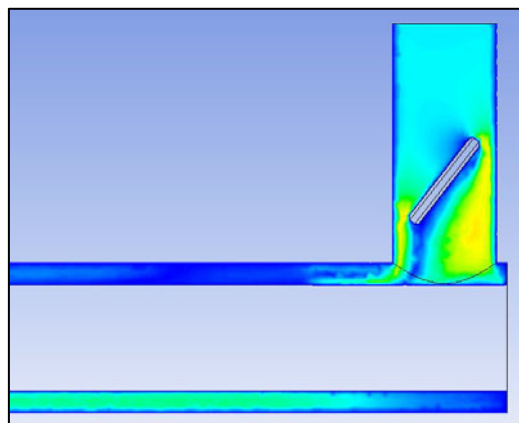
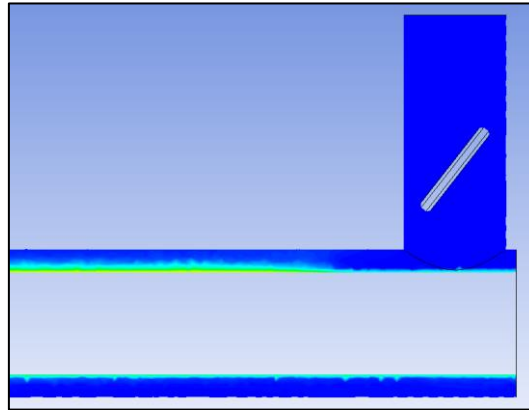


Figure 4-53: 2D velocity contour on X-Z plane using SST turbulence model.

There was no significant visually difference in the velocity contours between turbulence models.

## 2D Temperature Distribution

A cut was made on the X-Z plane in the cold-water domain and a temperature contour was created with 100 contours.



*Figure 4-54: 2D temperature contour on X-Z plane using  $k-\epsilon$  turbulence model.*

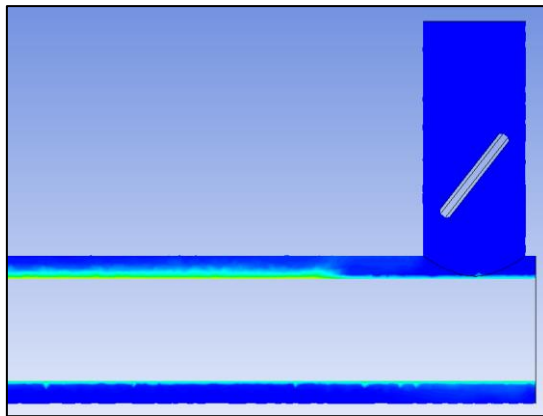


*Figure 4-55: 2D temperature contour on X-Z plane using  $k-\omega$  turbulence model.*

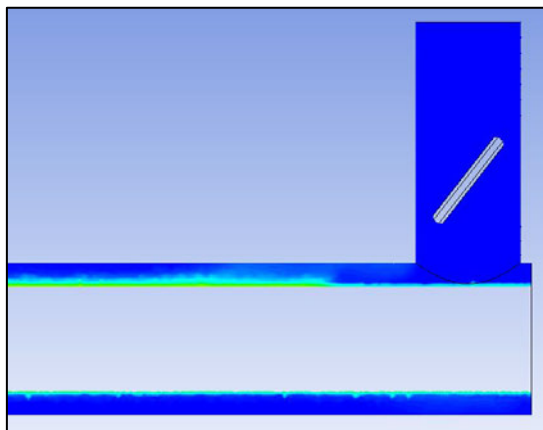


*Figure 4-56: 2D temperature contour on X-Z plane using SST turbulence model.*

There was no significant visual difference in the temperature contours between turbulence models.

### **Fluent Residuals**

Each set of calculations used identical geometry, mesh, material properties, setup, and boundary conditions with the only deviation being the turbulence model used. To compare the validity of the results, the Fluent scaled residuals were compared to ensure the results converged.

*Table 4-24: Summary of approximate scaled residuals for the different turbulence models.*

	<b>k-ε Model</b>	<b>k- ω - Standard</b>	<b>k- ω - SST</b>
Continuity	4.5E-4	2.6E-3	1.6E-2
X-velocity	5.0E-7	3.1E-6	1.8E-5
Y-velocity	5.0E-7	2.0E-6	1.0E-5
Z-velocity	7.0E-7	2.2E-6	1.0E-5
Energy	1.0E-8	1.2E-7	6.3E-7
K	4.5E-6	8.0E-6	5.0E-5
Omega/Epsilon	4.0E-5	2.1E-5	1.0E-4
Comments	Best – Considered Converged	Considered Converged	1 order of magnitude less

All three methods produced similar results that would appropriate for this study, however the velocity streamlines from the **k-ω** models seemed to be the most realistic following the sharp corner. With the SST model not converging appropriately, the standard **k-ω** model was chosen as the turbulence model for section 5 of this study.

#### **4.5.4 Mesh Independence Study**

A mesh independence study was performed to ensure the results being obtained were stable and correct. Since many computations were to be performed a mesh independence study was completed to find a mesh size suitable for getting accurate calculates whilst minimizing computation time to complete the study. To complete this study, 14 fluent studies were run with various mesh sizing and the results tabulated. The model from 4.5.2 was used with the **k-ω** turbulence model from section 4.5.3 for the independence study.

Three resulting categories were reviewed and compared.

- **Convergence Error Representation:** Each study was compared to the baseline for the X,Y&Z velocity, continuity equation and energy equation residuals. To compare to the baseline, any value larger than the baseline was averaged and compared to the baseline in percentage error
- **Wall Pressure:** The wall pressure of the hot and cold domains 30mm from the start of the main tube was compared to the baseline as a percentage error
- **Mass Flow Rate:** The mass flow rate of the hot and cold domains 30mm from the start of the main tube was compared to the baseline as a percentage error
- **Element Reduction:** Each study was compared to the based for the total elements generated through the mesh setup. The mesh was compared to the baseline using a percentage

- A subject visual inspection of the streamlines around the valve and following the sharp corner was also performed to ensure no unusual results were being missed at lower mesh element counts.

The full results of the mesh independence study can be found in Appendix E. The resulting elements were plotted against the dependant variables to determine if the study was mesh dependant. Analysis of the results in figure 4-57 below shows that the results are mesh dependant and stability is achieved with a mesh count of approximately 375,000 elements.



Figure 4-57: Mesh independence study results showing stability after approximately 375,000 elements.

Since this is not significantly reducing the elements amount and accuracy is important for this study, the mesh was left at the max element settings.

Hot water Domain:

- **Method:** Sweep mesh, using hot water entry face as source and outlet as the target
- **Mesh Type:** All Quad
- **Divisions:** 60
- **Edge Divisions:** 52
- **Bias:** No Bias.

Hot water Domain:

- **Method:** Tetrahedrons
- **Body Sizing:** 0.0007m
- **Face Sizing:** Around the valve – 0.0002m.

Resulting Mesh: 465,279 elements.

#### 4.5.5 Comparative model without Valve

To investigate if any local hot spots are due to the valve or not, a control model was created without the valve in the entry region. This control model was the same with the only adjustment being the removal of the valve feature. The mesh was re-generated without the face sizing as the valve no longer exists in this model, resulting in 426,856 elements.

The Fluent software was setup with the same boundary conditions, material properties and configurations as the model with the valve including the use of the **k- $\omega$**  standard turbulence model. The calculation was run with 500 iterations. The results without the valve are in the figures below.

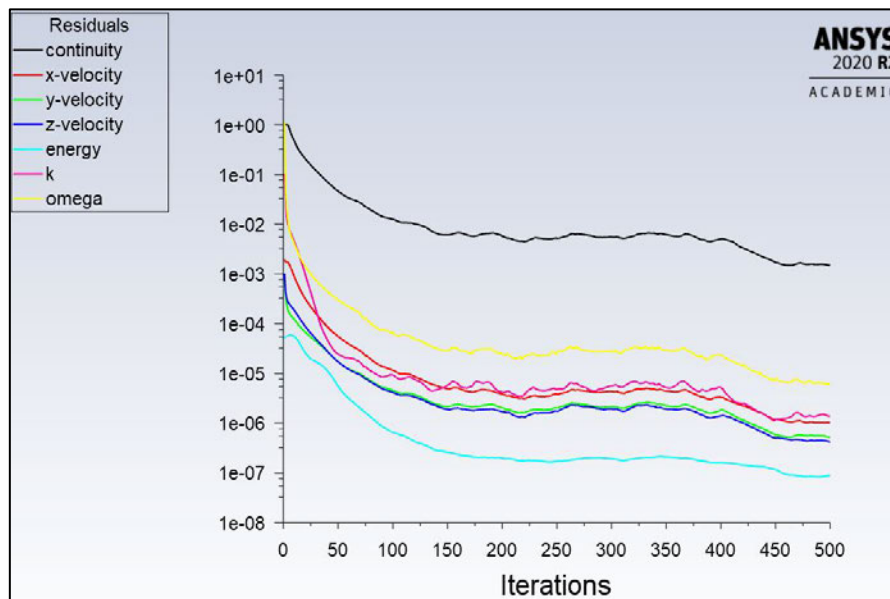


*Figure 4-58: Residuals for the entry region model without valve.*

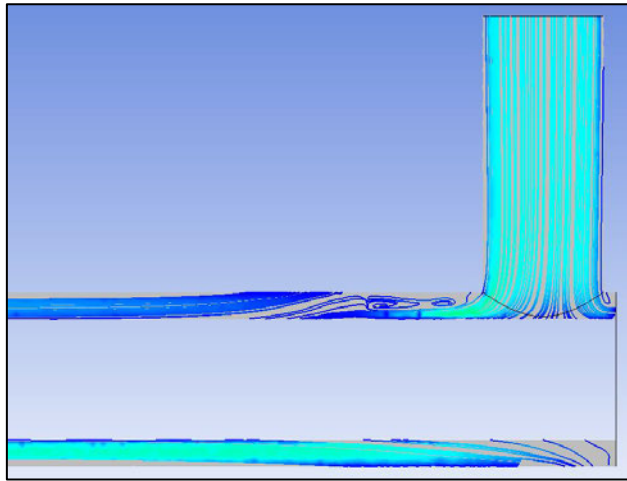


*Figure 4-59: 2D velocity streamlines for the entry region model without valve.*

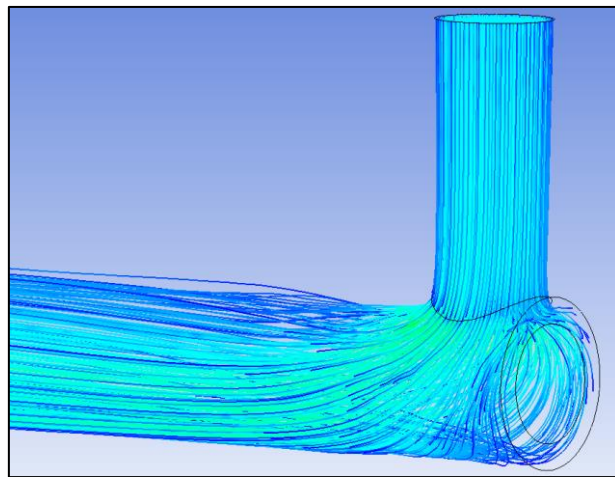


*Figure 4-60: 3D velocity streamlines for the entry region model without valve.*

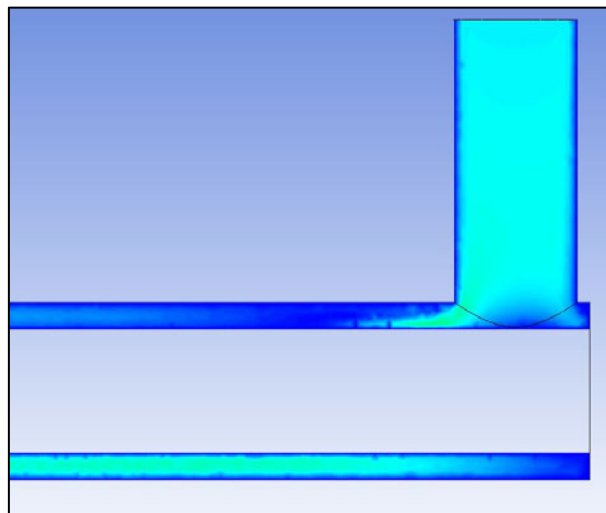


*Figure 4-61: 2D velocity contour for the entry region model without valve.*

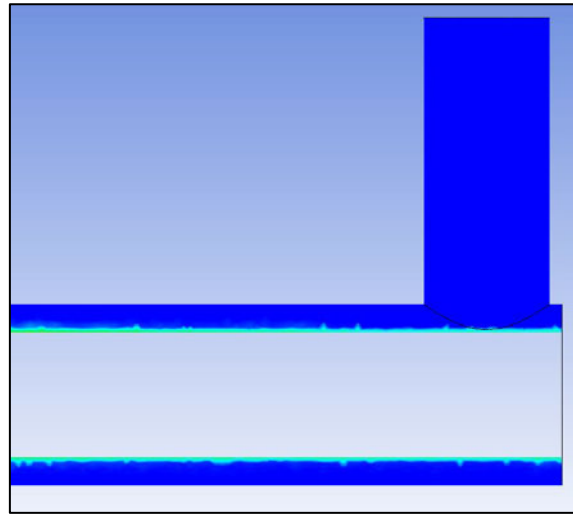


*Figure 4-62: 2D temperature contour for the entry region model without valve.*

#### 4.5.6 Analysis

Cross-section cuts were made through the CFD models, and the lowest, highest, and average temperatures analysed between the two scenarios. As the heat distribution is likely to be most affected closest to the valve, cuts were made every 1mm for the first 12mm, 2mm for the next 12mm and 5mm up to 49mm from the cold-water domain start wall. As the fouling is most likely to occur in the hot water side, the measurements were taken by creating the cut with a radius of 4.5mm in the cold-water domain, resulting in a sample of <1mm from the transfer wall as shown in figure 4-63 below.

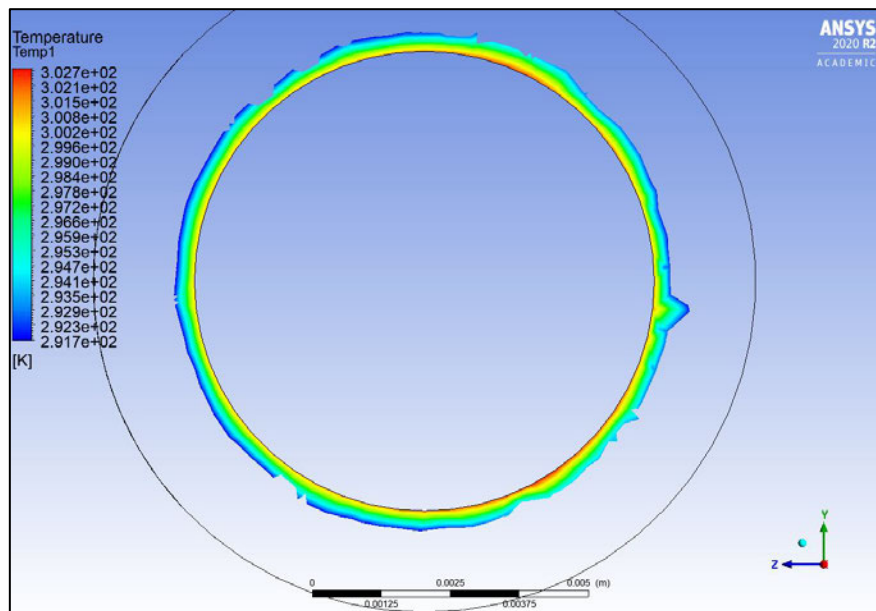


*Figure 4-63: Example of sample cut to measure min, max and average temperature close to transfer wall.*

Data was collected from multiple experiments at various valve open positions to investigate if valve position influences the heat distribution. The angles chosen were 15°, 30°, 45° and 60° from the valve being fully open. Note: 75 degrees was attempted, however the gap around the valve was too small causing flow to stop and the calculations did not converge.

To get the values, the function calculator in the ANSYS results module was used at each cut location for each of the models. For maximum temperature the “maxVal” function was used, for minimum temperature the “minVal” function was used, and for average temperatures the “massFlowAve” function was used.

**Results**

The ANSYS experiments were completed and the data tubulised which can be seen in full in appendix F. To analyse the data the temperature results were compared across the various valve positions. Figure 4-64 shows the minimum temperatures in the wall region for each model. This data shows very little variation in minimum temperature with less than 1 degree difference at any location along the test length. Figure 4-65 shows the maximum temperatures in the wall region for each model. This data shows significant variation between the baseline data and the data from the valves with the highest angle from fully open. This data is discussed in more detail later in this section. Figure 4-66 shows the average temperature in the wall region for each model. This data shows very little variation in the average temperatures between each model. Two outliers can be seen and are being considered irrelevant to the study due to this location being right near the sharp corner and an understanding that the average temperature would not really fluctuate to that degree.

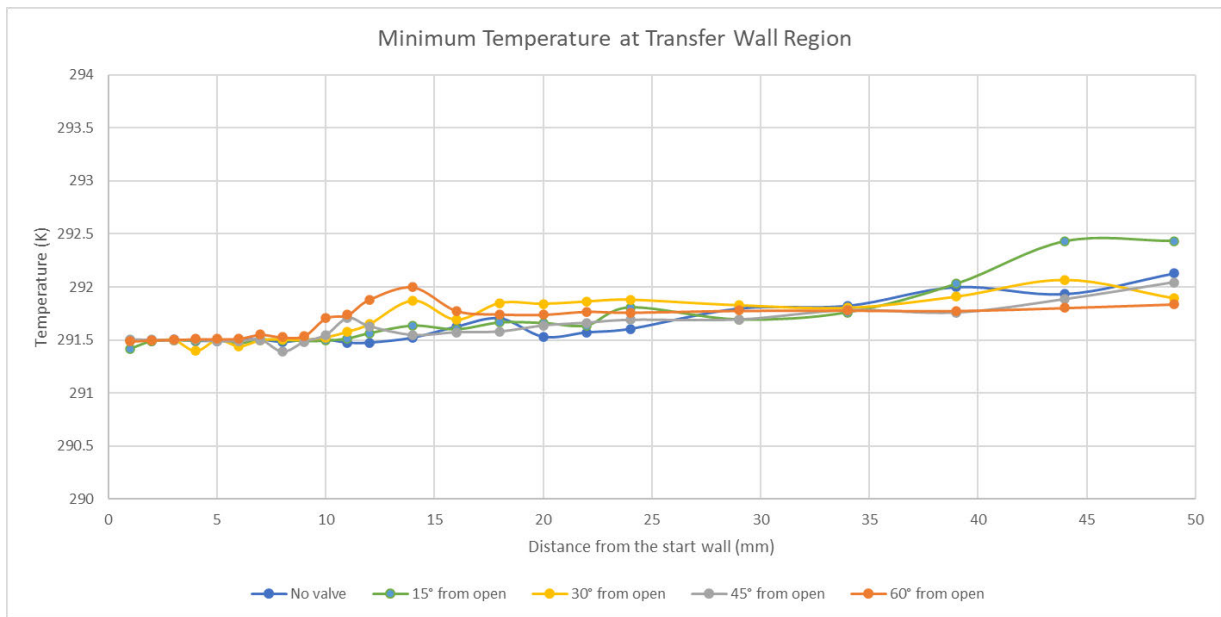


**Figure 4-64:** Minimum temperature at the transfer wall region at various valve positions.

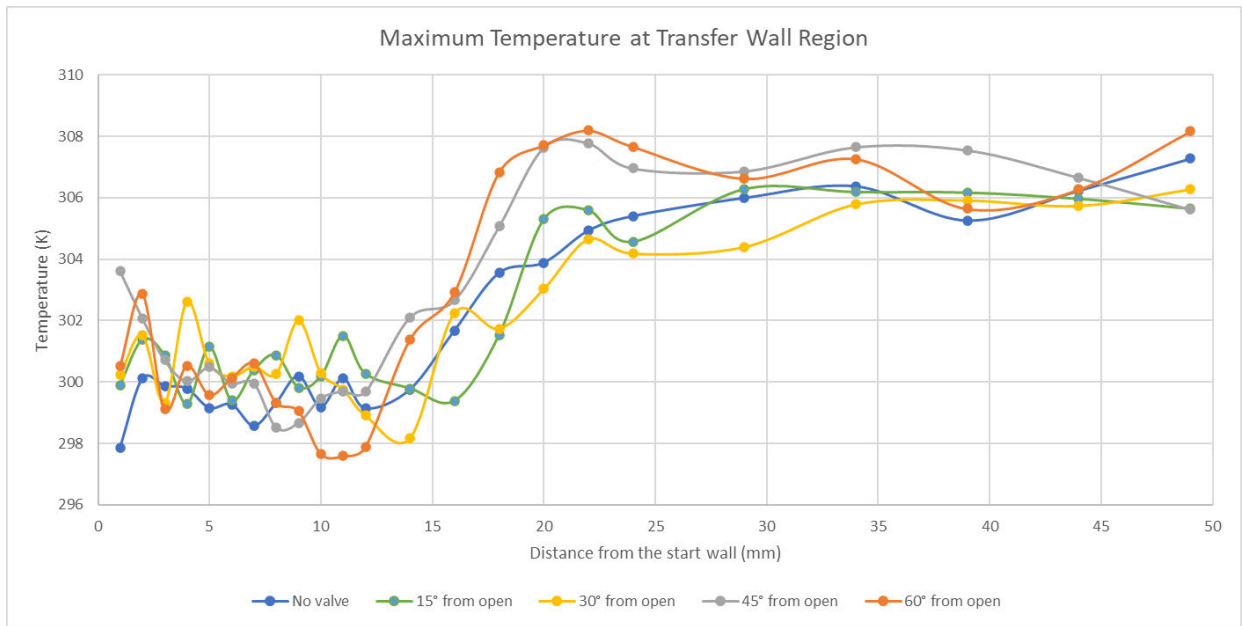


**Figure 4-65:** Maximum temperature at the transfer wall region at various valve positions.

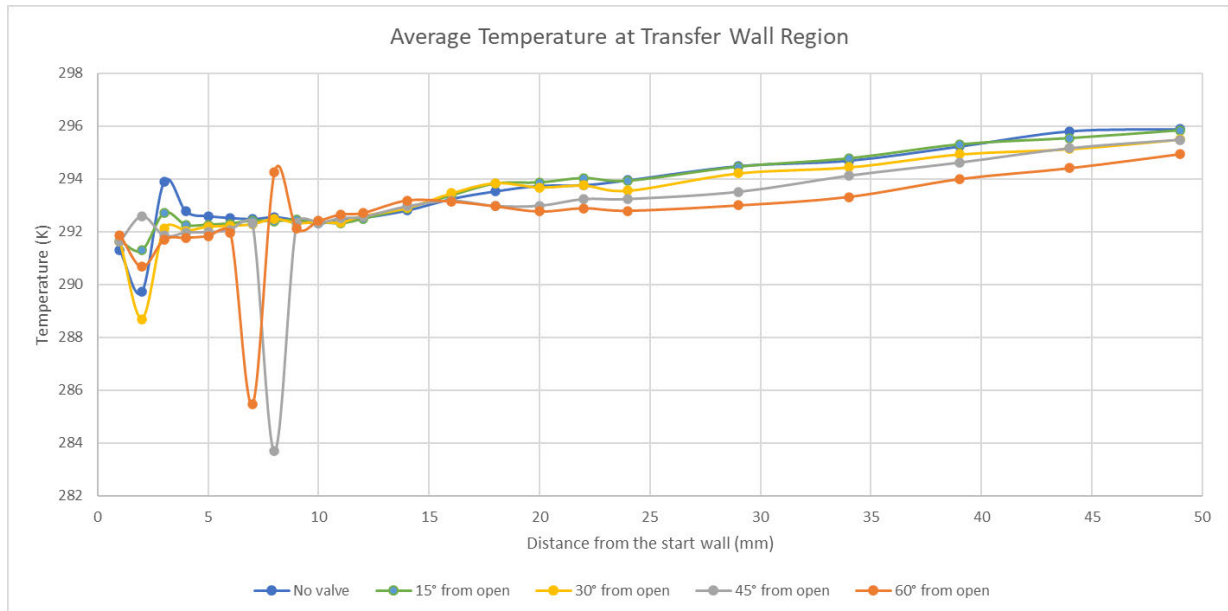


**Figure 4-66:** Average temperature at the transfer wall region at various valve positions.

Figure 4-65 shows that the maximum temperatures of the different valve position trendlines seem to fluctuate significantly in the first 15mm of tube crossing each other and not showing any notable trend. This is shown in more detail in figure 4-67 below. Each valve positions temperature trend then takes an independent path between 15mm and 30mm from the start of the tube with significant variation between valve position trends. This is shown in more detail in figure 4-68 below.

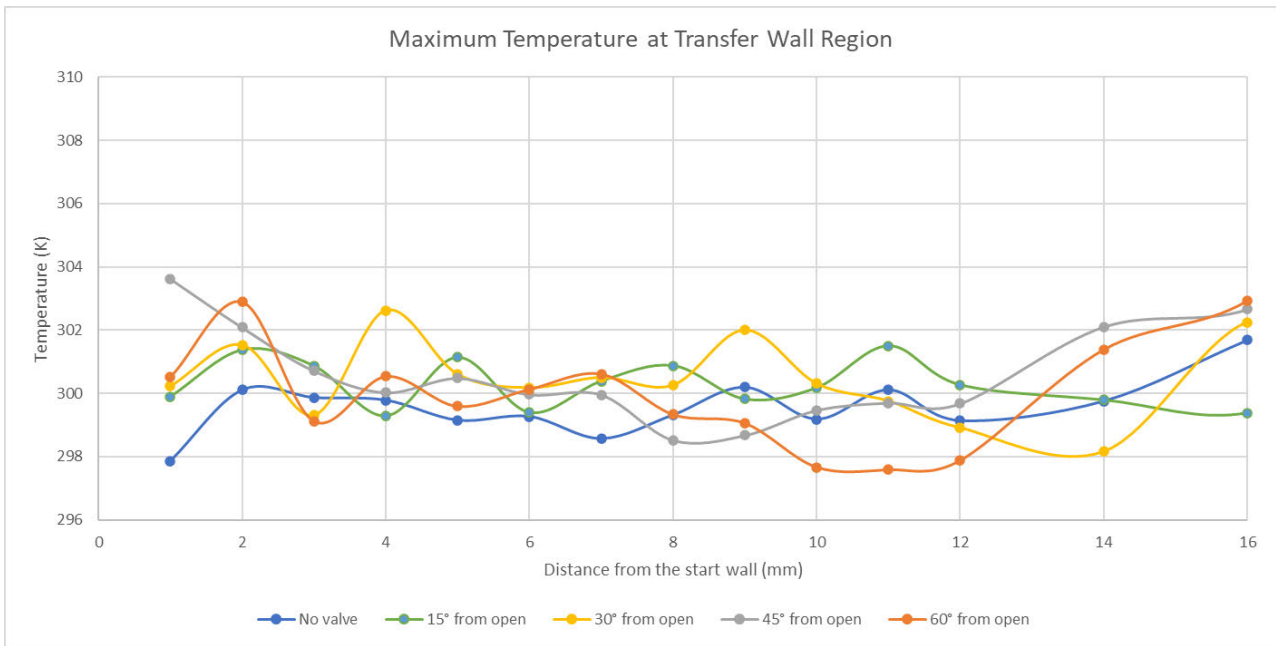


**Figure 4-67:** Maximum temperature at the transfer wall region at various valve positions refined to 0-16mm.

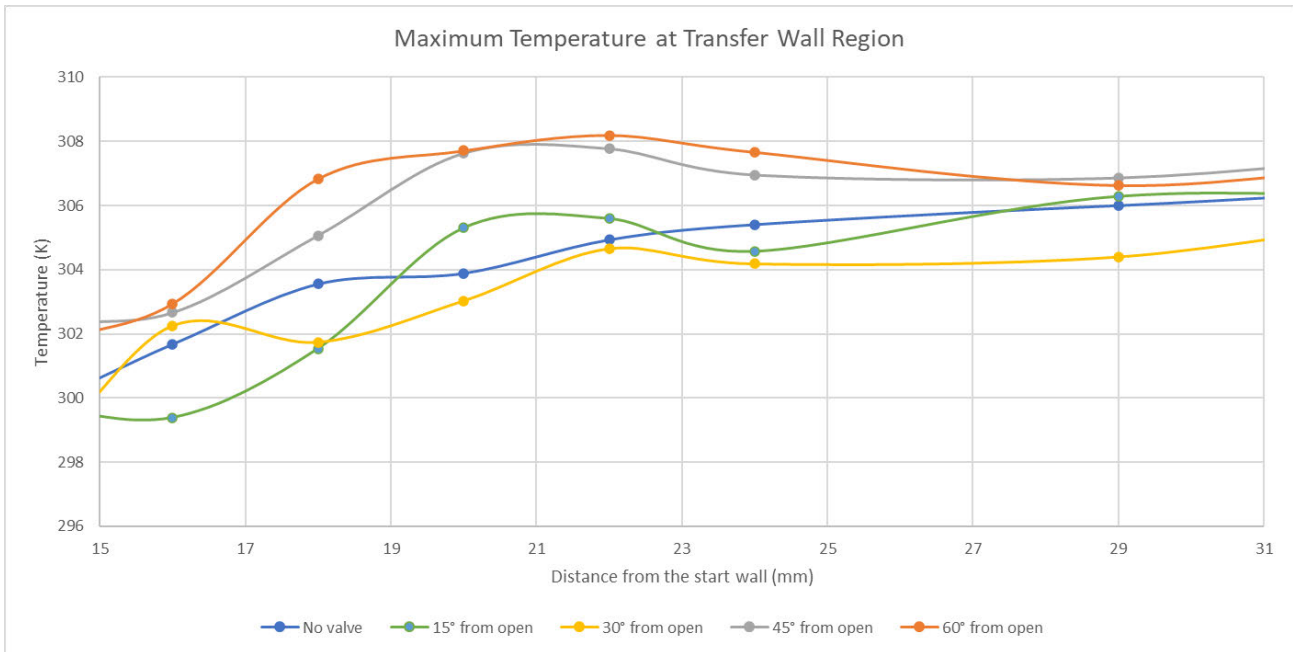


**Figure 4-68:** Maximum temperature at the transfer wall region at various valve positions refined to 15-31mm.

In the region between 15 and 25mm from the cold-domain tube starting wall, it can be seen the two experiments with valves closed at 45° and 60° are showing maximum temperatures consistently above the baseline. With the 60° valve angle the temperatures can be seen to differ 3-4 degrees consistently through several data points. The two other experiments with valves at 15° and 30° have values which fluctuate below and above the baseline, however they both follow its' general trend.

### ***Findings***

This section analysed the entry region of the heat exchanger comparing CFD models with and without a valve. The data is showing when the valve angle is closed, to significantly change the flow rate of the fluid, there is higher maximum temperatures between 15-25mm in the tube's transfer wall region.

The author does not feel confident making a statement on the hypothesis at this stage until more experimental data is reviewed.

It is important to also note the limitations of these findings. As the valve got a higher angle the CFD calculations converged less, therefore indicating more error in the results. This was likely due to the high turbulence and erratic velocities.

## 5.0 Chapter 5: Scale and Optimisation

### 5.1 Introduction

Chapter 4 describes experiments that were performed and noted the resulting initial findings regarding the temperature distribution effects of a control valve in the entry region of a heat exchanger. These experiments were performed on a small-scale educational heat exchanger model with low temperature differentials. Real-life sized industrial applications of a heat exchanger are likely to be exposed to more extreme conditions and fluids which could change the outcome of the experiments.

In this chapter of the dissertation, the CFD models have been scaled up to better represent a real-life application of a heat exchanger. As noted in section 3.2.2, in an industrial real-life application it is unlikely a dual-tube style exchanger would be used but is none the less being used for this study.

### 5.2 Design of Experiment

Six experiments were performed on upsized models to verify if greater flow rates, large diameters and larger temperature differences reveal similar results to the small controlled experiments from chapter 4. The experiments performed were:

- Complete heat exchanger model with no valve in entry region
- Complete heat exchanger model with valve at real-life position
- Complete heat exchanger model with valve at near-closed position
- Entry-region heat exchanger model with no valve in entry region
- Entry-region heat exchanger model with valve at real-life position
- Entry-region heat exchanger model with valve at near-closed position.

Experiments 1 to 3 will be conducted to determine if the control valve influences the global temperature distribution throughout the heat exchanger core. Experiments 4 to 6 will determine if the control valve influences the local temperature distribution in the entry region transfer wall of the heat exchanger.

### 5.3 Data for Model

To scale this study to the application of a large engine test dynamometer, data was required on the heat generated in the application. Data for a high horse power (HHP) industrial engine was found on the internet (Cummins Inc 2016) and will be used as a broad example of real-life engine heat output. Note: these large engines often have two coolant circuits – main jacket water and low temperature circuits. Only the main water jacket data is to be used as it outputs significantly more heat:

- **Engine Model:** QSK78-G12
- **Power Output:** 2737kW
- **Heat Rejection to Coolant:** 48.3 MJ/min (805 kW)
- **Max Flow Rate:** 2222 L/min ( $0.037 \frac{m^3}{s}$ )

- **Max Outlet Temp:** 104°C.

To calculate the heat in the exchanger system, some assumptions on the heat exchanger needed to be made. A suitable industrial product available on the market was chosen. The product chosen is the PowerTest JW4500 suitable for engines producing up to 3356kW of power. Some key specifications (PowerTest 2015):

- **Inlet/Outlet Diameter:** 152mm
- **Flow Rate:** 1174 L/min ( $0.020 \frac{m^3}{s}$ )
- **Max Heat Rejection:** 89075 BTU/min (1566 kW)
- **Max Coolant Inlet Temp:** 110°C
- **Coolant Outlet Temp:** 71-96°C
- **Process (cold) Fluid:** Water
- **Cooling (Hot) Fluid:** 50/50 Glycol/Water Mixture.

An industrial-type cooling tower which uses ambient air to cool was assumed to control the temperature of the cooling/process water. It was also assumed the water inlet temperature was 45°C. This is higher than the heat exchanger manufacturer’s recommended inlet temperature, however, is more realistic in the application’s environment. Process water will be assumed to be clean pure water. The system was assumed to be perfectly insulated with no losses and the heat exchanger will cool all the heat that has been rejected to the coolant.

The purpose of the heat exchanger in this application is to maintain the temperature outlet of the heat exchanger hot circuit to be 85°C, simulating a radiator. This allows the dynamometer test operators to identify when the test engine is producing too much heat during operation.

To calculate the required information, some material properties are required and were sourced as shown in table 5-1.

*Table 5-1: Material properties of heat exchanger fluids.*

<b>Material</b>	<b>Density (kg/m<sup>3</sup>)</b>	<b>Specific Heat (J/(kg K))</b>	<b>Source</b>
Water @ 45°C	990.1	4180	Cengel & Ghajar 2015
50/50 Glycol/Water mixture @ 100°C	1030	3718	Engineering ToolBox 2013

## 5.4 Calculations

To create scaled models in CFD software, four additional pieces of information were required:

- Dimensions of the heat exchanger for optimal cooling
- Hot water inlet temperature at operating conditions
- Cold water flow rate at operating conditions
- Angle of the control valve at operating conditions.

### Heat Exchanger Dimensions

A simple system diagram was created as seen in figure 5-1 from the data in section 5.2 for the heat exchanger with parameters for the maximum cooling capacity. The hot water outlet temperature was assumed to be 85°C as this is approximately the middle of the specified range of the example equipment. The cold-water inlet is assumed to be 30°C which is the inlet temperature the equipment is rated at.

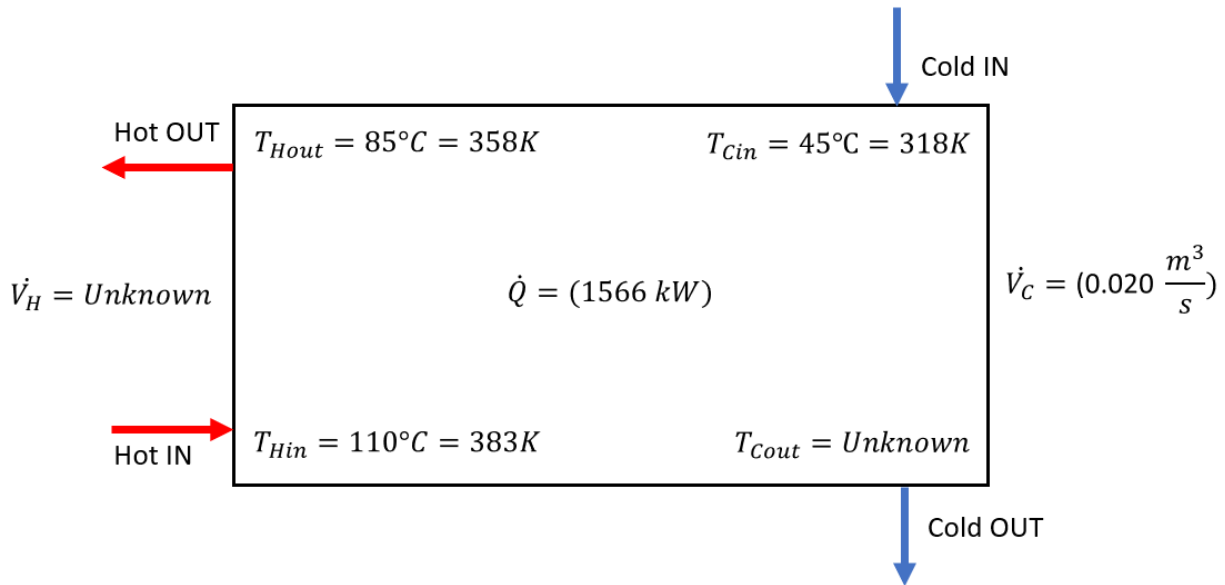


Figure 5-1: System diagram of scaled model for maximum cooling capacity.

To find the cold-water outlet temperature (Cengel & Ghajar 2015 [formula 11-9]):

$$\dot{Q} = \dot{m}_c c_{p,c} (T_{cold,out} - T_{cold,in})$$

To find  $\dot{m}_c$ ;

$$\dot{m}_c = \dot{V}_c * \rho_c$$

$$\dot{m}_c = 0.020 \frac{m^3}{s} * 990.1 \frac{kg}{m^3}$$

$$\dot{m}_c = 19.80 \frac{kg}{s}$$

Substituting  $\dot{m}_c$  back in:

$$\dot{Q} = \dot{m}_c c_{p,c} (T_{cold,out} - T_{cold,in})$$

$$1566 \text{ kW} = 19.80 \frac{kg}{s} * 4180 \frac{J}{kg * K} (T_{cold,out} - 318K)$$

$$1566000 \frac{J}{s} = 19.80 \frac{kg}{s} * 4180 \frac{J}{kg * K} * (T_{cold,out} - 318K)$$

$$18.92 = T_{cold,out} - 318K$$

$$T_{cold,out} = 336.92K \approx 337K$$

To find the length of the heat exchanger (Cengel & Ghajar 2015 [formula 11-10]) was used in conjunction with the log mean temperature method.

$$\dot{Q} = U * A_s * \Delta T_m$$

A few assumptions had to be made:

- From the available data the overall heat transfer coefficient (U) could not be accurately calculated from forced convection formula. Instead, a U value of  $1700 \frac{W}{m^2.K}$  was chosen from a combination of reviewing standard tables (Cengel & Ghajar 2015 [Table 11-1]) (Engineering Toolbox 2003).
- The inner tube to annulus outside diameter ratio was kept the same as the original heat exchanger model with the annulus outside diameter considered to be the 152mm inlet sizing from the supplier information

To find the annulus inside diameter:

$$\frac{8.925}{14} = \frac{D_a}{152}$$

$$D_a = 96.9mm \approx 97mm$$

To find the log mean temperature difference of the exchanger (Cengel & Ghajar 2015 [formula 11-25]):

$$\Delta T_{lm} = \frac{\Delta T_1 - \Delta T_2}{\ln\left(\frac{\Delta T_1}{\Delta T_2}\right)}$$

For counter-flow exchangers, delta T values are found from:

$$\Delta T_1 = T_{hot,in} - T_{cold,out}$$

$$\Delta T_1 = 383K - 337K$$

$$\Delta T_1 = 46K$$

And:

$$\Delta T_2 = T_{hot,out} - T_{cold,in}$$

$$\Delta T_2 = 358K - 318K$$

$$\Delta T_2 = 40K$$

Substituting back in:

$$\Delta T_{lm} = \frac{46 - 40}{\ln\left(\frac{46}{40}\right)}$$

$$\Delta T_{lm} = 42.93 \text{ K}$$

Substituting back in:

$$\dot{Q} = U * A_s * \Delta T_m$$

$$1566000 \text{ W} = 1700 \frac{\text{W}}{\text{m}^2 \cdot \text{K}} * A_s * 43.93 \text{ K}$$

$$A_s = 20.97 \text{ m}^2$$

To find the length:

$$A_s = \pi D L$$

$$L = \frac{A_s}{\pi * D}$$

$$L = \frac{20.97 \text{ m}^2}{\pi * 0.097 \text{ m}}$$

$$L = 68.81 \text{ m} \approx 69 \text{ m}$$

Whilst this length looks abnormally long, it is important to note the context of the size of the equipment and the heat being rejected into the system. This length is one of the reasons the industrial equipment in applications like this do not use a dual-tube type heat exchanger. Much more efficient plate-style heat exchangers are used. Plate style heat exchangers get much more surface area into a compact space. As an example, the PowerTest JW4500 plate-type heat exchanger these boundary conditions are based off, fits into a  $4 \text{ m}^3$  space.

### ***Hot Water Inlet Temperature***

To calculate the hot water inlet temperature, a simple system diagram was created from the data in section 5.2 for the heat exchanger with parameters modified to represent actual figures for the engine model rather than the maximum capacity. This can be seen in figure 5-2 below.

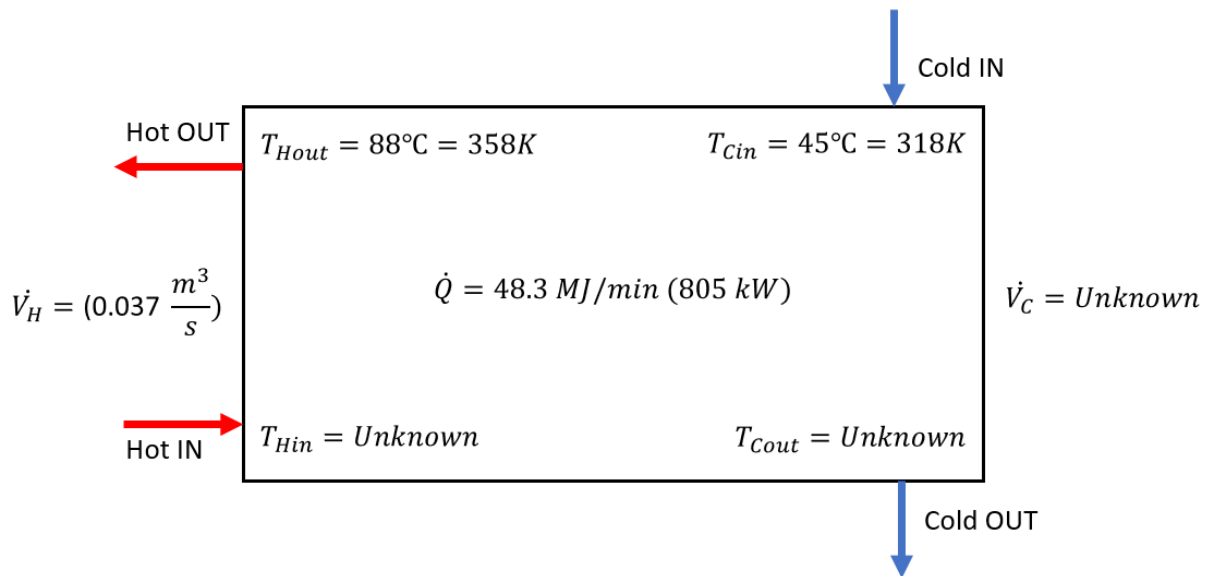


**Figure 5-2:** System diagram of scaled model at operating conditions.

To find the hot water inlet temperature (Cengel & Ghajar 2015 [formula 11-10]):

$$\dot{Q} = \dot{m}_h c_{ph} (T_{hot,in} - T_{hot,out})$$

To find  $\dot{m}_h$ ;

$$\dot{m}_h = \dot{V}_h * \rho_h$$

$$\dot{m}_h = 0.037 \frac{m^3}{s} * 1030 \frac{kg}{m^3}$$

$$\dot{m}_h = 38.11 \frac{kg}{s}$$

Substituting  $\dot{m}_h$  back in:

$$\dot{Q} = \dot{m}_h c_{ph} (T_{hot,in} - T_{hot,out})$$

$$805 \frac{kJ}{s} = 38.11 \frac{kg}{s} * 3718 \frac{J}{kg * K} * (T_{hot,in} - 358K)$$

$$805000 \frac{J}{s} = 38.11 \frac{kg}{s} * 3718 \frac{J}{kg * K} * (T_{hot,in} - 358K)$$

$$5.68K = T_{hot,in} - 358K$$

$$T_{hot,in} = 363.7K$$

### **Cold Water Flow Rate**

Due to the engine not producing as much heat as the heat exchanger is rated for, the cooling capacity is required to be decreased and the cold-water flow rate reduced.

To find the mean temperature:

$$\dot{Q} = U * A_s * \Delta T_m$$

$$805000W = 1700 \frac{W}{m^2.K} * 18.51 m^2 * \Delta T_m$$

$$\Delta T_m = 25.58K$$

Using the log mean temperature difference:

$$\Delta T_{lm} = \frac{\Delta T_1 - \Delta T_2}{\ln\left(\frac{\Delta T_1}{\Delta T_2}\right)}$$

$$25.58K = \frac{\Delta T_1 - \Delta T_2}{\ln\left(\frac{\Delta T_1}{\Delta T_2}\right)}$$

Understanding:

$$\Delta T_1 = T_{hot.in} - T_{cold,out}$$

$$\Delta T_1 = 363.7K - T_{cold,out}$$

And:

$$\Delta T_2 = T_{hot.out} - T_{cold,in}$$

$$\Delta T_2 = 358K - 318K$$

$$\Delta T_2 = 40K$$

Substituting back in:

$$25.58K = \frac{368.7K - T_{cold,out} - 60K}{\ln\left(\frac{368.7K - T_{cold,out}}{60K}\right)}$$

$$25.58K = \frac{308.7K - T_{cold,out}}{\ln\left(\frac{368.7K - T_{cold,out}}{60K}\right)}$$

This is not solvable algebraically, so excel solver module was used to optimise the data and find a result using an iterative method. The initial data was entered as per figure 5-3 with the cold-water outlet estimated at 360K. The solver was run with target of T\_mean value of 25.58 changing the cold-water outlet value. The solution can be seen in figure 5-4.

Known		Intermediate Values	
Hot Water Outlet	358	T_1	3.7
Hot Water Inlet	363.7	T_2	40
Cold Water Inlet	318		

Unknown		Outputs	
Cold Water Outlet	360	T_mean	15.2486

Figure 5-3: Initial values in Excel.

Known		Intermediate Values	
Hot Water Outlet	358	T_1	15.12838
Hot Water Inlet	363.7	T_2	40
Cold Water Inlet	318		

Unknown		Outputs	
Cold Water Outlet	348.5716	T_mean	25.58001

Figure 5-4: Solved values in Excel.

$$T_{cold,out} = 348.57K$$

The cold-water flow rate was found using:

$$\dot{Q} = \dot{m}_c c_{p,c} (T_{cold,out} - T_{cold,in})$$

$$805kW = \dot{m}_c * 4180 \frac{J}{kg * K} (348.57K - 303K)$$

$$\dot{m}_c = \frac{805000 \frac{J}{s}}{4180 \frac{J}{kg * K} (348.57K - 303K)}$$

$$\dot{m}_c = 4.23 \frac{kg}{s}$$

Converting to volumetric flow rate:

$$\dot{m}_c = \dot{V}_c * \rho_c$$

$$\dot{V}_c = \frac{\dot{m}_c}{\rho_c}$$

$$\dot{V}_c = \frac{4.23 \frac{kg}{s}}{990.1 \frac{kg}{m^3}}$$

$$\dot{V}_c = 0.0043 \frac{m^3}{s}$$

### Control Valve Angle

To use a mathematical equation to calculate the flow rate by valve angle, pressures that are unknown to industry equipment would need to be known. The chart in figure 5-5 (Johnson Controls, 1996), was used to estimate the valve position.

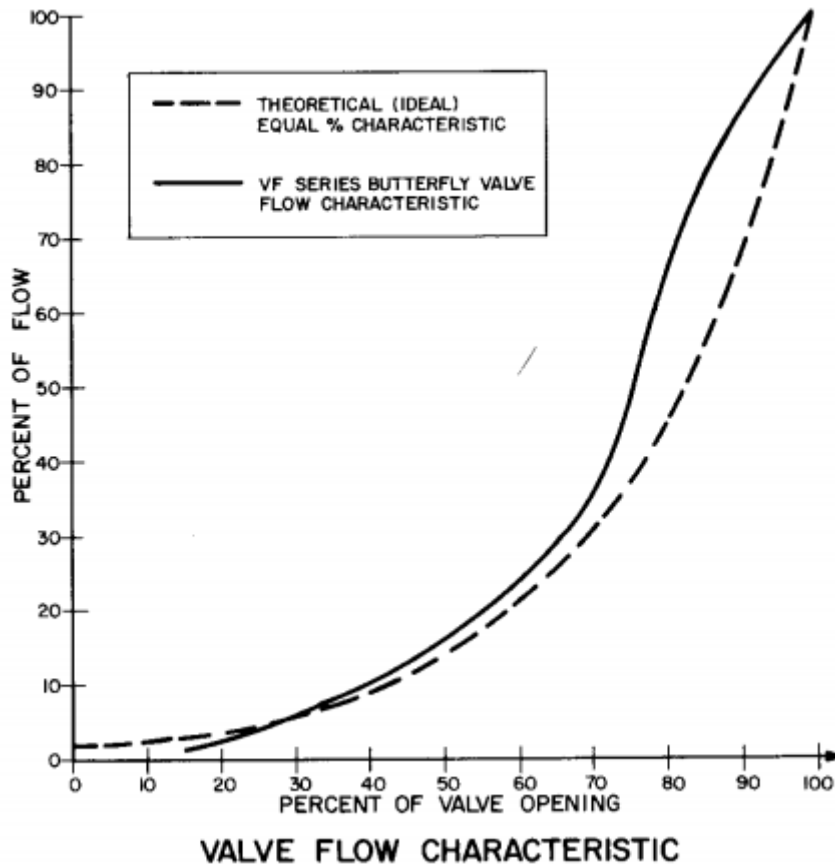


Figure 5-5: Valve flow rate percent vs valve opening percentage (Johnson Controls 1996).

With the valve fully open, the system required a flow rate of  $0.020 \frac{m^3}{s}$  and at operating conditions the system flow rate required to maintain the desired temperatures dropped to  $0.0043 \frac{m^3}{s}$ . This results in a flow of 21.5% of the pump capacity. Using the chart in figure 5-7 the approximate valve position will be 50° from fully closed.

## 5.5 Global Distribution model

Experiments 1 to 3 for chapter 5 CFD modelling was completed on the complete heat exchanger system to see if the addition of the valve influences the global temperature distribution.

### 5.5.1 Model Creation

#### *3D Model*

As the model was significantly larger in size compared to earlier models it was created as one continuous dual wall shape with a right-angle entry point for the cold-water entry to reduce the elements required. The tube was created with 5 bends to keep the shape in a length/width ratio ideal for viewing for analysis on a screen. The five bends were created with 2m radius giving 3.14m of transfer length each. Each of the 6 main lengths was therefore created at 8.88m of length to get the total required length of 69m.

All bends were created with radii or simple corners to sweep each part without sharp corners. A valve was created in the cold-water entry region with 0.14m outside diameter, 0.02m thickness and 0.004m chamfers. The cold-water domain was created by making a subtractive Boolean and the three resulting parts combined to make one part.

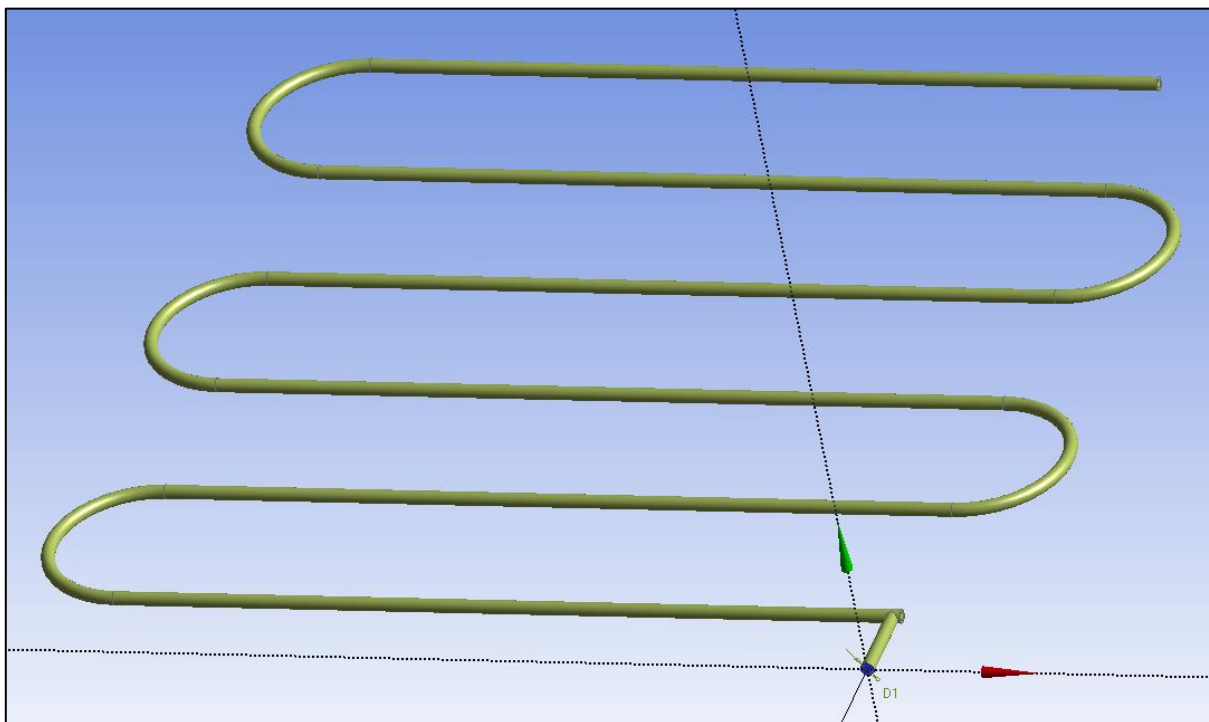


*Figure 5-6: 3D Model for the scaled model.*

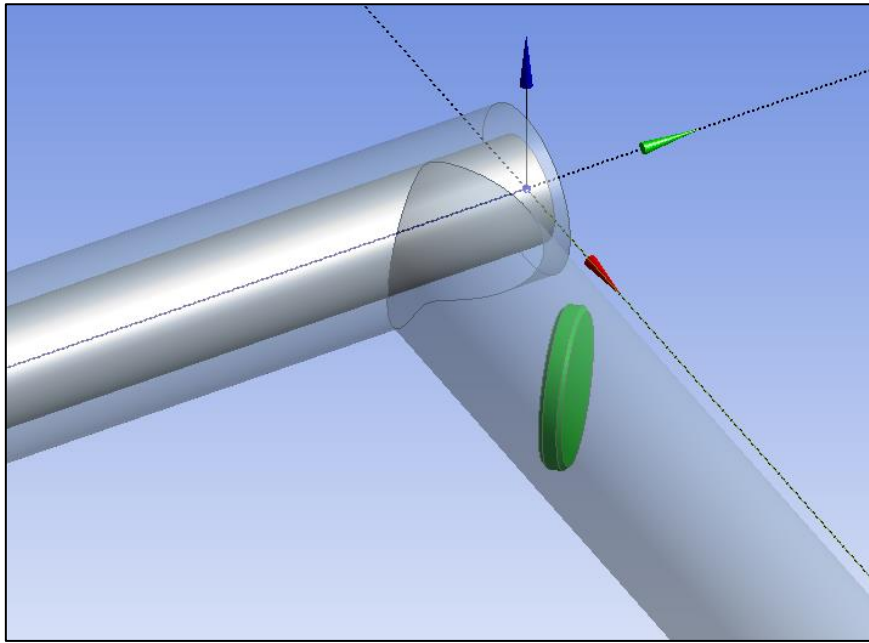


*Figure 5-7: Valve in the entry region of scaled model.*

### ***Mesh and Named Selections***

The mesh was created using a similar method to the model from section 4.2.2 and 4.4.2. It was created using a 2800 division sweep mesh through the hot-water domain, 0.035m body tetrahedron mesh in the cold-water domain and finer face mesh around the valve body. The setup was refined until a final element count of 400,987 elements was obtained, understanding that some free elements would be needed for the conductive shell transfer wall generated by Fluent. Due to the size of the model, it was difficult to create a stable mesh for this part that stayed under the 512,000-element limit of the ANSYS student version so a mesh independence study was not completed for this model. These results are presented with the understanding that this mesh independence study was not performed to verify the data is reliable.

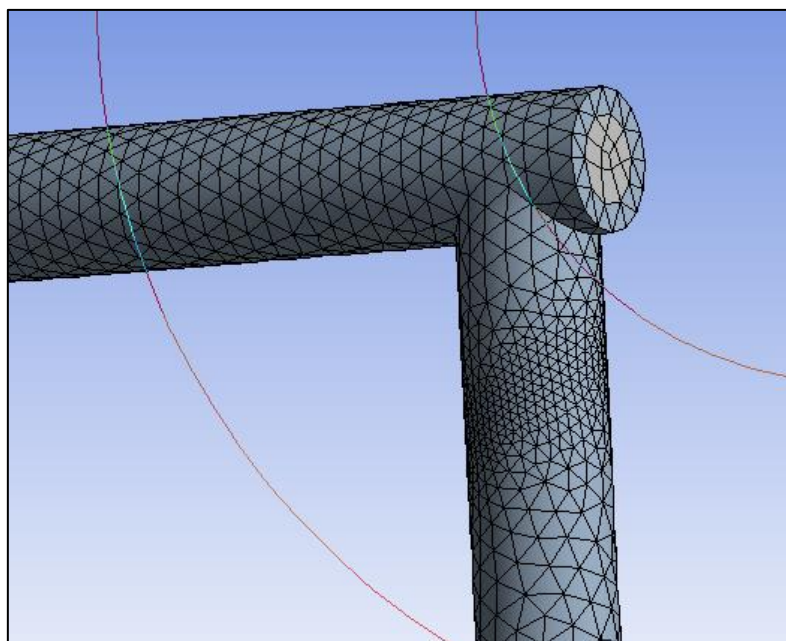


*Figure 5-8: Exterior view of the mesh elements for the global model.*

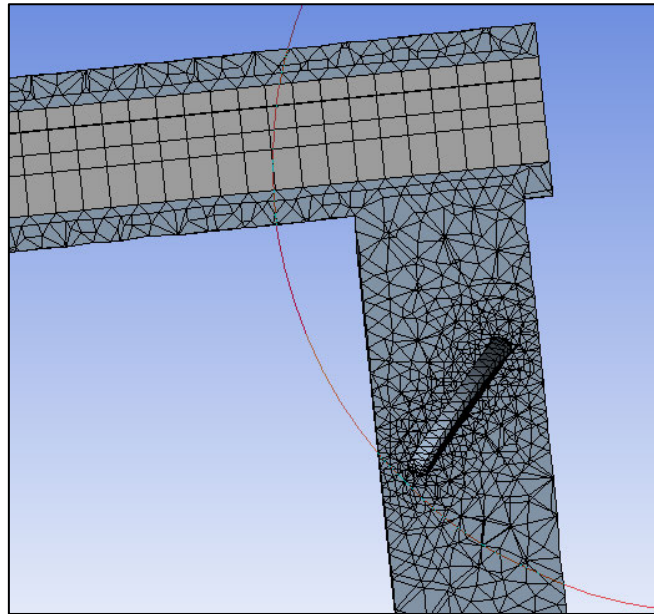


**Figure 5-9:** Sectioned view of the mesh elements for the global model.

The named selection choice was refined from the earlier model to a more simplified model without losses from convection. The following areas of the model were named:

- All external walls were named as insulation walls
- all internal walls were named as transfer walls
- the inlets and outlets
- the cold-water and hot-water domains.

### **Fluent Setup**

The model was setup with material properties as per table 5-2 below.

**Table 5-2:** Scaled model material properties.

<b>Material</b>	<b>Density (kg/m<sup>3</sup>)</b>	<b>Specific Heat (J/(kg K))</b>	<b>Thermal Conductivity (W/(m K))</b>	<b>Viscosity (kg/(m s))</b>	<b>Source</b>
Water @ 20°C	998.2	4182	0.6	0.001003	ANSYS Library
50/50 Glycol/Water mixture @ 93.3C	1030	3690	0.6	0.0007	(Engineering ToolBox 2013) - interpolated
Stainless Steel	7900	477	14.9	N/A	(Cengel & Ghajar 2015)

The model was setup with the boundary condition as per table 5-3 below.

*Table 5-3: Scaled model boundary conditions.*

<b>Parameter</b>	<b>Value</b>
Hot Water In	363.7 K
Hot Water Mass Flow	38.11 kg/s
Cold Water In	318 K
Cold Water Mass Flow	4.23 kg/s

The model was setup with the parameters and settings as per table 5-4 below.

*Table 5-4: Scaled model parameter setup.*

<b>Area</b>	<b>Parameter</b>	<b>Comments</b>
Setup – Models	Energy Equation	Turned on
Setup – Models	Viscous Model	k-epsilon Realizable Enhanced Wall Treatment
Setup – Materials	Fluids	Water-liquid and coolant setup
Setup – Materials	Solids	Steel-stainless setup
Setup - Cell Zone Conditions	Cold water domain Hot water domain Valve domain	Cold Water as fluid – water-liquid Hot Water as fluid – coolant Valve domain as acrylic
Setup - Boundary Conditions	Hot water out Cold water out	Setup as pressure outlets (better results than mass flow in this case)
Setup - Boundary Conditions	Hot water in Cold water in	Setup as mass flow inlet Setup flow rate as normal to boundary with flow rate and temperature as per table 5-3
Setup - Boundary Conditions	Insulated Wall – Cold water domain Insulated Wall – Hot water domain	Setup as no heat transfer
Setup - Boundary Conditions	Transfer wall	Setup as coupled transfer with the shadow equivalent. Setup as single layer stainless shell conduction with wall thickness of 0.004m
Setup - Boundary Conditions	Cold water domain to valve wall	Acrylic with no heat transfer
Solution – Method	Scheme	Coupled
Solution – Monitors	Residuals	All changed to 1E-06
Solution – Initialization	Method	Hybrid Initialization
Run Calculation	Number of Iterations	600

**Initial Calculations and Verification**

For the initial calculations and verification, the model was adjusted to remove the valve in the inlet. This allowed for a baseline model to be created and validation of the model compared to the mathematical model in section 5.4.

The stainless-steel material conduction transfer rate parameters and calculations were adjusted multiple times until the outlet temperatures matched the mathematical model. This step was necessary as some parameters could not be directly transferred to the CFD model, an example being the overall heat transfer coefficient. Table 5-5 shows the final outlet temperatures compared between the mathematical model and the CFD model. It was found after many configuration changes, the model could not be configured to perfectly match the mathematical model. It is the author’s thoughts that this is a problem with the meshing in the model. Due to the size of the model and the fine size of the mesh it is not possible within the limits of the modelling to correctly model this scenario.

*Table 5-5: Comparison of mathematical vs CFD model outlet temperatures.*

Parameter	Mathematical Model	CFD Model	Error
Cold Outlet	348.57 K	349.10 K	0.15%
Hot Outlet	358.00 K	358.91 K	0.25%

The residuals were inspected and show that the results converged as seen in figure 5-17 below.

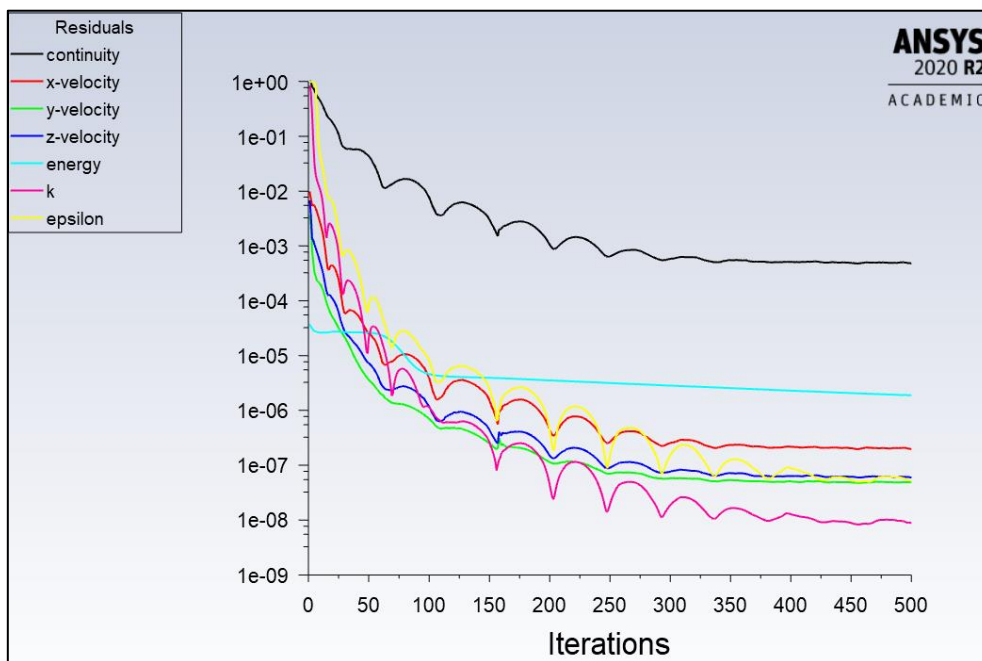


*Figure 5-10: Residuals for the scaled global model without valve.*

The mass flow rate was checked to ensure the two fluid paths did not mix and no other major problem were evident in the CFD model as shown in figure 5-11.

Mass Flow Rate	(kg/s)
cold_inlet	4.23
cold_outlet	-4.2300272
hot_inlet	38.11
hot_outlet	-38.11
Net	-2.7230147e-05

Figure 5-11: Mass Flow Rates of the scaled global CFD model without the valve.

A plane cut was made through the X-Z axis and a temperature contour plot made. The temperature contours show the continual cooling of the hot water and heating of the cold water expected to see in this arrangement. The contour was inspected for any unintentional mixing of the two fluids or any other unusual or unexpected results. The heat distribution in the cold-water domain was seen to vary significantly more than the model from section 4.2 due to the higher temperature difference.

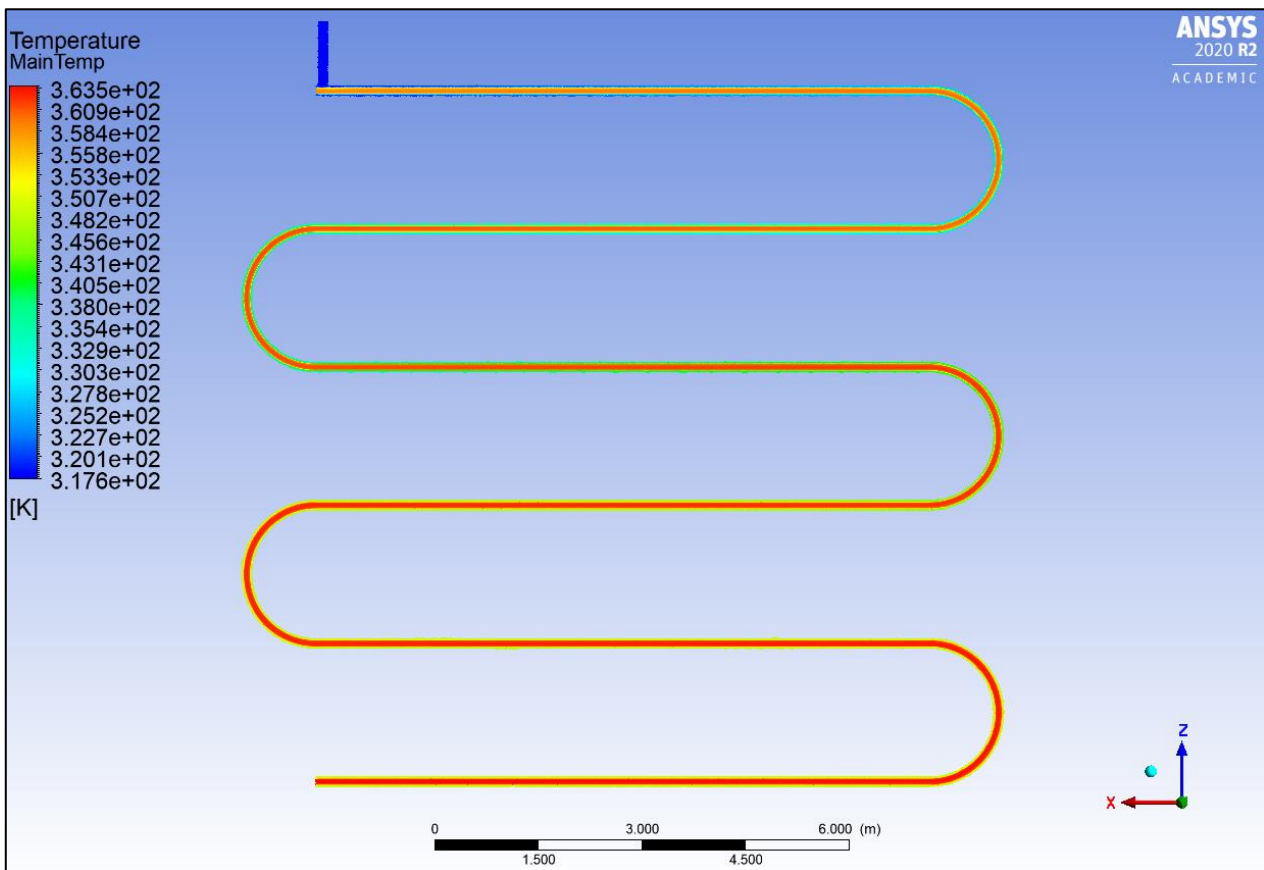


Figure 5-12: Temperature distribution of the scaled global CFD model without the valve.

### 5.5.2 Analysis

The model was updated to have valves in both the realistic case (49.5°) and extreme case (25°) scenarios. The meshing process and calculations were run again to get data for these two scenarios.

Several cuts were made in the result modules across the cold and hot domains at various points through the heat exchanger. The chosen measurements points were at equal positions throughout the exchanger core. The

temperatures results were collected using the function calculator: mass-weighted average method. The results were tabulated (table 5-6) and plotted (figure 5-13) to see if there was any notable difference between scenarios.

*Table 5-6: Results of global temperature distribution at various valve angles.*

	Location						
	0	1	2	3	4	5	6
Hot Water - No Valve	363.7	363.22	362.661	362.059	361.21	360.119	358.906
Cold Water - No Valve	318	328.006	335.876	343.06	347.818	348.699	349.097
Hot Water - 49.5°	363.7	363.225	362.663	362.059	361.211	360.124	358.891
Cold Water - 49.5°	318	328.102	335.975	343.06	347.832	348.737	349.14
Error - 49.5°	0.00%	-0.01%	-0.01%	0.00%	0.00%	-0.01%	0.00%
Hot Water - 25°	363.7	363.224	362.661	362.057	361.21	360.122	358.883
Cold Water - 25°	318	328.045	336.025	343.105	347.86	348.678	349.113
Error - 25°	0.00%	-0.01%	-0.02%	-0.01%	-0.01%	0.00%	0.00%

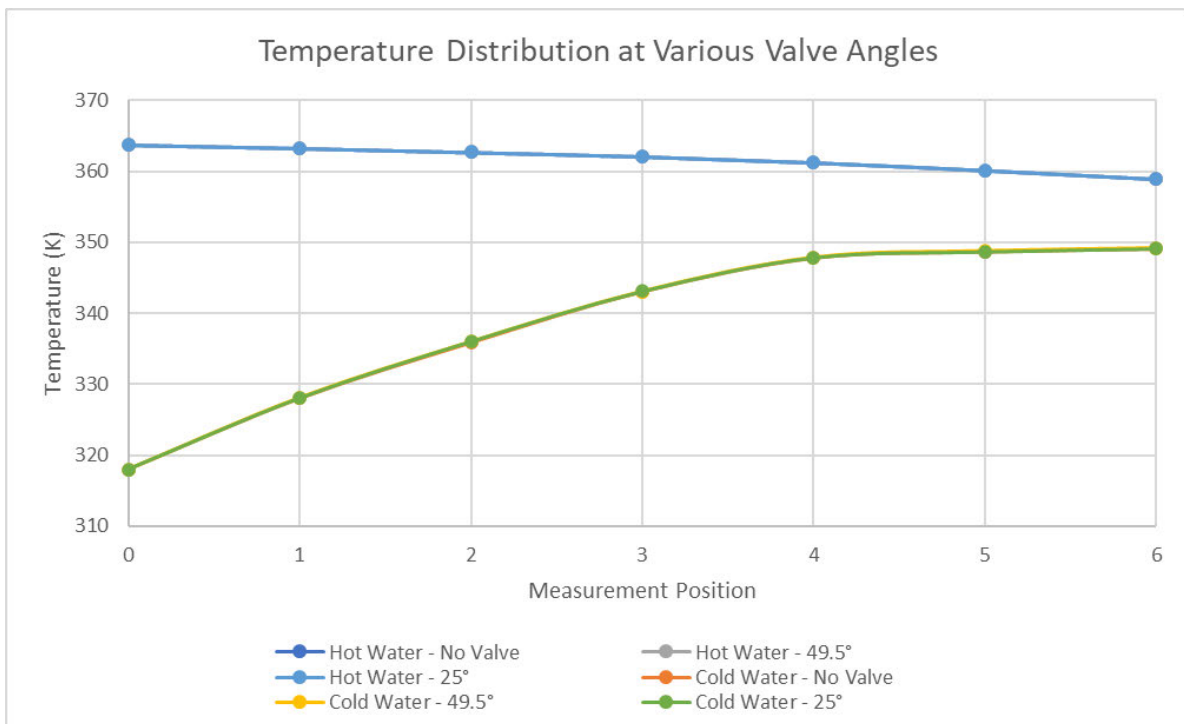


*Figure 5-13: Global temperature distribution at various valve angles.*

### 5.5.3 Findings

These results indicate no influence from the control valve on the global temperature distribution throughout the heat exchanger core.

## 5.6 Local Distribution Model

CFD modelling was completed on the entry region of the heat exchanger to see if the addition of the valve influences the local temperature distribution.

### 5.6.1 Model Creation

#### 3D Model

The entry region model was created in a similar way to the model from section 4.5. The main transfer region was created with a length of 1.5m to have a length of approximately 10x the valve diameter. A valve was created in the cold-water entry region with 0.14m outside diameter and 0.02m thickness and 0.004m chamfers. The cold-water domain was created by making a subtractive Boolean and the three resulting parts combined to make one part.

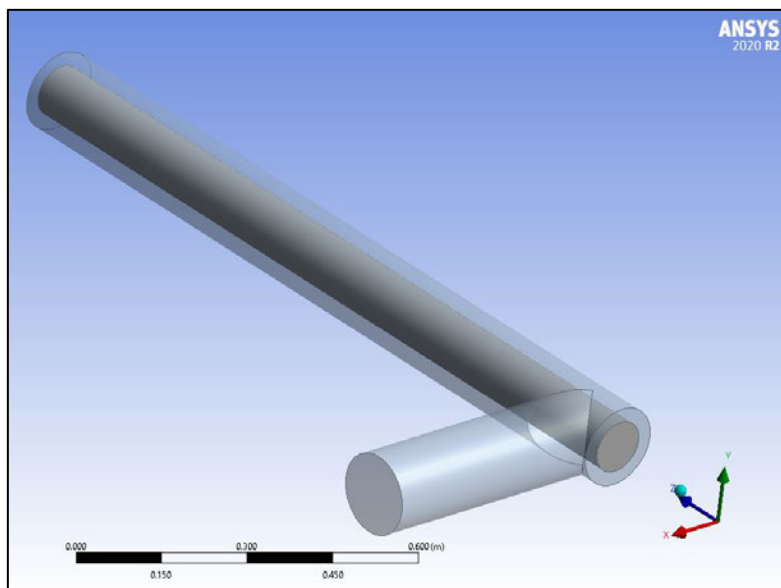


*Figure 5-14: 3D model for the entry region scaled model.*

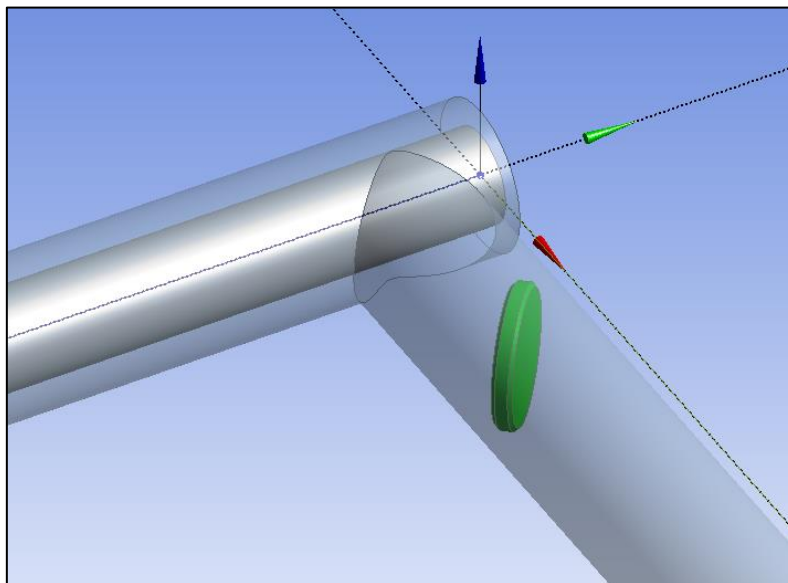


*Figure 5-15: Valve in the entry region of scaled model.*

### ***Mesh and Named Selections***

The mesh was created using a similar method to the model in section 4.5 using a swept mesh for the hot-water domain and 0.008m body tetrahedron mesh in the cold-water domain with finer face mesh around the valve body. The setup was refined until a final element count of 407,185 elements was achieved, without the valve, with the understanding free elements will be needed for the conductive shell transfer wall generated by Fluent.

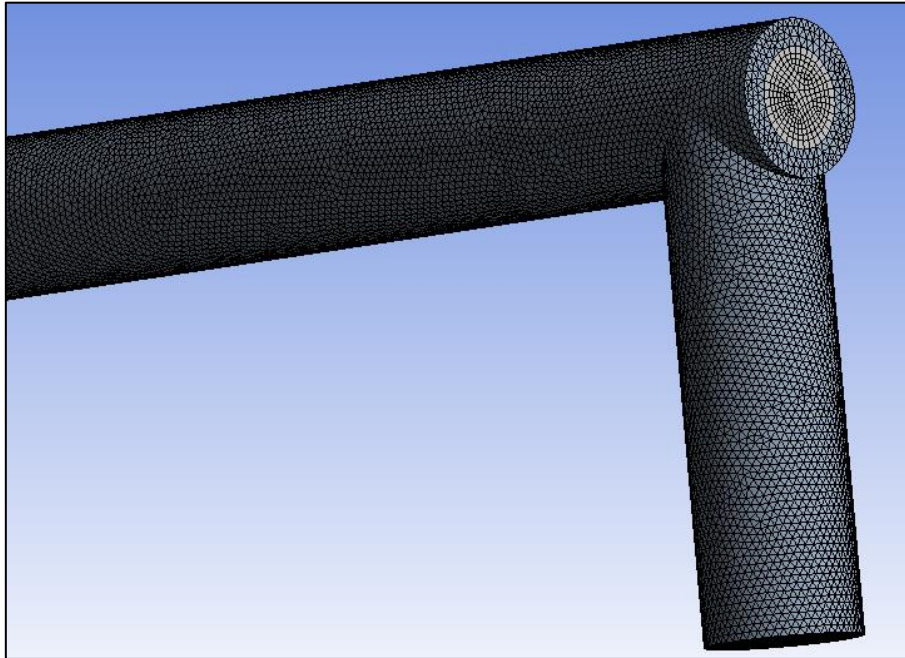


*Figure 5-16: Initial mesh for the entry region scaled model.*

The named selections were refined from the earlier model to be a simplified model without losses from convection. The following areas of the model were named:

- All external walls were named as insulation walls
- All internal walls were named as transfer walls
- The inlets and outlets
- The cold-water and hot-water domains.

### ***Fluent Setup***

The model was setup with material properties as per table 5-2 in section 5.5.1. To get the entry condition of the hot water, a plane was created on the global model from section 5.5, 1.5 from the tube beginning shown in table 5-7.

*Table 5-7: Scaled entry region model boundary conditions.*

<b>Parameter</b>	<b>Value</b>
Hot Water In	359.11 K
Hot Water Mass Flow	38.11 kg/s
Cold Water In	318 K
Cold Water Mass Flow	4.23 kg/s

The model was setup in Fluent as per table 5-8 below. Note in this section the **k- $\epsilon$**  turbulence model was used even though the **k- $\omega$**  model was found more accurate in section 4.5. In this case with multiple experiments performed, the **k- $\epsilon$**  model was found to converge an order of magnitude lower and show more realistic turbulence results.

**Table 5-8: Scaled model parameter setup.**

<b>Area</b>	<b>Parameter</b>	<b>Comments</b>
Setup – Models	Energy Equation	Turned on
Setup – Models	Viscous Model	k-epsilon Realizable Enhanced Wall Treatment
Setup – Materials	Fluids	Water-liquid and coolant setup
Setup – Materials	Solids	Steel-stainless setup
Setup - Cell Zone Conditions	Cold water domain Hot water domain Valve domain	Cold Water as fluid – water-liquid Hot Water as fluid – coolant Valve domain as acrylic
Setup - Boundary Conditions	Hot water out Cold water out	Setup as pressure outlets (better results than mass flow in this case)
Setup - Boundary Conditions	Hot water in Cold water in	Setup as mass flow inlet Setup flow rate as normal to boundary with flow rate and temperature as per table 5-24
Setup - Boundary Conditions	Insulated Wall – Cold water domain Insulated Wall – Hot water domain	Setup as no heat transfer
Setup - Boundary Conditions	Transfer wall	Setup as coupled transfer with the shadow equivalent. Setup as single layer steel-stainless shell conduction with wall thickness of 0.004m
Setup - Boundary Conditions	Cold water domain to valve wall	Acrylic with no heat transfer
Solution – Method	Scheme	Coupled
Solution – Monitors	Residuals	All changed to 1E-06
Solution – Initialization	Method	Hybrid Initialization
Run Calculation	Number of Iterations	500

**Initial Calculations and Verification**

To validate this model, the boundary conditions were compared to the values from the global model in section 5.5. The error as per table 5-9 was found to be insignificant, validating the model.

*Table 5-9: Comparison of mathematical vs CFD model outlet temperatures.*

Parameter	Global Model	Entry-Region Model	Error
Cold Outlet	319.92 K	319.82K	0.031%
Hot Outlet	358.91 K	358.88K	0.001%

The residuals were inspected and show that the results converged as seen in figure 5-17 below.

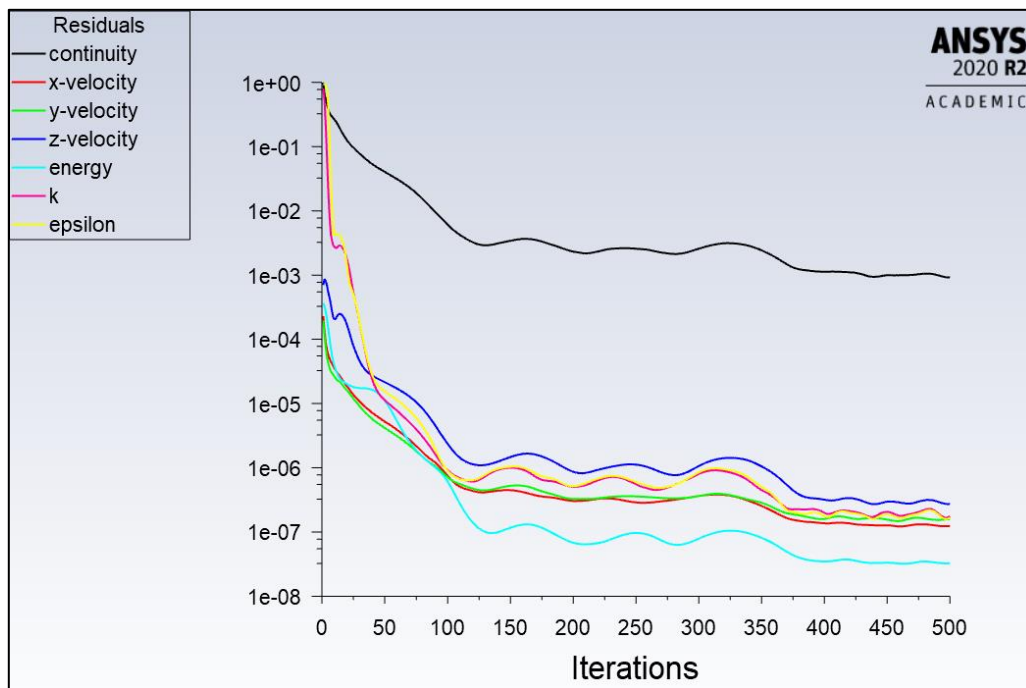


*Figure 5-17: Residuals for the scaled entry region model without valve.*

The mass flow rate was checked to ensure the two fluid paths did not mix and no other major problems were evident in the CFD model as shown in figure 5-18.

Mass Flow Rate	(kg/s)
cold_inlet	4.23
cold_outlet	-4.2300038
hot_inlet	38.11
hot_outlet	-38.11
Net	-3.7751514e-06

*Figure 5-18: Mass flow rates of the scaled entry region CFD model without the valve.*

### ***Mesh Independence Study***

Since many computations are to be performed, a mesh independence study was conducted to find a mesh size suitable to acquire accurate calculations whilst minimizing computation time to complete the study. To complete this study, 17 fluent studies were run with various mesh sizing and the results tabulated.

Four resulting categories were reviewed and compared.

- **Convergence Error Representation:** Each study was compared to the baseline for the X,Y&Z velocity, continuity equation and energy equation residuals. To compare to the baseline, any value larger than the baseline was averaged and compared to the baseline in percentage error
- **Outlet Temperatures:** The outlet temperatures of both the hot and cold domains were compared to the baseline as a percentage error
- **Wall Pressure:** The wall pressure of the hot and cold domains 75mm from the start of the main tube was compared to the baseline as a percentage error
- **Mass Flow Rate:** The mass flow rate of the hot and cold domains 75mm from the start of the main tube was compared to the baseline as a percentage error
- **Element Reduction:** Each study was compared to the based for the total elements generated through the mesh setup. The mesh was compared to the baseline using a percentage
- **A subject visual inspection of the streamlines around the valve and following the sharp corner was also performed to ensure no unusual results were being missed at lower mesh element counts.**

The full results of the mesh independence study can be found in Appendix H. The resulting elements were plotted against the dependant variables to determine if the study was mesh dependant. Analysis of the results in figure 5-19 below shows that the results are mesh dependant and stability is achieved with a mesh count of approximately 375,000 elements.

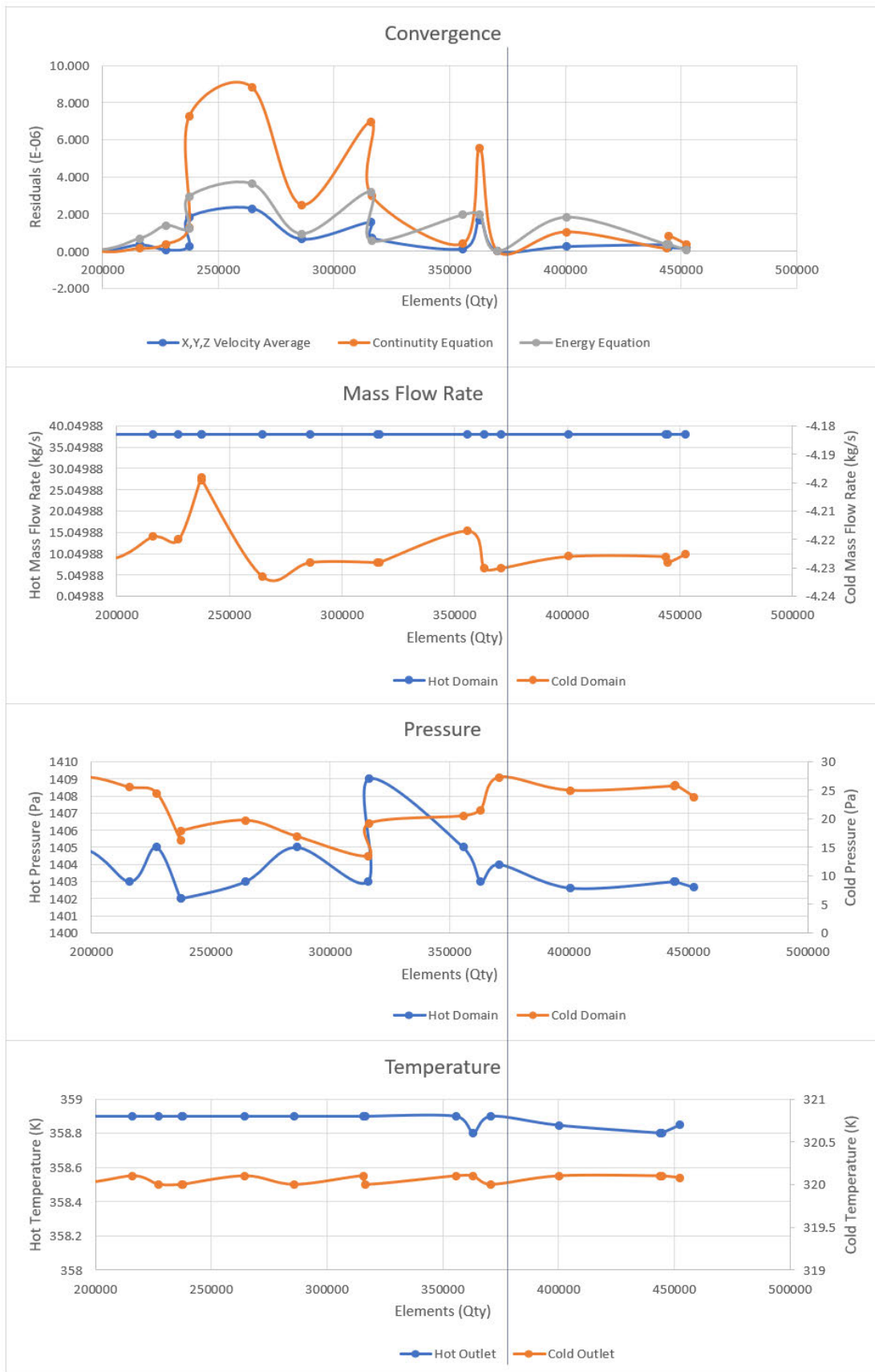


**Figure 5-19:** Mesh Independence Study results showing stability after approximately 375,000 elements.

Since this is not significantly reducing the elements amount and accuracy is important for this study, the mesh was left at the max element settings.

Hot water Domain:

- **Method:** Sweep mesh, using hot water entry face as source and outlet as the target
- **Mesh Type:** All Quad
- **Edge Divisions:** 36
- **Bias:** No Bias.

Hot water Domain:

- **Method:** Tetrahedrons
- **Body Sizing:** 0.008m.

Resulting Mesh: 452,359 elements.

### 5.6.2 Analysis

The model was updated to have valves in both the realistic case (50°) and extreme case (25°) scenarios. The meshing process and calculations were run again to get data for these two scenarios.

Cross-section cuts were made through the CFD models with and without the valve. The lowest, highest, and average temperatures were analysed. As the heat distribution is likely to be most affected closest to the valve, cuts were made every 10mm for the first 150mm, 20mm for the next 150mm and 50mm up to 490mm from the cold-water domain start wall. As the fouling is most likely to occur in the hot water side, the measurements were taken by creating the cut with a radius of 0.055m, in the cold-water domain, resulting in a sample close to the transfer wall as shown in figure 5-20 below.

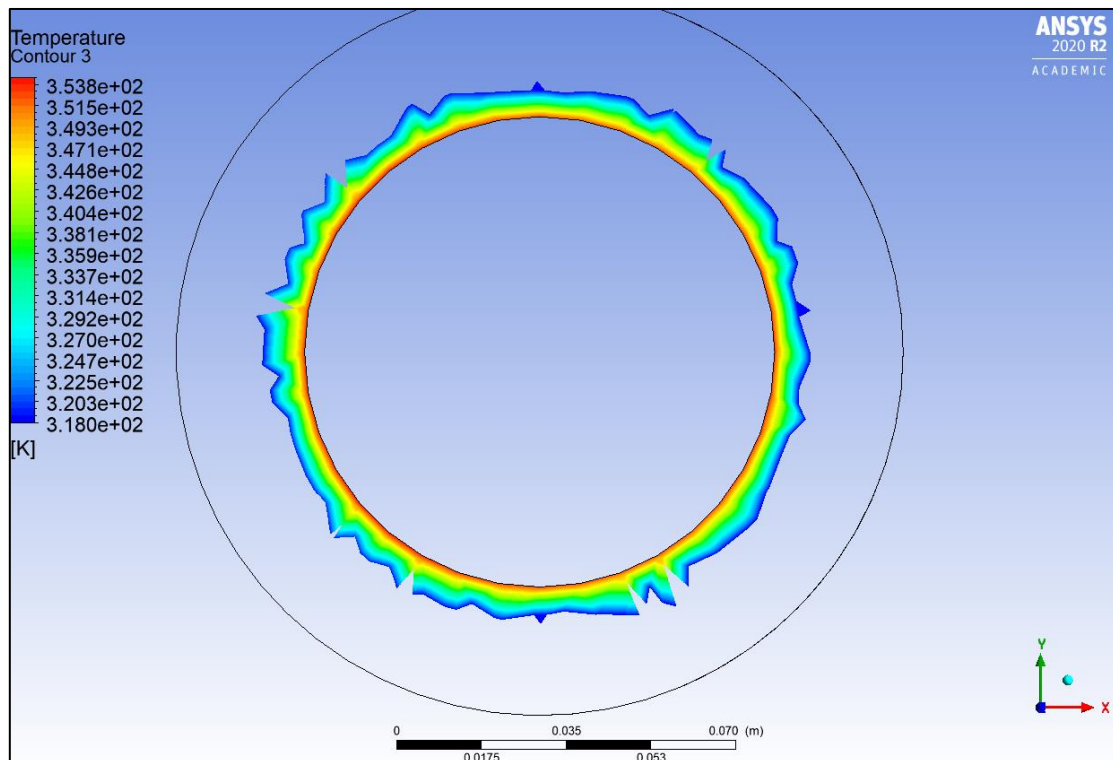
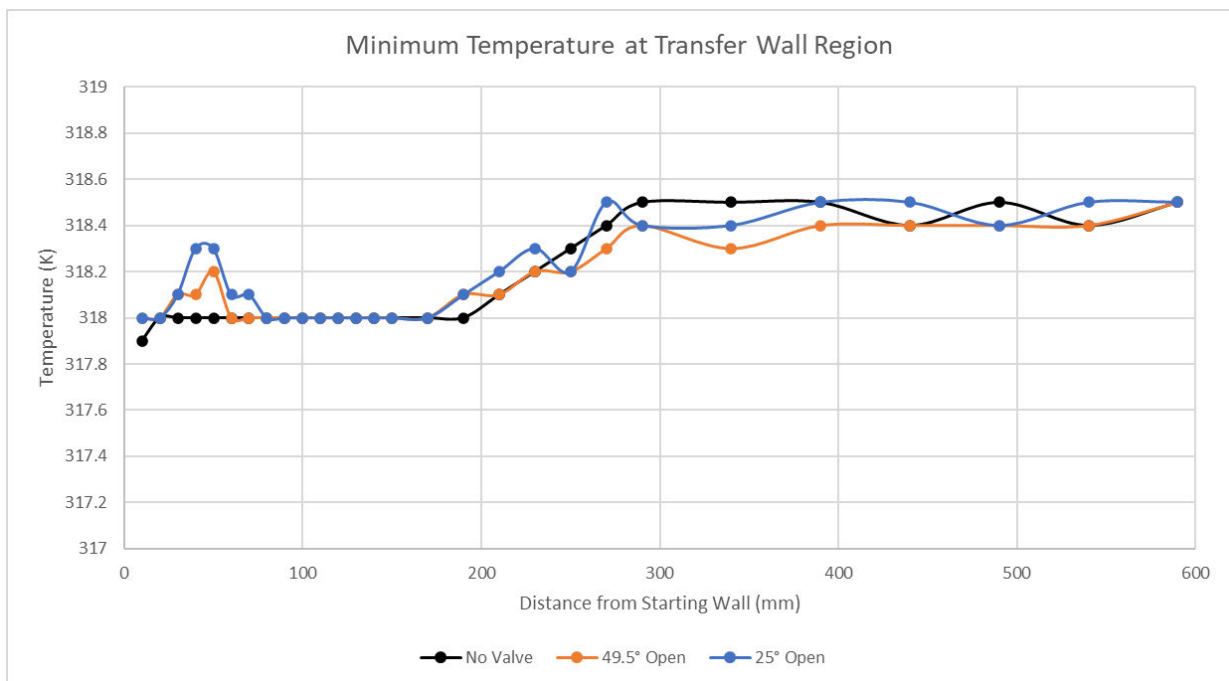


Figure 5-20: Example of sample cut to measure min, max and average temperature close to transfer wall.

To get the data values, the function calculator in the ANSYS results module was used at each cut location for each of the models. For maximum temperature the “maxVal” function was used, for minimum temperature the “minVal” function was used, and for average temperatures the “massFlowAve” function was used.

The ANSYS experiments were completed, the data tabulised and can be seen in full in appendix G. Figure 5-21 shows the minimum temperatures in the wall region for each model. This data shows little variation in minimum temperature with less than 1 degree difference at any location along the test length. Figure 5-22 shows the maximum temperatures in the wall region for each model. This data shows significant variation between the model without a valve and the two models with valves. This data is reviewed and discussed in more detail later in this section. Figure 5-23 shows the average temperature in the wall region for each model. This data shows very little variation in the average temperatures between each model. Some temperature variations can be seen between the model with the valve and the two models without a valve, however it is erratic and does not show a trend.



**Figure 5-21:** Minimum temperature at the transfer wall region at various valve positions.

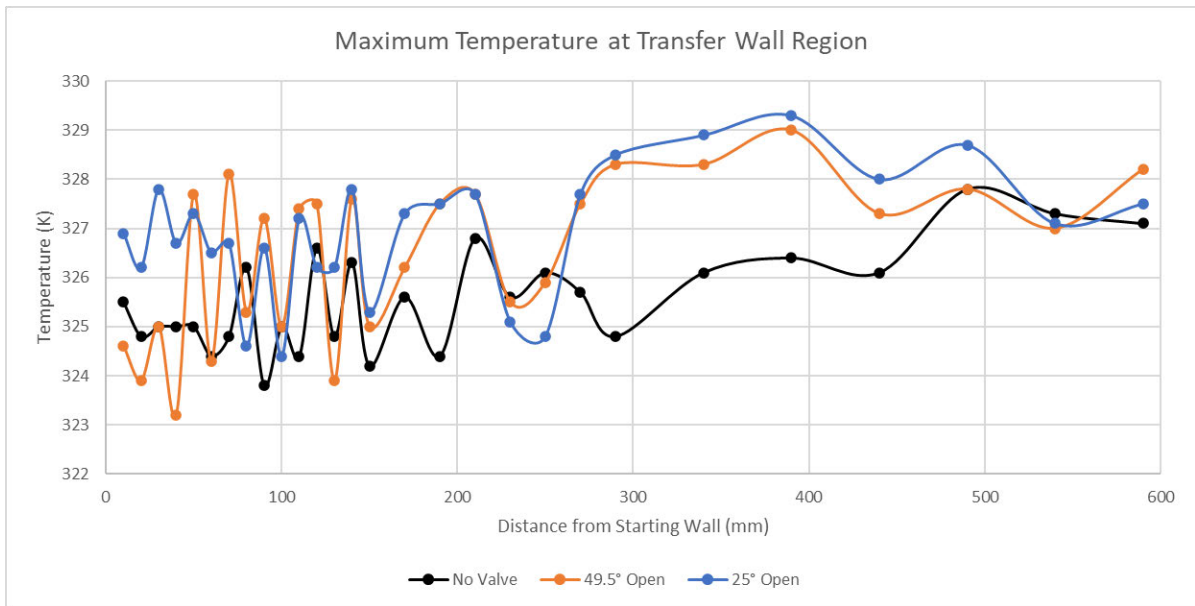


**Figure 5-22:** Maximum temperature at the transfer wall region at various valve positions.

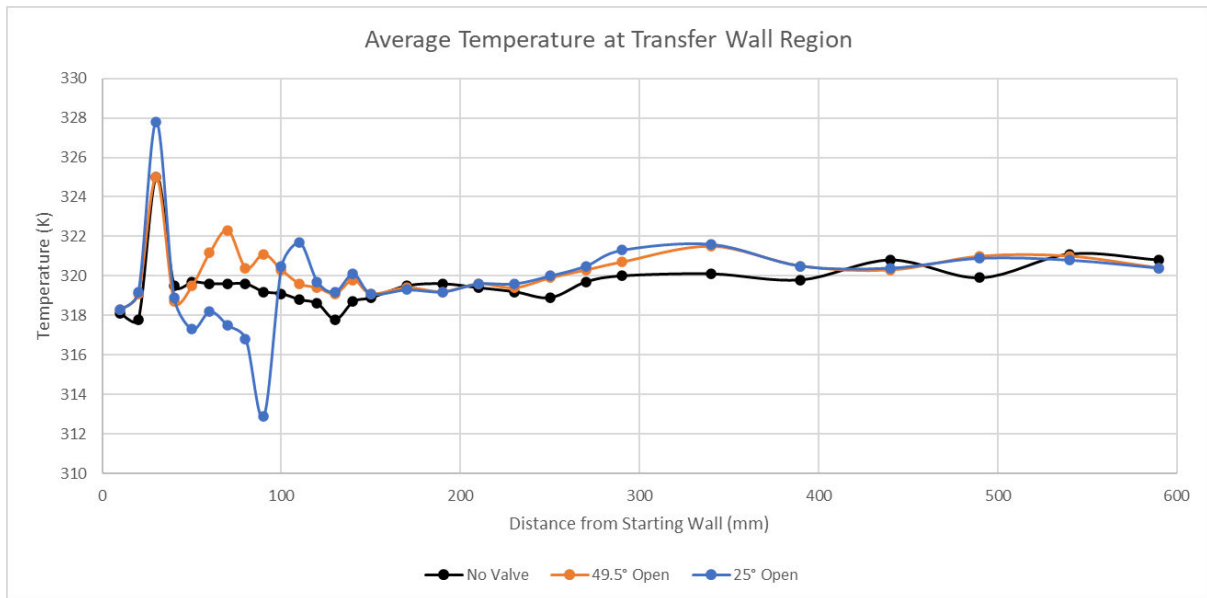


**Figure 5-23:** Average temperature at the transfer wall region at various valve positions.

Figure 5-22 shows the maximum temperatures fluctuate significantly in the first 250mm of tube between the different models with the temperature trend lines crossing each other and not showing any notable trend. This is shown in more detail in figure 5-24 below. In the section 250 – 475mm from the starting wall, the temperature trend lines on the two models with the valve can be seen to trend significantly above the baseline trend line. This is shown in more detail in figure 5-25 below.

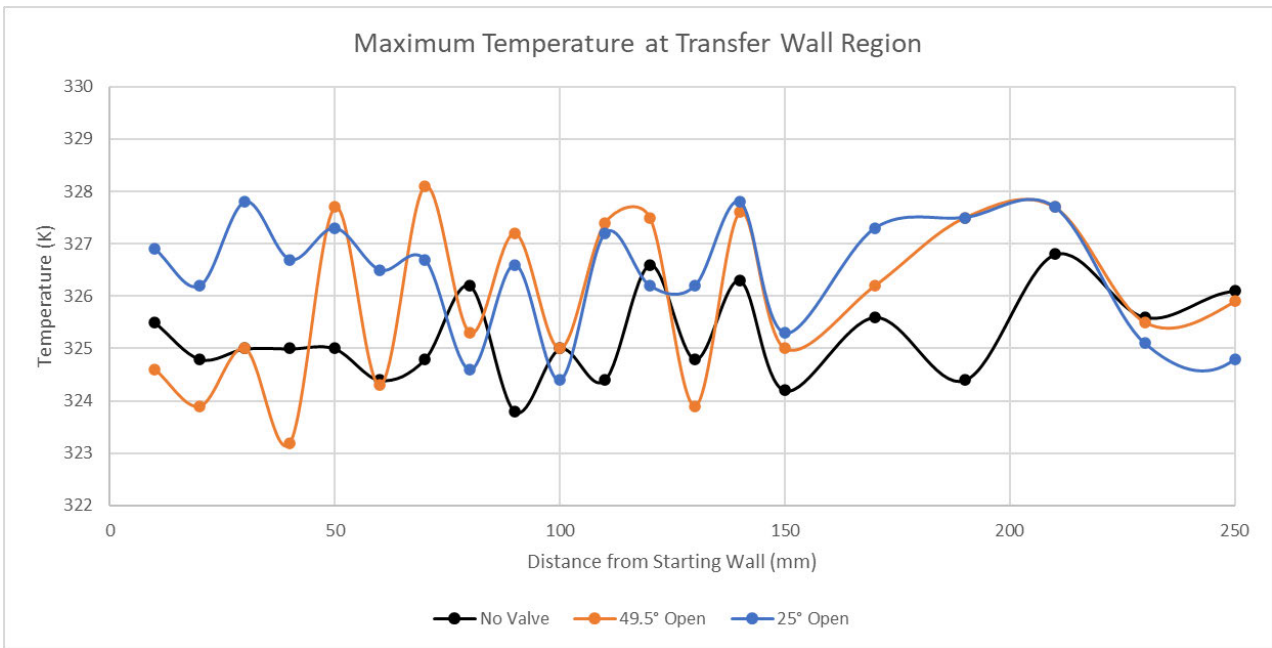


Figure 5-24: Maximum temperature at the transfer wall region at various valve positions refined for 0-250mm.

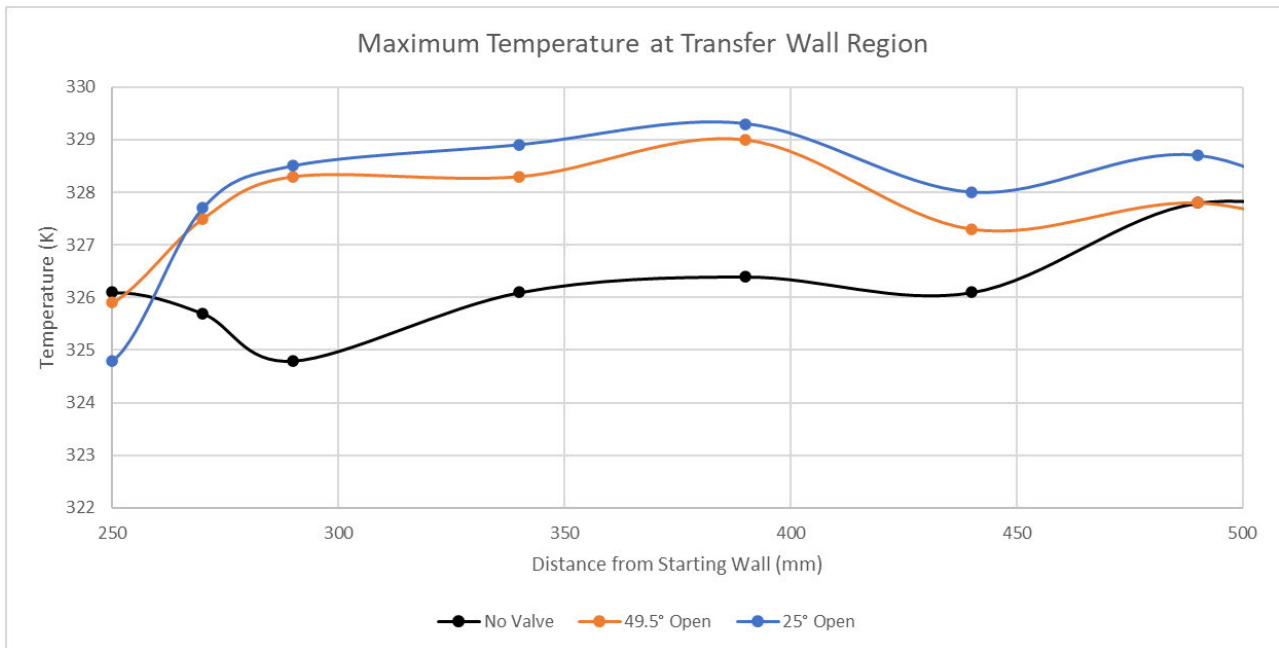


Figure 5-25: Maximum temperature at the transfer wall region at various valve positions refined for 250-500mm.

In both models the maximum temperature trend lines trend 2-4 degrees above the baseline trend line between the distances of approximately 275-425mm from the hot water exit point.

### 5.6.3 Findings

This section analysed the entry region of the heat exchanger comparing CFD models of a heat exchanger scaled to an industrial application with and without a valve. The data has shown that when the valve angle is closed to significantly change the flow rate of the fluid there is higher maximum temperatures on the transfer wall between 275-425mm into the tube's transfer wall region.

This was noted to produce similar results to those produced on the Armfield models in section 4.5, however at different locations. It was also noted that the entry region and valve geometry was significantly different between the Armfield and scaled models with 8.25mm diameter valve compared to 140mm diameter valve. To investigate this further, the two datasets were normalised by changing the distance to a scale of units of valve diameter to compare. The extreme valve closed cases from section 4.5 and 5.6 were used for clarity. The plot of these results can be seen in figure 6-1 below.

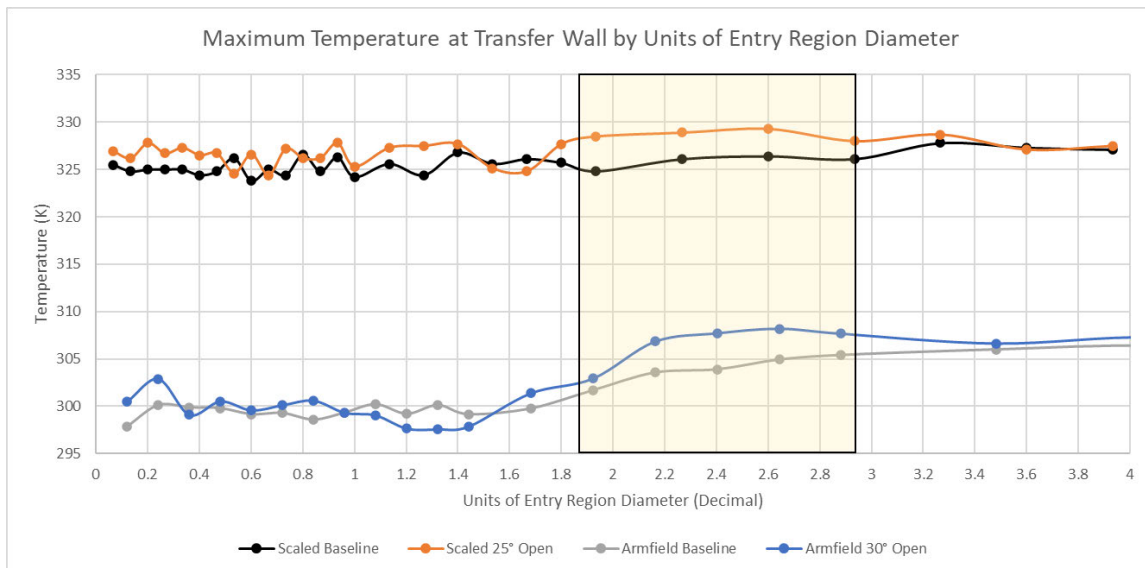


Figure 5-26: Maximum temperature at transfer wall by units of valve diameter.

Both the Armfield and scaled models have shown a significant deviation in the temperature trend lines at a location between approximately 1.9 and 2.9x the diameter of the entry region into the heat exchanger.

These two experimental datasets combined gives the author confidence these findings are valid. There is genuine influence from the valve on the maximum temperature spikes found on the transfer wall in the entry to the head exchanger.

## 5.7 Valve Angle Influence

The results discussed in both section 4.5.6 and 5.6.3 have shown deviations from the baseline (no valve) transfer wall temperature distribution can be caused from the control valve. For further verification and to understand if the valve angle had an influence on the amount of temperature spikes experienced, further studies were completed on the area 210-550mm from the starting wall on the scaled model.

The existing model, meshing and boundary conditions from chapter 5.6 were used. For finer resolution, measurement spacing was changed to collect 18 sets of data through the 210-550mm section of interest identified in the previous section resulting in 20mm spacing between measurements.

The full set of tubulised data from these experiments can be found in appendix I. Figure 5-26 below shows the maximum temperature at the transfer wall at various locations for valve opening positions at every 5° angle. To give a more clarity, the data was smoothed by averaging each reading with the previous and following values.

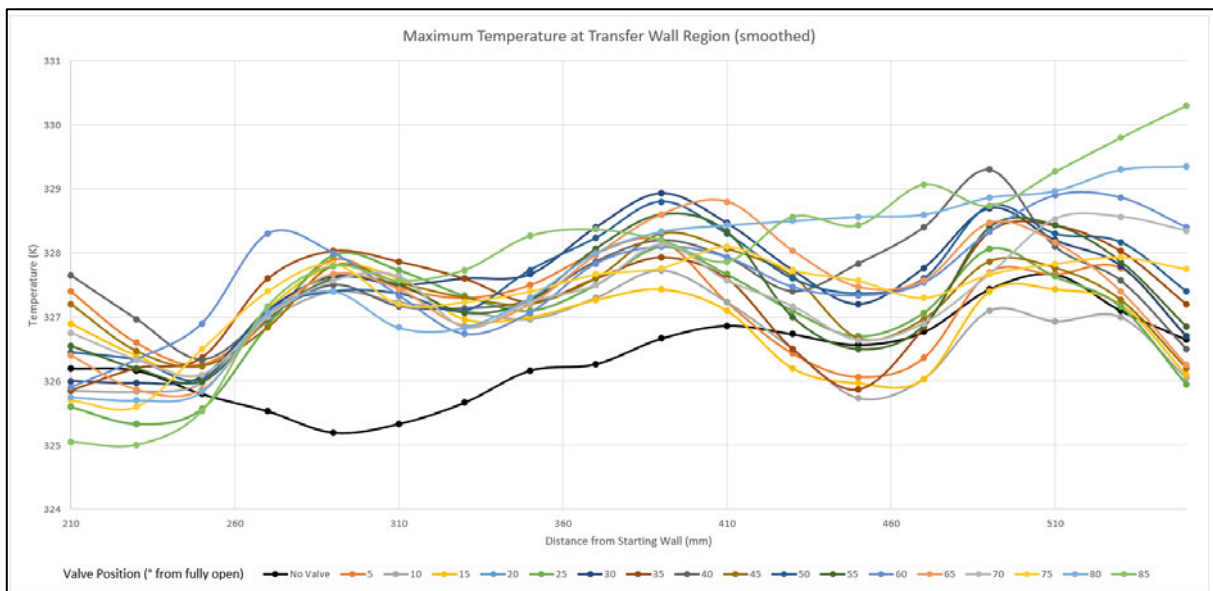


Figure 5-27: Maximum temperature at transfer wall for various valve open angles (smoothed).

This graph whilst busy, shows that in general all the models with the valve trend higher than the baseline through the 200-400mm region. Between the 400-520mm region of the graph some temperature trend lines stayed higher than the baseline, however some trended under. The more-closed valves appear to have higher deviations from this chart.

To investigate this further, the temperature differences for each valve open position was averaged and the maximum deviation was calculated. This data was plotted as shown in figure 5-27 below. The general trendlines show that as the valve is closed, the maximum temperature spikes on the transfer wall increase in both on average across the region and in maximum value measured.

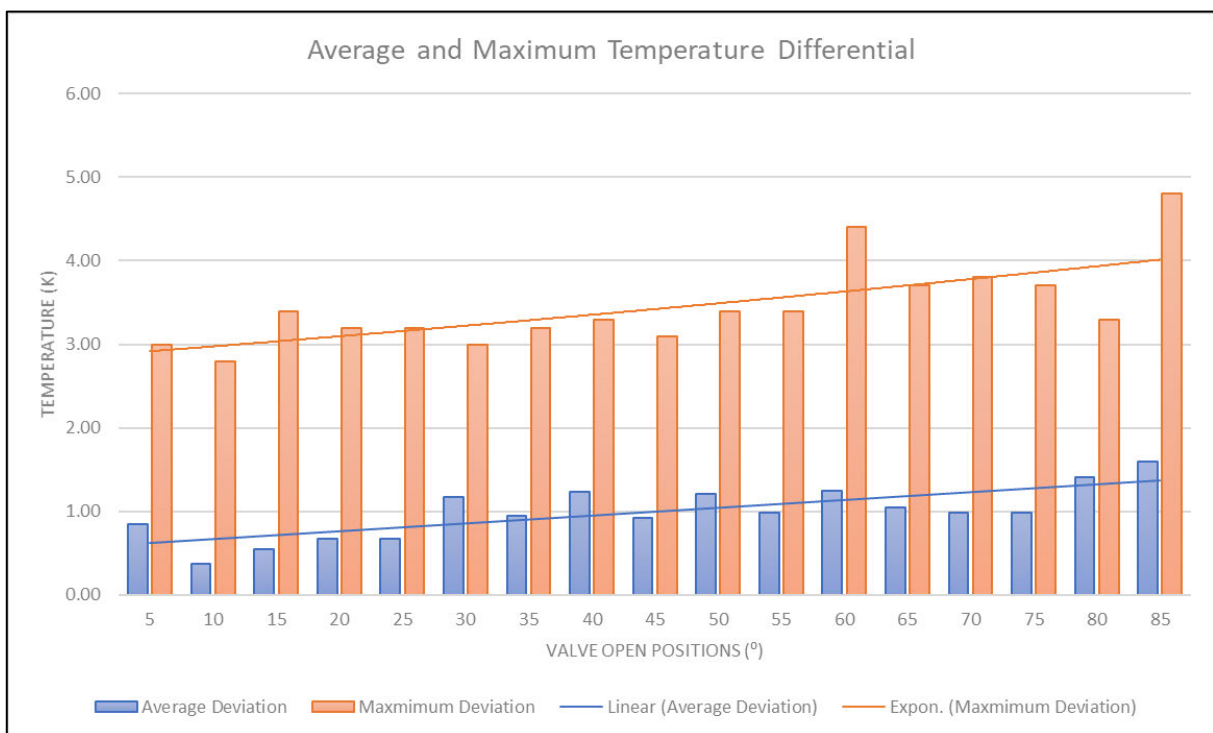


Figure 5-28: Average and maximum temperature differential with various valve open angles.

## 6.0 Chapter 6: Conclusion

### 6.1 Findings and Discussions

This dissertation set out to investigate the claims that a variable speed pump used in heat exchanger control system would create a better heat distribution throughout the exchanger, compared to a fixed output pump with butterfly control valve at the process water entry point.

ANSYS Computational Fluid Dynamics software was used to analyse a series of 3D models of fluid paths within a dual tube heat exchanger. The initial simple models were verified with physical experiments. Subsequent models were then created with greater complexity and size and verified with models. The initial models were created to simulate the Armfield HT36 educational heat exchanger at the University of Southern Queensland. Subsequent models were scaled and modified to simulate the conditions of an industrial application.

In both the smaller and scaled models and simulations, two hypotheses were tested:

- If an entry region control valve would influence the global temperature distribution of fluids within the heat exchanger
- If an entry region control valve would influence the local temperature maximums on the transfer wall of the heat exchanger close to the entry region.

Following these findings, a third hypothesis was tested as further work to further validate the results:

- If there was a valve angle which would produce the maximum temperature spike.

#### ***Global Temperature Distribution***

In section 4.4, the global temperature distribution was compared across the whole Armfield HT36 heat exchanger core in both physical and CFD experiments. The physical experiments found a temperature difference of 0.31% and a difference of 0.55% in the boundary conditions. The CFD experiments found an error of 3.51% and the same 0.55% difference in the boundary conditions. The CFD models however revealed a departure in boundary conditions compared to previous models when the valve was added. This is likely due to some slight differences in meshing required and boundary conditions in the model.

In section 5.5, the global temperature distribution was compared across a scaled model of a heat exchanger with the sizing, fluid and boundary conditions changed to match the requirements of an industrial application. These CFD experiments showed a maximum error of 0.02% between models for all the measurement locations across the model heat exchanger.

The combination of these tests gives the author confidence that a control valve near the entry region of the heat exchanger has no influence on the global temperature distribution throughout the heat exchanger.

### ***Local Transfer Wall Maximum Temperatures***

In section 4.5, a CFD model was created isolating the entry region of the Armfield HT36 heat exchanger to investigate influence of a valve on the transfer wall area. The experiments with a valve at a significantly closed position revealed maximum temperature trend lines that deviated from the baseline trend line. This occurred between 15 and 25mm from the hot water exit wall. The variation was between 3-4 degrees through this region.

In section 5.6, a similar experiment was performed with a scaled model of a heat exchanger with the sizing, fluid and boundary conditions changed to match the requirements of an industrial application. Like the first experiment, this CFD modelling found the maximum temperature trend lines that deviated from the baseline trend line by 2-4 degrees. This was noted to be at 275 to 425mm from the hot water exit wall.

In section 5.6.3 the results from section 4.5 and 5.6 were compared by dividing the data location into the exchanger by the valve diameter. Comparing the results found the temperature spikes occurred at the same relative location of 1.9-2.9x the valve diameter into the heat exchanger.

The combination of these tests gives the author confidence that a control valve near the entry region of the heat exchanger does have influence on the local temperature distribution at the transfer wall of the heat exchanger.

### ***Valve Angle Influence***

In section 5.7 a series of computational fluid dynamic experiments were completed on the scaled heat exchanger model with valves in various open positions incrementing by 5° each experiment. These results of this data showed the temperature spikes generally increased as the valve was further closed. This set of data also reinforced the findings about the local transfer wall discussed above with the experiments with the valve showing temperatures spikes above the baseline.

## **6.2 Recommendations**

In chapter 1 it was discussed that this project was inspired by the sales pitch of a supplier indicating their heat exchanger product was better due to the use of variable speed pumps instead of butterfly control valves. Based on the findings of this dissertation the author agrees it is possible the use of a control valve could create hot locations within the transfer wall region of the heat exchanger core. Possible mitigation to these localised hot locations could be:

- The removal of the control valve through a variable speed pump
- Relocation of the control valve to more than 10x valve diameter away from the entry region.

Aside from the findings in this study, the use a variable speed pump does have the other benefits:

- Efficiency improvements from using less power when variable speed pump has less output
- Longer pump life due to less cavitation from the throttling affect.

### **6.3 Further Work**

As discussed in section 3.2.2, the technology used in most industrial application is not dual-wall type heat exchangers but often plate-type heat exchangers. To verify the results of this study for industrial equipment, this study should be repeated with real models of equipment. This would likely require sponsorship of a supplier as the geometry of such equipment would likely be proprietary.

The mesh in section 5 had to be coarser than the author would have liked due to the element limitation of ANSYS student edition. Further work could be done to complete a mesh independency study on the models from this section using a full version of ANSYS to verify the results are stable and accurate. In the literature review section 2.4.2, it was found other available studies required element counts of >3,000,000 elements for stability where the use of ANSYS student version in this study limited the models to 512,000 elements.

A further study could be completed on the temperature trend deviation found between 1.9 and 2.9x the entry region diameter to understand if and how the deviation varies at different entry temperatures, geometry, and valve angles. The scope of these experiments would be unfeasible within this dissertation as it would likely involve many hundreds of experiments of considerable analysis. It would be interesting to further study what combination of temperature difference, valve angle, valve geometry and heat exchange geometry causes the most affect to the local temperature spikes. The CFD study could also be refined to include more data points in the region identified to be most affected.

The temperature differences found in the heat exchanger transfer wall were on 3-4 degrees. Further work could be completed to understand what level of temperature spikes on the transfer wall would lead to undesirable effects such as fouling and nucleate boiling.

# References

- Aghayari, R, Maddah, H, Ashori, F, Hakiminejad, A & Aghili, M 2015, 'Effect of nanoparticles on heat transfer in mini double-pipe heat exchangers in turbulent flow', *Heat and Mass Transfer*, vol. 51, no. 3, pp. 301-6, <https://doi.org/10.1007/s00231-014-1415-0>.
- Amanowicz, L 2018, 'Influence of geometrical parameters on the flow characteristics of multi-pipe earth-to-air heat exchangers – experimental and CFD investigations', *Applied Energy*, vol. 226, pp. 849-61, [https://usq.primo.exlibrisgroup.com/permalink/61UOSQ\\_INST/1d4atb2/cdi\\_gale\\_infotracacademiconefile\\_A547117828](https://usq.primo.exlibrisgroup.com/permalink/61UOSQ_INST/1d4atb2/cdi_gale_infotracacademiconefile_A547117828).
- Andersson, B 2012, *Computational fluid dynamics for engineers*, Cambridge University Press, Cambridge [England], [https://usq.primo.exlibrisgroup.com/permalink/61UOSQ\\_INST/dodgkr/alma991006123992804691](https://usq.primo.exlibrisgroup.com/permalink/61UOSQ_INST/dodgkr/alma991006123992804691).
- Ansys Inc 2009, *4.5 Standard and SST k-omega Models*, Ansys Inc, afs.enea.it, viewed 15 August, <https://www.afs.enea.it/project/neptunius/docs/fluent/html/th/node65.htm>.
- Armfield Limited 2015, *Extended Tubular Heat Exchanger Teaching Extracts*, ISSUE 9 edn, Armfield Limited, United Kingdom.
- Bashtani, I & Esfahani, JA 2019, 'ε-NTU analysis of turbulent flow in a corrugated double pipe heat exchanger: A numerical investigation', *Applied Thermal Engineering*, vol. 159, p. 113886, [https://usq.primo.exlibrisgroup.com/permalink/61UOSQ\\_INST/1d4atb2/cdi\\_crossref\\_primary\\_10\\_1016\\_j\\_applthermaleng\\_2019\\_113886](https://usq.primo.exlibrisgroup.com/permalink/61UOSQ_INST/1d4atb2/cdi_crossref_primary_10_1016_j_applthermaleng_2019_113886).
- Chun, M-H & Kang, M-G 1996, 'Effects of heat exchanger tube geometries on nucleate pool boiling heat transfer in a scaled in-containment refueling water storage tank', *International communications in heat and mass transfer*, vol. 23, no. 1, pp. 23-34, [https://usq.primo.exlibrisgroup.com/permalink/61UOSQ\\_INST/1d4atb2/cdi\\_scopus\\_primary\\_126402585](https://usq.primo.exlibrisgroup.com/permalink/61UOSQ_INST/1d4atb2/cdi_scopus_primary_126402585).
- Cummins Inc 2016, *Generator Set Data Sheet - QSK78-G12*, Cummins Inc, CIGroup-US, viewed 19 May, <https://cigroup-us.com/wp-content/uploads/2019/09/Cummins-Diesel-Generator-DQLE-QSK78-Data-Sheet.pdf>.
- Del Toro, A, Johnson, MC & Spall, RE 2015, 'Computational Fluid Dynamics Investigation of Butterfly Valve Performance Factors', *Journal - American Water Works Association*, vol. 107, no. 5, pp. E243-E54, [https://usq.primo.exlibrisgroup.com/permalink/61UOSQ\\_INST/1d4atb2/cdi\\_crossref\\_primary\\_10\\_5942\\_jawwa\\_2015\\_107\\_0\\_052](https://usq.primo.exlibrisgroup.com/permalink/61UOSQ_INST/1d4atb2/cdi_crossref_primary_10_5942_jawwa_2015_107_0_052).
- Denkenberger, DC, Brandemuehl, MJ, Zhai, J & Pearce, JM 2021, 'Finite Difference Heat Exchanger Model: Flow Maldistribution with Thermal Coupling', *Heat transfer engineering*, vol. 42, no. 11, pp. 889-903, [https://usq.primo.exlibrisgroup.com/permalink/61UOSQ\\_INST/1d4atb2/cdi\\_informaworld\\_taylorfrancis\\_310\\_1080\\_014576\\_32\\_2020\\_1756060](https://usq.primo.exlibrisgroup.com/permalink/61UOSQ_INST/1d4atb2/cdi_informaworld_taylorfrancis_310_1080_014576_32_2020_1756060).
- Dielectric Manufacturing 2020, *Acrylic*, Dielectric Manufacturing, viewed 01 May, <https://dielectricmfg.com/knowledge-base/acrylic-thermoplastic/>.
- Energy Education 2020, *Thermal conductivity*, Energy Education,, viewed 01 May, [https://energyeducation.ca/encyclopedia/Thermal\\_conductivity](https://energyeducation.ca/encyclopedia/Thermal_conductivity).
- Engineering ToolBox 2003, *Ethylene Glycol Heat-Transfer Fluid*, Engineering ToolBox, viewed 24 August, [https://www.engineeringtoolbox.com/ethylene-glycol-d\\_146.html](https://www.engineeringtoolbox.com/ethylene-glycol-d_146.html).
- Engineering ToolBox 2003, *Heat Exchanger Heat Transfer Coefficients*, Engineering Toolbox, viewed 25 August, [https://www.engineeringtoolbox.com/heat-transfer-coefficients-exchangers-d\\_450.html](https://www.engineeringtoolbox.com/heat-transfer-coefficients-exchangers-d_450.html).
- Engineers Edge 2021, *Parallel and Counter Flow Designs*, Engineers Edge, <https://www.engineersedge.com/>, viewed 21 July, [https://www.engineersedge.com/heat\\_transfer/parallel\\_counter\\_flow\\_designs.htm](https://www.engineersedge.com/heat_transfer/parallel_counter_flow_designs.htm).
- Fisher 2001, *Control Valve Handbook*, Fisher Controls International Inc, <https://www.chemicalprocessing.com/>, viewed 03 August, [https://www.chemicalprocessing.com/assets/Media/MediaManager/control\\_valves.pdf](https://www.chemicalprocessing.com/assets/Media/MediaManager/control_valves.pdf).

- Fridman, E & Mahajan, HS 2014, *Heat transfer virtual lab for students and engineers : theory and guide for setting up*, Momentum Press, New York, [New York] (222 East 46th Street, New York, NY 10017), [https://usq.primo.exlibrisgroup.com/permalink/61UOSQ\\_INST/dodgkr/alma991006123950304691](https://usq.primo.exlibrisgroup.com/permalink/61UOSQ_INST/dodgkr/alma991006123950304691).
- Iqbal, M & Syed, KS 2011, 'Thermally developing flow in finned double-pipe heat exchanger', *International journal for numerical methods in fluids*, vol. 65, no. 10, pp. 1145-59, [https://usq.primo.exlibrisgroup.com/permalink/61UOSQ\\_INST/1d4atb2/cdi\\_istex\\_primary\\_ark\\_67375\\_WNG\\_MLB0NJVK\\_3](https://usq.primo.exlibrisgroup.com/permalink/61UOSQ_INST/1d4atb2/cdi_istex_primary_ark_67375_WNG_MLB0NJVK_3).
- Johnson Controls 1996, *Valve Basics and Sizing Information Section, Section Vb2: Butterfly Valves*, Johnson Controls, viewed August 2021, [https://cgproducts.johnsoncontrols.com/MET\\_PDF/347VB2.PDF?x=86&x=86](https://cgproducts.johnsoncontrols.com/MET_PDF/347VB2.PDF?x=86&x=86).
- Kapustenko, P, Dobromyslova, O, Dobromyslov, O, Perevertaylenko, O, Arsenyeva, O, Ilyunin, O & Shabanov, E 2009, 'Control of Plate Heat Exchanger Outlet Temperature Using Butterfly Valve and Parametric Model Control Technique', *Chemical engineering transactions*, vol. 18, [https://usq.primo.exlibrisgroup.com/permalink/61UOSQ\\_INST/1d4atb2/cdi\\_doaj\\_primary\\_oai\\_doaj\\_org\\_article\\_fd22405378014792ab1c0b689b09ce91](https://usq.primo.exlibrisgroup.com/permalink/61UOSQ_INST/1d4atb2/cdi_doaj_primary_oai_doaj_org_article_fd22405378014792ab1c0b689b09ce91).
- Lazarevic, S, Congradac, V, Andjelkovic, A, Kljajic, M & Kanovic, Z 2019, 'District heating substation elements modeling for the development of the real-time model', *Thermal science*, vol. 23, no. 3 Part B, pp. 2061-70, [https://usq.primo.exlibrisgroup.com/permalink/61UOSQ\\_INST/1d4atb2/cdi\\_doaj\\_primary\\_oai\\_doaj\\_org\\_article\\_63191ae7693442e3ab5f21de277a1e05](https://usq.primo.exlibrisgroup.com/permalink/61UOSQ_INST/1d4atb2/cdi_doaj_primary_oai_doaj_org_article_63191ae7693442e3ab5f21de277a1e05).
- Luyben, WL 2011, 'Heat-Exchanger Bypass Control', *Industrial & engineering chemistry research*, vol. 50, no. 2, pp. 965-73, [https://usq.primo.exlibrisgroup.com/permalink/61UOSQ\\_INST/1d4atb2/cdi\\_crossref\\_primary\\_10\\_1021\\_ie1020574](https://usq.primo.exlibrisgroup.com/permalink/61UOSQ_INST/1d4atb2/cdi_crossref_primary_10_1021_ie1020574).
- Pedlosky, J 1987, *Geophysical fluid dynamics*, Springer, New York, <https://archive.org/details/geophysicalfluid00jose/page/10>.
- PowerTest Inc. 2015, *Closed Loop Cooling System - Stationary*, PowerTest Inc, viewed 24 August, <https://powertestdyno.com/wp-content/uploads/sites/2/2020/04/CLCS-SpecSheet-Combined.pdf>.
- Rajeshkumar, M, Logesh, K, Thangaraj, M & Govindan, S 2021, 'Heat transfer study on finned tube heat exchanger using CFD', *International journal of ambient energy*, vol. 42, no. 3, pp. 239-43, [https://usq.primo.exlibrisgroup.com/permalink/61UOSQ\\_INST/1d4atb2/cdi\\_crossref\\_primary\\_10\\_1080\\_01430750\\_2018\\_1542621](https://usq.primo.exlibrisgroup.com/permalink/61UOSQ_INST/1d4atb2/cdi_crossref_primary_10_1080_01430750_2018_1542621).
- Ramsey, MS 2019, 'Chapter Six - Rheology, Viscosity, and Fluid Types', in MS Ramsey (ed.), *Practical Wellbore Hydraulics and Hole Cleaning*, Gulf Professional Publishing, Cambridge, USA, pp. 217-37, <https://www.sciencedirect.com/science/article/pii/B978012817088500006X>.
- Rao, JS 2017, *Simulation Based Engineering in Fluid Flow Design*, Springer International Publishing, India, [https://usq.primo.exlibrisgroup.com/permalink/61UOSQ\\_INST/dodgkr/alma991005950709704691](https://usq.primo.exlibrisgroup.com/permalink/61UOSQ_INST/dodgkr/alma991005950709704691).
- Sayed Ahmed, SAE, Mesalhy, OM & Abdelatif, MA 2015, 'Flow and heat transfer enhancement in tube heat exchangers', *Heat and Mass Transfer*, vol. 51, no. 11, pp. 1607-30, [https://usq.primo.exlibrisgroup.com/permalink/61UOSQ\\_INST/1d4atb2/cdi\\_springer\\_primary\\_2015\\_231\\_51\\_11\\_1669](https://usq.primo.exlibrisgroup.com/permalink/61UOSQ_INST/1d4atb2/cdi_springer_primary_2015_231_51_11_1669).
- Sensata Technologies Inc 2021, *UF25B Ultrasonic Flow Meter*, Sensata Technologies Inc, viewed 25 May, <https://www.cynergy3.com/sites/default/files/cynergy3-uf25b-v4.pdf>.
- Shah, RK & Sekulic, DP 2003, *Fundamentals of Heat Exchanger Design*, Wiley & Sons, Inc, Hoboken, New Jersey, [https://usq.primo.exlibrisgroup.com/permalink/61UOSQ\\_INST/dodgkr/alma991006276133404691](https://usq.primo.exlibrisgroup.com/permalink/61UOSQ_INST/dodgkr/alma991006276133404691).
- Sharifi, K, Sabeti, M, Rafiei, M, Mohammadi, AH & Shirazi, L 2018, 'Computational fluid dynamics (CFD) technique to study the effects of helical wire inserts on heat transfer and pressure drop in a double pipe heat exchanger', *Applied Thermal Engineering*, vol. 128, pp. 898-910, <https://www.sciencedirect.com/science/article/pii/S1359431117323049>.
- Song, X, Wang, L & Park, Y 2009, 'Analysis and optimization of a butterfly valve disc', *Proceedings of The Institution of Mechanical Engineers Part E-journal of Process Mechanical Engineering - PROC INST MECH ENG E-J P M E*, vol. 223, pp. 81-

9,

[https://usq.primo.exlibrisgroup.com/permalink/61UOSQ\\_INST/1d4atb2/cdi\\_crossref\\_primary\\_10\\_1243\\_09544089JPME236](https://usq.primo.exlibrisgroup.com/permalink/61UOSQ_INST/1d4atb2/cdi_crossref_primary_10_1243_09544089JPME236).

Sung-Woong, C, Hyoung-Seock, S & Han-Sang, K 2021, 'Analysis of Flow Characteristics and Effects of Turbulence Models for the Butterfly Valve', *Applied sciences*, vol. 11, no. 6319, p. 6319, [https://usq.primo.exlibrisgroup.com/permalink/61UOSQ\\_INST/1d4atb2/cdi\\_doaj\\_primary\\_oai\\_doaj\\_org\\_article\\_19676a05567d4de7a4a47af9d34b19f0](https://usq.primo.exlibrisgroup.com/permalink/61UOSQ_INST/1d4atb2/cdi_doaj_primary_oai_doaj_org_article_19676a05567d4de7a4a47af9d34b19f0).

Taler, D 2019, *Numerical Modelling and Experimental Testing of Heat Exchangers*, 1st ed. 2019. edn, vol. 161, Studies in Systems, Decision and Control, Poland, [https://usq.primo.exlibrisgroup.com/permalink/61UOSQ\\_INST/dodgkr/alma991006396715204691](https://usq.primo.exlibrisgroup.com/permalink/61UOSQ_INST/dodgkr/alma991006396715204691).

Tomoe Valve n.d., *Data*, Tomoe Valve Co Ltd, viewed 05 Aug, <https://www.tomoevalve.com/english/pdf/ValveRelatedData.pdf>.

Wasserman, S 2016, *Choosing the Right Turbulence Model for Your CFD Simulation*, Engineering.com, viewed 19 May, <https://www.engineering.com/story/choosing-the-right-turbulence-model-for-your-cfd-simulation>.

Wojtkowiak, J 2006, 'Investigations of Butterfly Control Valve Flow Characteristics', *Foundations of Civil and Environmental Engineering*, vol. 7, pp. 382-95, <[https://www.researchgate.net/publication/242672823\\_INVESTIGATIONS\\_OF\\_BUTTERFLY\\_CONTROL\\_VALVE\\_FLOW\\_CHARACTERISTICS](https://www.researchgate.net/publication/242672823_INVESTIGATIONS_OF_BUTTERFLY_CONTROL_VALVE_FLOW_CHARACTERISTICS)>.

Yunus A Cengel, AJG 2015, *Heat and Mass Transfer*, McGraw-Hill Education, New York.

Yunus Cengel, JC, Afshin Ghajar 2016, *Fundamentals of Thermal-Fluid Sciences*, 5th edn, McGraw-Hill Education, Europe.

Zhang, K, Li, M-J, Liu, H, Xiong, J-G & He, Y-L 2021, 'A general and rapid method to evaluate the effect of flow maldistribution on the performance of heat exchangers', *International journal of thermal sciences*, vol. 170, [https://usq.primo.exlibrisgroup.com/permalink/61UOSQ\\_INST/1d4atb2/cdi\\_elsevier\\_sciencedirect\\_doi\\_10\\_1016\\_j\\_ijthermalsci\\_2021\\_107152](https://usq.primo.exlibrisgroup.com/permalink/61UOSQ_INST/1d4atb2/cdi_elsevier_sciencedirect_doi_10_1016_j_ijthermalsci_2021_107152).

## Appendix A – Project Specification

For: Terrence Clarke

Title: Heat exchanger performance and optimization

Major: Mechanical Engineering

Supervisor: Khalid Saleh

Enrollment: ENG4111 – ONC S1, 2021  
ENG4112 – ONC S2, 2021

Project Aim: To understand if, in an engine dynamometer test cooling application, using a fixed output water pump with butterfly valve produces localized hot spots in a fluid to fluid heat exchanger core compared to the use of a variable speed water pump without control valve.

Confidentiality: All information used for the project will be based on information available in the public domain, so will not require any specific confidentiality consideration. During the information gathering stage, if I find I need specifications outside the public domain I will work with USQ and supplier of information to consider if public access restriction is appropriate.

Communication Plan: Weekly update emails from Terrence to Khalid. Zoom calls or face-to-face meetings as/if required at time agreed by both parties.

**Programme: Version 1, 18 March 2021**

1. Research existing studies and literature available on temperature distribution throughout a head exchanger, comparing the use of throttling valves vs variable speed pump control systems.
2. Research industrial heat exchangers available for dynamometer testing of a large diesel engine.
3. Research information on the USQ laboratory fluid/fluid heat exchanger.
4. Learn how to complete a CFD study of heat exchanger using Ansys software.
5. Complete initial CFD studies using boundary conditions that could be simulated in the lab environment.
6. Complete physical experiment in the USQ lab with same boundary conditions as CFD studies. Compare results and confirm CFD and physical experimental data match.
7. Re-scale the CFD simulation to a set of real-life boundary conditions and complete a series of studies.
8. Analyse data and produce conclusion.

## Appendix B – Project Planning Timeline

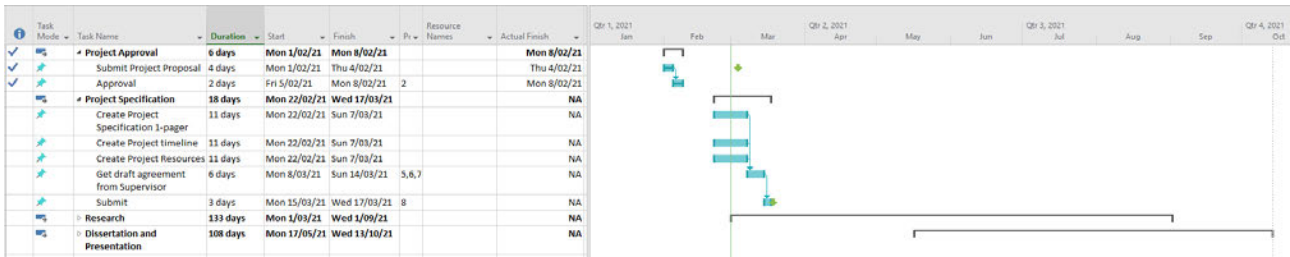


Figure B-1: Screenshot of project plan showing project approval and project specification plans.

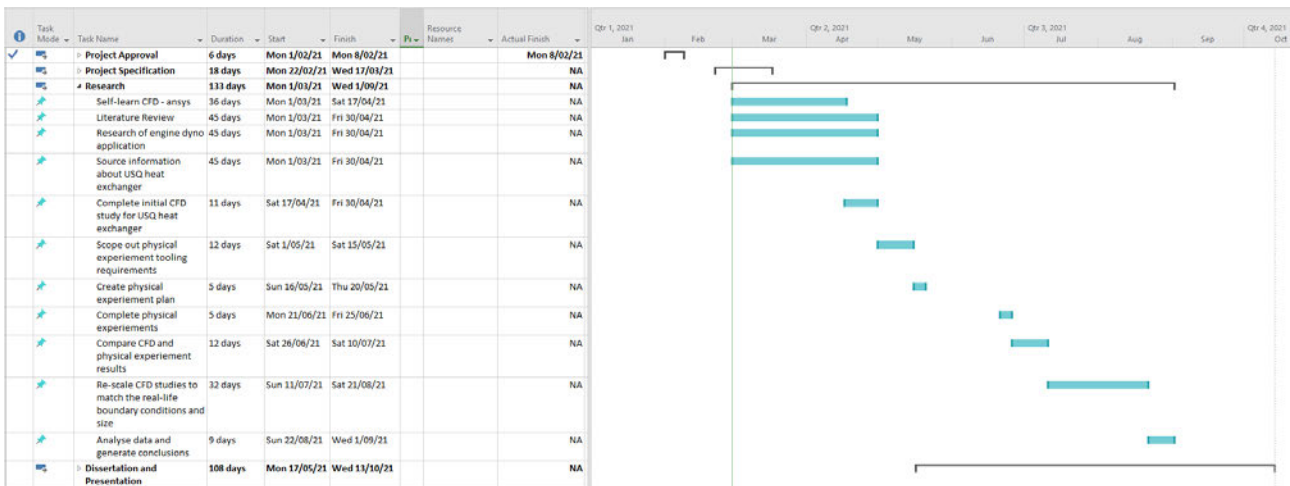


Figure B-2: Screenshot of project plan showing research plans.

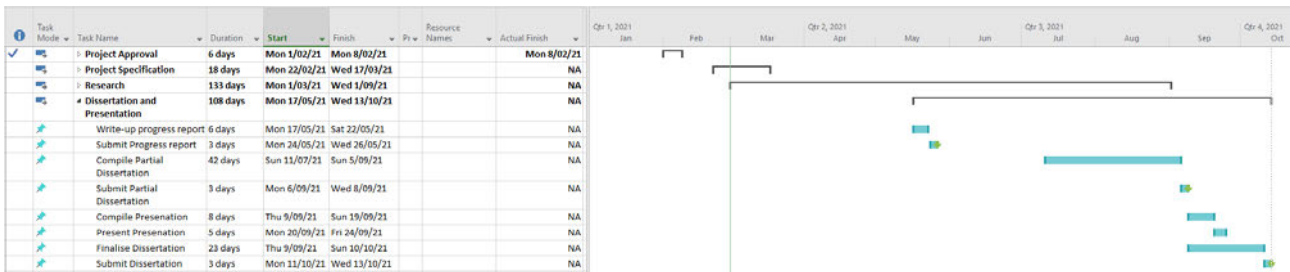


Figure B-3: Screenshot of project plan showing dissertation and presentation plans.

## Appendix C – Risk Assessment for Physical Experiments

This risk assessment was completed on, and approved in, the USQ Safety Risk Management System online system. Screenshots showing all the detail are in this appendix.

Safety Risk Management Plan					
Risk Management Plan ID:	Status:	Current User:	Author:	Supervisor:	Approver:
RMP_2021_5546	Approve				
Assessment Title:	Armfield HT36 Experiment for Terrence Clarke ENG4111 Dissertation			Assessment Date:	19/05/2021
Workplace (Division/Faculty/Section):	204070 - School of Mechanical and Electrical Engineering			Review Date:	31/12/2021 (5 years maximum)
Approver:	Supervisor: (for notification of Risk Assessment only)				
Khalid Saleh:	Mohan Trada:				
Context					
<b>DESCRIPTION:</b>					
What is the task/event/purchase/project/procedure?	Complete the Armfield HT36 Experiments as per experiment plan provided.				
Why is it being conducted?	Experimental data for ENG4111 dissertation				
Where is it being conducted?	USQ Lab				
Course code (if applicable)	ERP2021/ENG4111	Chemical Name (if applicable)	Water		
<b>WHAT ARE THE NOMINAL CONDITIONS?</b>					
Personnel involved	Terrence Clarke (student), Khalid Saleh (Supervisor) & Mohan Trada (Technical Staff)				
Equipment	Armfield HT36 test equipment				
Environment	Lab				
Other	Estimated Experiment Date: Monday 24 May 2021.				
Briefly explain the procedure/process	Performing Experiment A from the Armfield HT36 instruction manual and recording the data. This involves running cool and warm water through a heat exchanger test jig and logging temperatures through existing thermocouples.				
Assessment Team - who is conducting the assessment?					
Assessor(s):	Khalid Saleh (Supervisor), Belal Yousif (Examiner)				
Others consulted: (eg elected health and safety representative, other personnel exposed to risks)	Mohan Trada (Technical Staff)				

Figure C-1: Risk assessment header information.

Risk Register and Analysis											
Step 1	Step 2	Step 2a	Step 2b	Step 3			Step 4				
Hazards: From step 1 or more if identified	The Risk: What can happen if exposed to the hazard without existing controls in place?	Consequence: What is the harm that can be caused by the hazard without existing controls in place?	Existing Controls: What are the existing controls that are already in place?	Risk Assessment: Consequence x Probability = Risk Level			Additional Controls: Enter additional controls if required to reduce the risk level	Risk assessment with additional controls: Has the consequence or probability changed?			
				Probability	Risk Level	ALARP					
Example							Consequence	Probability	Risk Level	ALARP	
Working in temperatures over 35° C	Heat stress/heat stroke/exhaustion leading to serious personal injury/death	Catastrophic	Regular breaks, chilled water available, loose clothing, fatigue management policy.	Possible	High	No	temporary shade shelters, essential tasks only, close supervision, buddy system	Catastrophic	unlikely	med	No
1	Unidentified risks due to lack of familiarity of the equipment	Personal or equipment/facility damage	Moderate	Nil	Possible	High	Review of the Armfield HT36 manual and the task specific USQ Risk	Minor	Rare	Low	Yes
2	Injury from high temperature fluid contacting human	Eye damage Skin burns	Major	Eye protection is mandatory in the lab Experimental jig has been designed with a maximum temperature of 80DegC	Unlikely	Medium	Dissertation experiment designed to use approx 50DegC maximum Temperature. Flow cold water through experiment first to ensure no leaks or loose fittings. Experimental equipment not to be opened by student - seek technical assistance if faults found.	Minor	Unlikely	Low	Yes
3	Slip hazards from fluid on ground	Trips and falls resulting in personal injury	Major	Lab has cleanliness requirements Equipment maintenance	Unlikely	Medium	low cold water through experiment first to ensure no leaks or loose fittings.	Medium	Rare	Low	Yes
4	Electrical Shock	Electrical shock from water contacting electrical components of the experiment or internal electrical fault of the equipment	Catastrophic	USQ would have appropriate RCD devices. Armfield HT36 includes integrated RCD device.	Unlikely	Medium	Equipment power leads will have test labels checked to be in date before test commences  Before test complete the Armfield RCD test as described in the instruction manual.	Catastrophic	Rare	Low	Yes
5	Exposure to Water Borne Hazards	Sickness due to exposure to water borne hazards.	Major	Regular cleaning of rust, sludge, scale. Regular change of water	Unlikely	Medium	Student to view USQ records of cleaning, water changing and control plan for this risk before completing experiment.	Major	Rare	Low	Yes

Figure C-2: : Risk register and analysis.

Step 5 - Action Plan (for controls not already in place)					
	Additional Controls:	Exclude from Action Plan: (repeated control)	Resources:	Persons Responsible:	Proposed Implementation Date:
1	Review of the Armfield HT36 manual and the task specific USQ Risk Assessment	<input type="checkbox"/>	Armfield HT36 Manual and USQ 'Heat Exchanger Unit' SWP.	Terrence Clarke	19/05/2021
2	Dissertation experiment designed to use approx 50DegC maximum Temperature. Flow cold water through experiment first to ensure no leaks or loose fittings. Experimental equipment not to be opened by student - seek technical assistance if faults found.	<input type="checkbox"/>	Access to experimental jig	Terrence Clarke	24/05/2021
3	low cold water through experiment first to ensure no leaks or loose fittings.	<input type="checkbox"/>	Access to experimental jig	Terrence Clarke	24/05/2021
4	Equipment power leads will have test labels checked to be in date before test commences  Before test complete the Armfield RCD test as described in the instruction manual.	<input type="checkbox"/>	Access to experimental jig	Terrence Clarke	24/05/2021
5	Student to view USQ records of cleaning, water changing and control plan for this risk before completing experiment.	<input type="checkbox"/>	USQ Control Plan and Maintenance Records	Mohan Trada	21/05/2021

Supporting Attachments	
<a href="#">View Attachments</a>	
<a href="#">Click here to attach a file</a>	

Step 6 – Request Approval	
Drafters Name:	Terrence Clarke
Draft Date:	19/05/2021
Drafters Comments:	Completed to best of my knowledge. Ready for Supervisor Approval
Assessment Approval:	All risks are marked as ALARP
Maximum Residual Risk Level:	Low - Manager/Supervisor Approval Required
Document Status:	Approve

Step 6 – Approval	
Approvers Name:	Khalid Saleh
Approvers Position Title:	
Approvers Comments:	
I am satisfied that the risks are as low as reasonably practicable and that the resources required will be provided.	
Approval Decision:	Approve
Approve / Reject Date:	19/05/2021
Document Status:	Approve

Figure C-3: Action plan and approval.

## Appendix D – Mesh Independence Study for Heat Exchanger

	Base Li	Test 1	Test 2	Test 3	Test 4	Test 5	Test 6	Test 7	Test 8	Test 9	Test 10	Test 11	Test 12	Test 13	Test 14	Test 15	Test 16
Hot Water Sweep Divisions	2200	2200	2200	2200	2200	1900	1900	1900	1900	1900	1700	1700	1700	1700	1700	1600	1500
Hot water edge division	28	28	28	28	28	24	24	24	24	24	22	22	22	22	22	22	22
Cold water Body Sizing	0.0026	0.003	0.0035	0.004	0.005	0.0026	0.003	0.0035	0.004	0.005	0.0026	0.003	0.0035	0.004	0.005	0.0045	0.006
Cold water corner Face Size	0.0008	0.001	0.0015	0.002	0.0025	0.0008	0.001	0.0015	0.002	0.0025	0.0008	0.001	0.0015	0.002	0.0025	0.003	0.0035
Cold water transfer face size	0.0021	0.0025	0.0025	0.0025	0.0025	0.0021	0.0025	0.0025	0.0025	0.0025	0.0021	0.0025	0.0025	0.0025	0.0025	0.003	0.0035
Resulting Elements	443487	382876	326806	261251	219804	427587	366976	310906	245351	203904	416987	356376	300306	234751	193304	176712	149892
Average X,Y,Z Convergence	2.730	2.400	1.136	2.567	5.733	3.170	2.967	1.360	2.900	6.600	3.730	3.167	1.169	3.133	8.267	5.2	9.2333
Continuity Convergence (E-0)	1.750	1.150	0.900	1.190	1.600	0.850	1.900	0.600	1.300	1.800	1.900	1.200	0.980	1.250	1.900	2.8	1.5
Energy Convergence (E-07)	1.100	1.100	1.300	3.000	2.800	1.200	1.200	1.300	3.100	2.600	1.280	1.300	1.400	3.350	2.300	3.15	2.4
Hot Temp Out	315.26	315.23	315.27	315.51	315.66	315.29	315.23	315.27	315.49	315.62	315.28	315.23	315.27	315.49	315.6	315.67	315.58
Cold Temp Out	316.19	316.37	316.26	315.57	315.3	316.2	316.37	316.27	315.63	315.3	316.19	316.36	316.26	315.66	315.35	315.19	315.46
Hot Water Centre (T3)	320.29	320.27	320.26	320.25	320.28	320.29	320.27	320.26	320.25	320.27	320.29	320.27	320.26	320.25	320.27	320.28	320.29
Cold Water Centre (T8)	308.02	308.13	308.01	307.37	307.23	308.02	308.13	308	307.35	307.21	308.02	308.13	308	307.35	307.2	307.01	307.35
Hot Water Mass Flow Rate C	0.0499	0.0499	0.0499	0.0491	0.0499	0.0499	0.0499	0.0499	0.0499	0.0499	0.0499	0.0499	0.0499	0.0499	0.0499	0.0499	0.0499
Cold Water Mass Flow Rate	-0.016	-0.017	-0.017	-0.016	-0.016	-0.016	-0.017	-0.017	-0.016	-0.016	-0.016	-0.017	-0.017	-0.016	-0.016	-0.017	-0.016
Hot Water Pressure Centre	2495.7	2495.7	2495.7	2495.7	2495.7	2508.8	2508.8	2508.8	2508.8	2508.8	2565.9	2565.9	2565.9	2565.9	2565.5	2467.6	2471.8
Cold Water Pressure Centre	-980.6	-997.5	-1013	-921.5	-957.6	-980.7	-997.4	-1013	-921.6	-957.6	-980.7	-997.4	-1013	-921.6	-958.4	-935.6	-1213
Convergence Error Reprer	N/A	0%	6%	58%	88%	8%	9%	6%	63%	94%	21%	11%	9%	73%	107%	112%	119%
Temperature Error	N/A	0.11%	0.04%	0.50%	0.67%	0.01%	0.11%	0.04%	0.48%	0.66%	0.01%	0.11%	0.04%	0.47%	0.65%	0.78%	0.55%
Mass Flow Rate Error	N/A	0.16%	0.25%	2.44%	1.53%	0.00%	0.16%	0.25%	0.75%	1.53%	0.00%	0.16%	0.26%	0.76%	1.53%	1.24%	2.72%
Pressure Error	N/A	1.72%	3.33%	6.03%	2.35%	0.53%	2.23%	3.86%	6.55%	2.87%	2.82%	4.52%	6.15%	8.83%	5.07%	5.72%	24.64%
Element Reduction		14%	26%	41%	50%	4%	17%	30%	45%	54%	6%	20%	32%	47%	56%	60%	66%

Figure D-1: Mesh independence study results – for section 4.2.4.

## Appendix E – Mesh Independence Study for Cold-water Entry Region

	Base Line	Test 1	Test 2	Test 3	Test 4	Test 5	Test 6	Test 7	Test 8	Test 9
Hot Water Sweep Divisions	600	550	600	550	500	600	550	600	550	600
Hot water edge division	52	48	52	48	46	52	48	52	48	52
Cold water Body Sizing	0.0007	0.0007	0.0012	0.0012	0.0012	0.0009	0.0009	0.0011	0.0011	0.0008
Valve Face Size	0.0002	0.0002	0.0005	0.0005	0.0005	0.0003	0.0003	0.0004	0.0004	0.00025
Resulting Elements	465279	453479	303431	240165	223440	348830	290166	309910	248847	387359
Average X,Y,Z Convergence [E-06]	2.433	1.567	1.757	17.333	0.350	3.467	7.430	8.333	3.930	3.333
Continuity Convergence [E-03]	2.600	1.700	1.450	16.000	1.167	4.200	7.900	6.600	3.000	5.400
Energy Convergence [E-07]	1.200	1.300	1.300	7.000	1.000	1.900	4.000	3.500	2.300	1.800
Hot Water Mass Flow Rate Centre	0.04991	0.04991	0.04991	0.04991	0.04991	0.04991	0.04991	0.04991	0.04991	0.04991
Cold Water Mass Flow Rate Centre	-0.01614	-0.01614	-0.01597	-0.01596	-0.01604	-0.01598	-0.01601	-0.01612	-0.016	-0.01614
Hot Water Pressure Centre	54.55	54.59	54.55	54.3	54.83	54.55	54.3	54.55	54.3	54.55
Cold Water Pressure Centre	-139.235	-139.08	-257.69	-144.79	-102.78	-117.36	-139.74	-101.07	-124.2	-138.7
Subjective Pass/Fail of streamlines	Pass	Pass	Pass	Average	Average	Pass	Pass	Pass	Average	Pass
Convergence Error Representation	N/A	3%	3%	537%	0%	54%	214%	196%	56%	65%
Mass Flow Rate Error	N/A	0.00%	1.04%	1.12%	0.60%	0.94%	0.76%	0.10%	0.83%	0.04%
Wall Pressure Error	N/A	0.18%	85.08%	4.45%	26.70%	15.71%	0.82%	27.41%	11.26%	0.38%
Element Reduction		3%	35%	48%	52%	25%	38%	33%	47%	17%

Figure E-1: Mesh independence study results – for section 4.5.4.

## Appendix F – Local Temperature Distribution Data for Section 4.5.6

		Distance (mm)										
			1	2	3	4	5	6	7	8	9	10
Valve Position (degrees from fully open)	No valve	Min (K)	291.5	291.491	291.501	291.491	291.49	291.504	291.503	291.48	291.501	291.502
		Max (K)	297.859	300.107	299.865	299.783	299.149	299.267	298.569	299.316	300.19	299.184
		Average (K)	291.299	289.73	293.898	292.767	292.598	292.531	292.487	292.559	292.444	292.31
	15	Min (K)	291.418	291.49	291.499	291.494	291.5	291.47	291.501	291.5	291.488	291.493
		Max (K)	299.896	301.377	300.866	299.282	301.142	299.395	300.386	300.877	299.817	300.177
		Average (K)	291.625	291.289	292.698	292.243	292.263	292.302	292.413	292.387	292.453	292.363
	30	Min (K)	291.499	291.493	291.5	291.396	291.501	291.441	291.499	291.506	291.501	291.525
		Max (K)	300.23	301.527	299.313	302.621	300.599	300.177	300.501	300.257	302.001	300.306
		Average (K)	291.643	288.697	292.121	292.04	292.191	292.22	292.286	292.489	292.328	292.366
	45	Min (K)	291.503	291.501	291.497	291.502	291.488	291.49	291.5	291.389	291.483	291.549
		Max (K)	303.619	302.082	300.709	300.027	300.479	299.962	299.954	298.519	298.672	299.465
		Average (K)	291.64	292.59	291.853	291.971	291.984	292.064	292.306	283.693	292.325	292.329
	60	Min (K)	291.488	291.499	291.503	291.509	291.51	291.514	291.551	291.526	291.539	291.706
		Max (K)	300.514	302.886	299.117	300.534	299.588	300.126	300.608	299.33	299.057	297.666
		Average (K)	291.877	290.669	291.698	291.773	291.831	291.97	285.484	294.245	292.13	292.405

from the starting wall (mm)												
11	12	14	16	18	20	22	24	29	34	39	44	49
291.474	291.474	291.521	291.625	291.703	291.529	291.571	291.604	291.796	291.821	291.998	291.931	292.126
300.108	299.136	299.753	301.68	303.555	303.888	304.931	305.406	305.998	306.374	305.258	306.231	307.274
292.502	292.535	292.81	293.246	293.539	293.74	293.768	293.955	294.491	294.695	295.233	295.809	295.884
291.513	291.563	291.634	291.6	291.664	291.659	291.637	291.806	291.692	291.76	292.029	292.43	292.432
301.503	300.267	299.79	299.385	301.538	305.302	305.594	304.57	306.287	306.189	306.171	305.968	305.645
292.311	292.48	292.887	293.363	293.814	293.855	294.022	293.919	294.451	294.765	295.296	295.532	295.829
291.579	291.65	291.871	291.692	291.849	291.841	291.863	291.879	291.827	291.802	291.908	292.065	291.893
299.759	298.914	298.164	302.252	301.739	303.031	304.658	304.185	304.402	305.794	305.918	305.744	306.28
292.351	292.598	292.894	293.451	293.841	293.679	293.752	293.552	294.21	294.438	294.931	295.13	295.492
291.707	291.629	291.547	291.573	291.58	291.637	291.663	291.69	291.693	291.782	291.759	291.886	292.044
299.699	299.679	302.105	302.66	305.066	307.631	307.773	306.956	306.862	307.652	307.547	306.649	305.61
292.513	292.566	292.962	293.175	292.974	292.984	293.239	293.238	293.51	294.122	294.618	295.162	295.481
291.738	291.881	291.997	291.776	291.743	291.74	291.768	291.76	291.777	291.779	291.776	291.803	291.837
297.589	297.881	301.384	302.931	306.828	307.705	308.19	307.662	306.625	307.26	305.638	306.271	308.16
292.655	292.708	293.183	293.14	292.96	292.764	292.892	292.794	292.996	293.318	293.99	294.404	294.935

*Figure F-1: Data set from section 4.5.6 reporting temperatures at various distances by valve angle (image split for clarity).*

## Appendix G – Local Temperature Distribution Data for Section 5.6.2

		Distance from the starting wall (mm)						
			10	20	30	40	50	60
Valve Position (degrees from fully closed)	No valve	Min (K)	317.9	318	318	318	318	318
		Max (K)	325.5	324.8	325	325	325	324.4
		Average (K)	318.1	317.8	325	319.5	319.7	319.6
	49.5	Min (K)	318.0	318.0	318.1	318.1	318.2	318.0
		Max (K)	324.6	323.9	325.0	323.2	327.7	324.3
		Average (K)	318.3	319.1	325.0	318.7	319.5	321.2
	25	Min (K)	318.0	318.0	318.1	318.3	318.3	318.1
		Max (K)	326.9	326.2	327.8	326.7	327.3	326.5
		Average (K)	318.3	319.2	327.8	318.9	317.3	318.2

Distance from the starting wall (mm)										
70	80	90	100	110	120	130	140	150	170	190
318	318	318	318	318	318	318	318	318	318	318
324.8	326.2	323.8	325	324.4	326.6	324.8	326.3	324.2	325.6	324.4
319.6	319.6	319.2	319.1	318.8	318.6	317.8	318.7	318.9	319.5	319.6
318.0	318.0	318.0	318.0	318.0	318.0	318.0	318.0	318.0	318.0	318.1
328.1	325.3	327.2	325.0	327.4	327.5	323.9	327.6	325.0	326.2	327.5
322.3	320.4	321.1	320.3	319.6	319.4	319.1	319.8	319.1	319.4	319.2
318.1	318.0	318.0	318.0	318.0	318.0	318.0	318.0	318.0	318.0	318.1
326.7	324.6	326.6	324.4	327.2	326.2	326.2	327.8	325.3	327.3	327.5
317.5	316.8	312.9	320.5	321.7	319.7	319.2	320.1	319.1	319.3	319.2

Distance from the starting wall (mm)										
210	230	250	270	290	340	390	440	490	540	590
318.1	318.2	318.3	318.4	318.5	318.5	318.5	318.4	318.5	318.4	318.5
326.8	325.6	326.1	325.7	324.8	326.1	326.4	326.1	327.8	327.3	327.1
319.4	319.2	318.9	319.7	320	320.1	319.8	320.8	319.9	321.1	320.8
318.1	318.2	318.2	318.3	318.4	318.3	318.4	318.4	318.4	318.4	318.5
327.7	325.5	325.9	327.5	328.3	328.3	329.0	327.3	327.8	327.0	328.2
319.6	319.4	319.9	320.3	320.7	321.5	320.5	320.3	321.0	321.0	320.4
318.2	318.3	318.2	318.5	318.4	318.4	318.5	318.5	318.4	318.5	318.5
327.7	325.1	324.8	327.7	328.5	328.9	329.3	328.0	328.7	327.1	327.5
319.6	319.6	320.0	320.5	321.3	321.6	320.5	320.4	320.9	320.8	320.4

Figure G-1: Data set from section 5.6.2 reporting temperatures at various distances by valve angle (image split for clarity).

## Appendix H – Mesh Independence Study for Scaled Entry Region

	Base Line default	Test 1		Test 2		Test 3		Test 4		Test 5		Test 6		Test 7		Test 8		Test 9		Test 10		Test 11		Test 12		Test 13		Test 14		Test 15		Test 16			
		default	36	36	36	36	36	36	36	36	36	36	36	36	36	32	32	32	32	32	32	32	32	32	28	28	28	28	28	28	28	21			
Hot Water Sweep Divisions	0.008	0.0085	0.009	0.009	0.01	0.015	0.015	0.015	0.015	0.02	0.02	0.008	0.008	0.0085	0.009	0.009	0.009	0.009	0.01	0.015	0.015	0.02	0.008	0.008	0.009	0.01	0.01	0.015	0.15	0.15	0.01	0.01			
Hot water edge division	0.008	0.0085	0.009	0.009	0.01	0.015	0.015	0.015	0.015	0.02	0.02	0.008	0.008	0.0085	0.009	0.009	0.009	0.009	0.01	0.015	0.015	0.02	0.008	0.008	0.009	0.01	0.01	0.015	0.15	0.15	0.01	0.01			
Cold water Body sizing	0.008	0.0085	0.009	0.009	0.01	0.015	0.015	0.015	0.015	0.02	0.02	0.008	0.008	0.0085	0.009	0.009	0.009	0.009	0.01	0.015	0.015	0.02	0.008	0.008	0.009	0.01	0.01	0.015	0.15	0.15	0.01	0.01			
Resulting Elements	452359	400417	363067	315818	315818	264605	215969	443927	370694	355725	285915	227334	189666	316421	237560	108643	237426	237426	237426	237426	237426	237426	237426	237426	237426	237426	237426	237426	237426	237426	237426	237426	237426		
Average X,Y,Z Convergence [E-06]	0.140	0.253	1.691	1.550	1.550	2.300	0.353	0.353	0.018	0.135	0.654	0.077	0.137	0.225	0.714	1.830	3.413	3.413	3.413	3.413	3.413	3.413	3.413	3.413	3.413	3.413	3.413	3.413	3.413	3.413	3.413	3.413	3.413		
Continuity Convergence [E-03]	0.384	1.040	5.570	1.988	3.190	3.620	0.690	0.366	0.008	0.398	2.500	0.370	0.481	0.791	2.970	7.260	9.500	9.500	9.500	9.500	9.500	9.500	9.500	9.500	9.500	9.500	9.500	9.500	9.500	9.500	9.500	9.500	9.500		
Energy Convergence [E-07]	0.068	1.826	1.988	3.190	3.190	3.620	0.690	0.366	0.003	1.955	0.940	1.384	0.210	0.377	0.550	2.950	4.420	4.420	4.420	4.420	4.420	4.420	4.420	4.420	4.420	4.420	4.420	4.420	4.420	4.420	4.420	4.420	4.420		
Hot Water Mass Flow Rate Exit	-38.11	-38.11	-38.11	-38.11	-38.11	-38.11	-38.11	-38.11	-38.11	-38.11	-38.11	-38.11	-38.11	-38.11	-38.11	-38.11	-38.11	-38.11	-38.11	-38.11	-38.11	-38.11	-38.11	-38.11	-38.11	-38.11	-38.11	-38.11	-38.11	-38.11	-38.11	-38.11	-38.11		
Cold Water Mass Flow Rate Exit	-4.23	-4.23	-4.23	-4.23	-4.23	-4.23	-4.23	-4.23	-4.23	-4.23	-4.23	-4.23	-4.23	-4.23	-4.23	-4.23	-4.23	-4.23	-4.23	-4.23	-4.23	-4.23	-4.23	-4.23	-4.23	-4.23	-4.23	-4.23	-4.23	-4.23	-4.23	-4.23	-4.23		
Hot Water Mass Flow Rate Centre	38.11	38.11	38.11	38.11	38.11	38.11	38.11	38.11	38.11	38.11	38.11	38.11	38.11	38.11	38.11	38.11	38.11	38.11	38.11	38.11	38.11	38.11	38.11	38.11	38.11	38.11	38.11	38.11	38.11	38.11	38.11	38.11	38.11	38.11	
Cold Water Mass Flow Rate Centre	-4.22515	-4.22592	-4.23	-4.23	-4.23	-4.233	-4.219	-4.226	-4.23	-4.217	-4.228	-4.22	-4.226	-4.22	-4.226	-4.22	-4.226	-4.22	-4.226	-4.22	-4.226	-4.226	-4.226	-4.226	-4.226	-4.226	-4.226	-4.226	-4.226	-4.226	-4.226	-4.226	-4.226	-4.226	
Hot Water Pressure Centre	1402.67	1402.63	1403	1403	1403	1403	1403	1403	1403	1404	1405	1405	1405	1405	1405	1405	1405	1405	1405	1405	1405	1405	1405	1405	1405	1405	1405	1405	1405	1405	1405	1405	1405	1405	
Cold Water Pressure Centre	23.8396	24.9467	21.55	13.41	13.41	19.7	25.52	25.71	27.25	20.47	16.89	24.51	27.32	25.95	19.16	17.8	21.59	21.59	21.59	21.59	21.59	21.59	21.59	21.59	21.59	21.59	21.59	21.59	21.59	21.59	21.59	21.59	21.59	21.59	
Hot Water Outlet Temperature	358.848	358.846	358.8	358.9	358.9	358.9	358.9	358.8	358.9	358.9	358.9	358.9	358.9	358.9	358.9	358.9	358.9	358.9	358.9	358.9	358.9	358.9	358.9	358.9	358.9	358.9	358.9	358.9	358.9	358.9	358.9	358.9	358.9	358.9	358.9
Cold Water Outlet Temperature	320.08	320.1	320.1	320.1	320.1	320.1	320.1	320.1	320.1	320.1	320.1	320.1	320.1	320.1	320.1	320.1	320.1	320.1	320.1	320.1	320.1	320.1	320.1	320.1	320.1	320.1	320.1	320.1	320.1	320.1	320.1	320.1	320.1	320.1	
Subjective Pass/Fail of streamlines	Pass	Pass	Pass	Pass	Pass	Pass	Pass	Pass	Pass	Pass	Pass	Pass	Pass	Pass	Pass	Pass	Pass	Pass	Pass	Pass	Pass	Pass	Pass	Pass	Pass	Pass	Pass	Pass	Pass	Pass	Pass	Pass	Pass	Pass	
Convergence Error Representation	N/A	952%	1768%	2448%	2448%	3002%	358%	198%	0%	933%	737%	650%	79%	208%	599%	2423%	3720%	3720%	3720%	3720%	3720%	3720%	3720%	3720%	3720%	3720%	3720%	3720%	3720%	3720%	3720%	3720%	3720%	3720%	
Mass Flow Rate Error	N/A	0.02%	0.11%	0.07%	0.07%	0.19%	0.15%	0.02%	0.11%	0.19%	0.07%	0.12%	0.02%	0.07%	0.07%	0.62%	0.86%	0.86%	0.86%	0.86%	0.86%	0.86%	0.86%	0.86%	0.86%	0.86%	0.86%	0.86%	0.86%	0.86%	0.86%	0.86%	0.86%	0.86%	
Wall Pressure Error	N/A	4.65%	9.63%	43.77%	43.77%	17.39%	7.07%	8.01%	14.40%	14.30%	29.32%	2.98%	14.77%	9.02%	20.08%	25.38%	9.56%	9.56%	9.56%	9.56%	9.56%	9.56%	9.56%	9.56%	9.56%	9.56%	9.56%	9.56%	9.56%	9.56%	9.56%	9.56%	9.56%	9.56%	
Outlet Temperature Error	N/A	0.01%	0.02%	0.02%	0.02%	0.02%	0.02%	0.02%	0.04%	0.02%	0.04%	0.04%	0.04%	0.02%	0.04%	0.04%	0.04%	0.04%	0.04%	0.04%	0.04%	0.04%	0.04%	0.04%	0.04%	0.04%	0.04%	0.04%	0.04%	0.04%	0.04%	0.04%	0.04%	0.04%	
Element Reduction		11%	20%	30%	30%	42%	52%	2%	18%	21%	37%	50%	58%	2%	30%	47%	76%	76%	76%	76%	76%	76%	76%	76%	76%	76%	76%	76%	76%	76%	76%	76%	76%	76%	

Figure H-1: Mesh independence study results – for section 5.6.1.

# Appendix I – Temperature Distribution Data for Section 6.1

Temperature (K)	Distance from the Starting Wall (mm)																	
	210	230	250	270	290	310	330	350	370	390	410	430	450	470	490	510	530	550
0	326.8	325.6	326.1	325.7	324.8	325.1	326.1	325.8	326.6	326.4	327	327.2	326	326.5	327.8	328	327.2	326.1
5	329.1	325.7	325.0	328.1	327.8	327.8	326.8	327.3	328.4	328.3	327.9	325.5	325.9	326.8	326.4	329.9	326.7	326.7
10	327.0	324.7	325.8	327.4	327.6	327.2	326.9	327.2	326.8	327.9	328.5	325.3	325.7	326.2	326.2	328.9	325.7	326.4
15	328.7	325.1	325.4	327.8	328.2	327.4	327.2	326.3	327.5	328.0	326.8	326.5	325.3	326.1	326.7	329.4	326.2	326.0
20	327.1	324.1	324.8	327.8	328.0	328.1	327.1	326.8	327.4	328.3	328.6	326.1	326.6	327.4	327.2	329.6	326.1	325.8
25	327.1	324.1	324.8	327.8	328.0	328.1	327.1	326.8	327.4	328.3	328.6	326.1	326.6	327.4	327.2	329.6	326.1	325.8
30	327.3	324.7	325.9	327.6	327.8	327.5	327.2	328.1	327.7	329.4	329.7	326.3	327.2	328.1	328.0	330.0	326.6	326.8
35	327.4	324.3	326.9	327.9	328.0	328.2	327.4	327.2	327.1	328.5	328.2	326.1	325.2	326.3	329.0	329.7	326.6	327.8
40	329.7	325.6	325.6	327.8	327.6	327.1	326.8	327.5	327.5	328.6	328.5	326.7	327.0	329.8	328.4	329.7	326.2	326.8
45	328.3	326.1	325.0	327.6	327.9	327.9	326.8	327.2	327.6	328.0	329.3	326.9	326.7	326.4	327.8	329.4	326.1	326.3
50	327.9	325.0	326.1	327.0	328.2	327.0	326.9	327.4	328.9	328.4	329.1	327.4	326.3	328.4	328.1	329.7	327.1	327.7
55	327.8	325.3	325.3	327.2	328.2	327.4	326.9	326.9	328.0	329.3	328.5	327.2	325.3	327.0	328.3	329.9	327.1	326.6
60	326.8	325.0	327.2	328.5	329.2	326.3	326.5	327.4	327.3	328.8	328.2	326.8	327.4	327.8	327.4	329.8	329.5	327.3
65	327.7	325.1	324.8	327.7	328.5	326.8	327.0	326.8	327.8	329.3	328.7	328.4	327.0	327.0	328.7	329.7	326.1	326.4
70	327.6	325.9	325.5	326.9	328.6	327.2	327.1	326.2	328.4	327.9	328.1	326.7	326.7	326.5	327.5	329.0	329.1	327.6
75	326.7	324.7	325.4	329.4	327.4	326.7	327.5	327.5	327.2	328.3	327.8	328.2	327.2	327.3	327.4	328.3	327.8	327.7
80	327.4	324.1	325.6	327.8	327.8	326.6	326.1	327.8	328.0	328.2	328.8	328.3	328.4	329.0	328.4	329.2	329.3	329.4
85	326.5	323.6	324.9	328.1	328.5	326.8	327.4	329.0	328.4	327.7	328.5	327.4	329.8	328.1	329.3	328.8	329.7	330.9

Figure I-1: Mesh independence study results – for section 5.6.1.